

Muon reconstruction efficiency and momentum resolution of the ATLAS experiment in proton–proton collisions at $\sqrt{s} = 7$ TeV in 2010

The ATLAS Collaboration*

CERN, 1211 Geneva 23, Switzerland

Received: 18 April 2014 / Accepted: 19 August 2014 / Published online: 16 September 2014

© CERN for the benefit of the ATLAS collaboration 2014. This article is published with open access at Springerlink.com

Abstract This paper presents a study of the performance of the muon reconstruction in the analysis of proton–proton collisions at $\sqrt{s} = 7$ TeV at the LHC, recorded by the ATLAS detector in 2010. This performance is described in terms of reconstruction and isolation efficiencies and momentum resolutions for different classes of reconstructed muons. The results are obtained from an analysis of J/ψ meson and Z boson decays to dimuons, reconstructed from a data sample corresponding to an integrated luminosity of 40 pb^{-1} . The measured performance is compared to Monte Carlo predictions and deviations from the predicted performance are discussed.

1 Introduction

Muon identification and measurement in ATLAS relies on two complementary detectors, one of which is its huge Muon Spectrometer (MS). This is based on the use of three very large air core toroidal magnets, each containing eight superconducting coils, and three measuring planes of high-precision chambers. This system is designed for efficient muon detection even in the presence of very high particle backgrounds and for excellent muon momentum resolution up to very high momenta of ~ 1 TeV. This unprecedented stand-alone performance of the ATLAS muon spectrometer is due to the large field integral (ranging between 2 and 6 Tm for most of the detector), the very low multiple scattering in the material of the air core toroids (1.3 units of radiation length over a large fraction of the acceptance in the barrel toroid), the very high precision measurements along the muon trajectory (chamber resolution $35 \mu\text{m}$) and the extreme alignment precision of the measuring planes ($30 \mu\text{m}$).

The other very important component of the muon identification and measurement in ATLAS is the inner detector (ID). In ATLAS the very efficient muon detection and high

momentum resolution, with nominal relative momentum resolutions of $<3.5\%$ up to transverse momenta $p_T \sim 200$ GeV and $<10\%$ up to $p_T \sim 1$ TeV, are obtained by a combination of measurements from the ID and the MS [1, p.162]. The complementarity of these measurements can be exploited to provide measurements of the muon reconstruction efficiencies in both tracking systems. In this paper, the muon reconstruction efficiencies are measured using dimuon decays of J/ψ mesons to access the region $p_T < 10$ GeV and dimuon decays of Z bosons to access the region $20 \text{ GeV} < p_T < 100 \text{ GeV}$. The efficiency determination in the region $10 \text{ GeV} < p_T < 20 \text{ GeV}$ is not possible due to the limited sample of muons with p_T higher than 10 GeV in the J/ψ decays and difficulties in controlling the backgrounds in the sample of Z decays that lead to muons with p_T smaller than 20 GeV. For these analyses, one of the decay muons is reconstructed in both detector systems and the other is reconstructed by just one of the systems in order to probe the efficiency of the other. This method (known as *tag-and-probe*, and described in more detail in Sect. 4) is applied to the ATLAS proton–proton (pp) collision data recorded at the Large Hadron Collider (LHC) in 2010 at a centre-of-mass energy of 7 TeV.

Muon isolation criteria are used to select muons in many physics analyses, and measurements of the isolation efficiency performed using $Z \rightarrow \mu^+\mu^-$ decays are described in Sect. 9. The invariant mass distributions from these data are also used to extract the muon momentum resolutions. The analysed data sample corresponds to the full 2010 pp dataset with an integrated luminosity of 40 pb^{-1} [2] after applying beam, detector and data-quality requirements.

2 The ATLAS detector

A detailed description of the ATLAS detector can be found elsewhere [3]. Muons are independently measured in the ID and in the MS.

* e-mail: atlas.publications@cern.ch

The ID measures tracks up to $|\eta| = 2.5$ ¹ exploiting three types of detectors operated in an axial magnetic field of 2 T: three layers of silicon pixel detectors closest to the interaction point, four layers of semiconductor microstrip detectors (SCT) surrounding the pixel detector, and a transition radiation straw-tube tracker (TRT) covering $|\eta| < 2.0$ as the outermost part. The innermost pixel layer (known as the *b-layer*) has a radius of 50.5 mm in the barrel, whilst the outermost TRT tubes are at $r \approx 1$ m.

The electromagnetic and hadronic calorimeters surround the ID and cover the pseudorapidity range $|\eta| < 4.9$, far beyond the range over which muons are identified. In the barrel and end-cap, in the region $|\eta| < 3.2$ the electromagnetic calorimeter consists of lead absorbers with liquid-argon (LAr) as active material. The barrel hadronic tile calorimeter is a steel/scintillating-tile detector and is extended by two end-caps with LAr as the active material and copper as absorber. The total combined thickness of 11 interaction lengths (λ) includes 9.7λ of active calorimeter and 1.3λ of outer support.

The magnetic field of the MS is produced by three large air-core superconducting toroidal magnet systems (two end-caps, where the average field integral is about 6 Tm, and one barrel, where the field integral is about 2.5 Tm). The field is continuously monitored by approximately 1800 Hall sensors distributed throughout the spectrometer volume. The deflection of the muon trajectory in this magnetic field is measured via hits in three layers of precision monitored drift tube (MDT) chambers for $|\eta| < 2.0$ and two outer layers of MDT chambers in combination with one layer of cathode strip chambers (CSCs) in the innermost end-cap wheels ($2.0 \leq |\eta| < 2.7$). Three layers of resistive plate chambers (RPCs) in the barrel ($|\eta| < 1.05$) and three layers of thin gap chambers (TGCs) in the end-caps ($1.05 < |\eta| < 2.4$) are used by the muon trigger (see below). The RPCs, TGCs and CSCs also measure the muon trajectory in the non-bending (ϕ) plane of the spectrometer magnets. The following text frequently refers to chambers which make a measurement in the bending (η) plane as ‘precision chambers’, since these have a much better spatial resolution (important for a good momentum resolution) than the chambers used for triggering.

The chambers are monitored by an optical alignment system, designed to provide an accuracy of $30\ \mu\text{m}$ in the barrel and $40\ \mu\text{m}$ in the end-cap [4]. The absolute alignment combines information from the optical system and a track-based procedure (using cosmic data samples and special runs with-

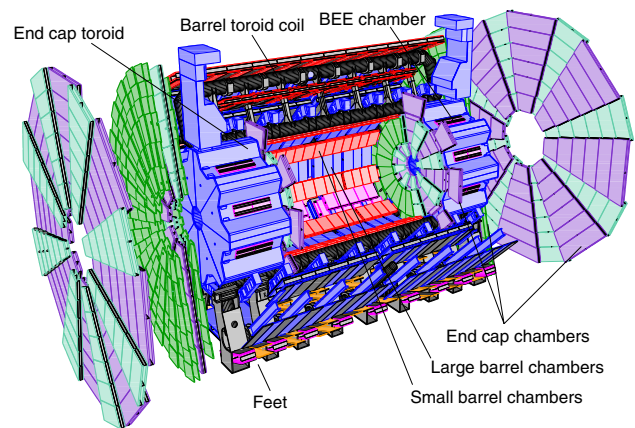


Fig. 1 Schematic drawing of the ATLAS muon spectrometer

out the toroidal field), and then the optical alignment is used continuously to monitor relative chamber displacements with time (for example, when the toroid magnet is turned on). With the limited 2010 data sample, the muon spectrometer alignment precision was around three times larger than designed.

The ATLAS detector has a three-level trigger system: level 1 (L1), level 2 (L2), and the event filter (EF). The MS provides a L1 hardware muon trigger which is based on hit coincidences in different RPC and TGC detector layers within programmed geometrical windows which define the muon p_T . The L2 and EF muon triggers perform a software confirmation of the L1 muon trigger using refined p_T measurements from the precision chambers.

Figure 1 shows a schematic drawing of the ATLAS MS. The barrel muon chambers are installed around the calorimeters in roughly cylindrical rings of approximately 5, 7 and 9 m radius. Large barrel chambers are mounted between the barrel toroid coil cryostats. Small barrel chambers are installed on the toroid coil cryostats. The barrel end-cap extra (BEE) chambers are mounted on the end-cap toroid cryostats. The end-cap chambers are arranged in disks with z axis positions of approximately 7, 13 and 21 m from the centre of the detector, and which are orthogonal to the proton beams.

3 Muon reconstruction and identification in ATLAS

Muon identification in ATLAS uses independent track reconstruction in the ID and MS, which are then combined. Track reconstruction in the muon spectrometer is logically subdivided into the following stages: pre-processing of raw data to form drift-circles in the MDTs or clusters in the CSCs and the trigger chambers, pattern-finding and segment-making, segment-combining, and finally track-fitting. Track segments are defined as straight lines in a single MDT or CSC station. The search for segments is seeded by a reconstructed pattern of drift-circles and/or clusters.

¹ ATLAS uses a right-handed coordinate system with its origin at the nominal interaction point (IP) in the centre of the detector and the z axis along the beam pipe. The x axis points from the IP to the centre of the LHC ring, and the y axis points upward. Cylindrical coordinates (r, ϕ) are used in the transverse plane, ϕ being the azimuthal angle around the beam pipe. The pseudorapidity is defined in terms of the polar angle θ as $\eta = -\ln \tan(\theta/2)$.

Full-fledged track candidates are built from segments, typically starting from the outer and middle stations and extrapolating back through the magnetic field to the segments reconstructed in the inner stations (though other permutations are also explored). Each time a reasonable match is found, the segment is added to the track candidate. The final track-fitting procedure takes into account all relevant effects (e.g. multiple scattering, field inhomogeneities, inter-chamber misalignments, etc.). More details about the muon reconstruction can be found in Ref. [1, p. 165].

A similar approach is followed by the ID track reconstruction where the pattern recognition uses space-points formed from the pixel and SCT clusters to generate track seeds. These seeds are then extended into the TRT and drift circles are associated. Finally the tracks are refitted with the information coming from all three detectors. More details about the ID track reconstruction can be found in Ref. [1, p. 19].

The analyses presented here make use of three classes of reconstructed muons, as described below.

- *Stand-alone (SA) muon*: the muon trajectory is reconstructed only in the MS. The direction of flight and the impact parameter of the muon at the interaction point are determined by extrapolating the spectrometer track back to the point of closest approach to the beam line, taking into account the energy loss of the muon in the calorimeters.
- *Combined (CB) muon*: track reconstruction is performed independently in the ID and MS, and a combined track is formed from the successful combination of a SA track with an ID track.
- *Segment-tagged (ST) muon*: a track in the ID is identified as a muon if the track, extrapolated to the MS, is associated with at least one segment in the precision muon chambers.

The main goals of this paper are the measurement of the reconstruction efficiencies, for combined (CB) and combined-plus-segment-tagged (CB+ST) muons, and reconstruction resolutions, for MS and ID muons. The use of the ID for CB and CB+ST muons limits their acceptance to $|\eta| < 2.5$. Stand-alone muons are employed to measure the muon reconstruction efficiency in the ID.

The CB muon candidates constitute the sample with the highest purity. The efficiency for their reconstruction is strongly affected by acceptance losses in the MS, mainly in the two following regions:

- at $\eta \sim 0$, the MS is only partially equipped with muon chambers in order to provide space for services of the ID and the calorimeters;
- in the region ($1.1 < |\eta| < 1.3$) between the barrel and the end-caps, there are regions in ϕ where only one layer of

chambers is traversed by muons in the MS, due to the fact that some chambers were not yet installed in that region during the 2010–2012 data-taking. Here no stand-alone momentum measurement is available and the CB muon reconstruction efficiency is decreased.

The reconstruction algorithms for ST muons have higher efficiency than those for CB muons as they can recover muons which did not cross enough precision chambers to allow an independent momentum measurement in the MS. They are also needed for the reconstruction of low- p_T muons which only reach the innermost layer of the muon chambers. Due to their lower purity and poorer momentum resolution, ST muons are only used in cases where no CB muon can be reconstructed.

In the early phase of the LHC operation, ATLAS used two entirely independent strategies for the reconstruction of both the CB and ST muons. These two approaches, known as *chain 1* and *chain 2* in the following, provide an invaluable cross-check on the performance of a very complex system, and allow ATLAS to ultimately take the best aspects of both. The chains have slightly different operating points, with chain 1 typically more robust against background, whilst chain 2 has a slightly higher efficiency.

In chain 1, the momentum of the muon is obtained from a statistical combination of the parameters of the tracks reconstructed by the ID and MS [1, p. 166]. SA muon tracks are required to have a sufficient number of hits in the precision and trigger chambers, to ensure a reliable momentum measurement. In chain 2, the combined muon momentum is the result of a simultaneous track fit to the hits in the ID and the MS. The requirements applied to the hit multiplicities in the MS are less stringent than in chain 1 because certain information, such as the trajectory in the plane transverse to the proton beams, is better provided by the ID in the simultaneous fit. In both chains, muon track segments can additionally be assigned to ID tracks to form ST muons, based on the compatibility of the segment with the extrapolated ID track.

To illustrate the high purity of the ATLAS muon identification and the size of the dimuon dataset, Fig. 2 shows the reconstructed invariant mass distribution of opposite-sign muon candidate pairs. The events are selected by an unscaled, 15 GeV p_T threshold single muon trigger, which is reconfirmed offline by requiring at least one muon to have $p_T > 15$ GeV. Both muons are required to be of CB type and to pass the ID track selection criteria of Sect. 6.2. The distance of closest approach of the muon to the primary vertex is limited to 5 mm in the transverse plane and $200 \text{ mm}/\sin \theta$ in the longitudinal direction. The J/ψ , Υ and Z peaks are clearly visible, and the muon reconstruction has the capability to resolve close-by resonances, such as the J/ψ and ψ' as well as the $\Upsilon(1S)$ and $\Upsilon(2S)$. The shoulder near $m_{\mu\mu} \approx 15$ GeV is caused by the kinematic selection.

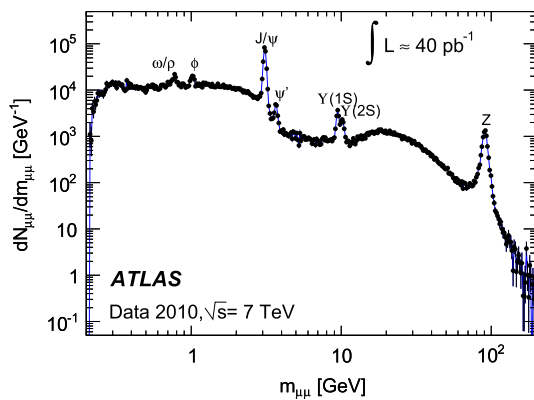


Fig. 2 Reconstructed invariant mass, $m_{\mu\mu}$, distribution of muon candidate pairs. The number of events is normalised by the bin width. The uncertainties are statistical only

4 The tag-and-probe method

As track reconstruction is performed independently in the ID and MS, the reconstruction efficiency for CB or ST muons is the product of the muon reconstruction efficiency in the ID, the reconstruction efficiency in the MS, and the matching efficiency between the ID and MS measurements (which includes the refit efficiency in the case of chain 2). It is therefore possible to study the full reconstruction efficiency by measuring these individual contributions. A tag-and-probe method is employed, which is sensitive to either the ID efficiency or the combined MS and matching efficiency.² This technique is applied to samples of dimuons from the J/ψ and Z decays.

For $Z \rightarrow \mu^+\mu^-$ decays, events are selected by requiring two oppositely charged isolated tracks with a dimuon invariant mass near the mass of the Z boson. One of the tracks is required to be a CB muon candidate, and to have triggered the readout of the event (see Sect. 6). This muon is called the *tag*. The other track, the so-called *probe*, is required to be a SA muon if the ID efficiency is to be measured. If the MS reconstruction and matching efficiency is to be measured the probe must be an ID track. The ID reconstruction efficiency is defined as the fraction of SA probes which can be ascribed to an inner detector track. The combined MS and matching efficiency is the fraction of ID probes which can be associated to a CB or ST muon.

The invariant mass spectra of Z boson tag-and-probe pairs, shown in Fig. 3, illustrate how muon isolation requirements (see Sects. 6 and 9) almost entirely remove contributions from background processes, resulting in a relatively pure

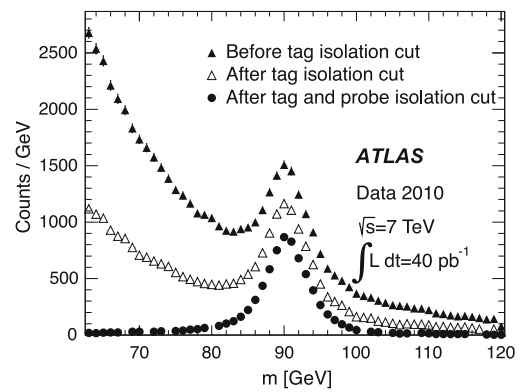


Fig. 3 Invariant mass, m , distribution of pairs of tag muons (chain 2) and ID track probes for different sets of muon isolation requirements for the Z boson analysis, as indicated in the legend

sample of muon tag-and-probe pairs. Monte Carlo studies show that the contribution from other sources is below 0.1 % when MS probes are used and below 0.7 % when ID probes are used. These backgrounds arise from $Z \rightarrow \tau^+\tau^-$, $W^\pm \rightarrow \mu^\pm(\bar{\nu}_\mu)$, $W^\pm \rightarrow \tau^\pm(\bar{\nu}_\tau)$, $b\bar{b}$, $c\bar{c}$, and $t\bar{t}$. The presence of backgrounds in the data leads to an apparent decrease in the muon efficiency in the range $p_T \lesssim 30$ GeV, for both reconstruction chains. This is taken into account by comparing the measured efficiencies to efficiencies predicted using simulated samples which include these background contributions.

To investigate the reconstruction efficiency at lower transverse momenta, dimuon pairs from $J/\psi \rightarrow \mu^+\mu^-$ decays are used in the same way as those from $Z \rightarrow \mu^+\mu^-$ decays. Because J/ψ mesons are produced inside jets, isolation requirements cannot be used to select a pure sample. In this case, the invariant mass distribution of the tag-and-probe pairs is fitted using the sum of a quadratic background term and a Gaussian signal term [5]. This is illustrated in Fig. 4 for probe muons selected in the range $0.1 < |\eta| < 1.1$ and $3 \text{ GeV} < p_T < 4 \text{ GeV}$. The invariant mass spectra are shown for tag-and-probe pairs in which the probes are matched to reconstructed muons (see Sect. 6.5) and for unmatched tag-and-probe pairs. The muon reconstruction efficiency is then extracted from a simultaneous fit to the distributions obtained from the matched and unmatched tag-and-probe pairs.

5 Monte Carlo samples and expectations

The measurements presented in this paper are compared with predictions of Monte Carlo (MC) simulations. For the efficiency measurements in the region $p_T > 20$ GeV, five million $Z \rightarrow \mu^+\mu^-$ events were simulated with PYTHIA 6.4 [6], passed through the full simulation of the ATLAS detector

² Efficiencies determined with the tag-and-probe method, and with an alternative method based on Monte Carlo generator-level information, were found to agree to within statistical uncertainties [1, p. 221], which also shows that any possible correlations between the tag and probe muons are negligible.

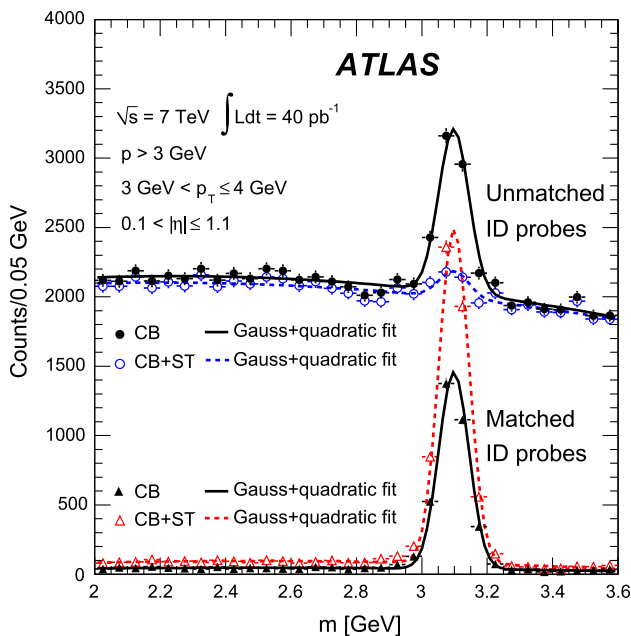


Fig. 4 Distribution of the invariant mass, m , of the unmatched (upper distributions) and matched (lower distributions) tag-and-probe pairs for CB and CB+ST muons of chain 2, for the J/ψ analysis with a probe muon selection as described in the legend. Also shown are the results of the fit using a Gaussian signal and a quadratic background contribution

[7], based on GEANT4 [8,9], and reconstructed with the same reconstruction programs as the experimental data.

During the 2010 data taking, the average number of pp interactions per bunch crossing was about 1.5. This “pile-up” is modelled by overlaying simulated minimum bias events on the original hard-scattering event. It is found to have a negligible impact for these measurements. The following background samples were used: $Z \rightarrow \tau^+\tau^-$, $W^\pm \rightarrow \mu^\pm \bar{\nu}_\mu$, $W^\pm \rightarrow \tau^\pm \bar{\nu}_\tau$, $b\bar{b}$, $c\bar{c}$, and $t\bar{t}$. More details can be found in Ref. [10].

The reconstruction efficiency at low p_T was studied with a simulated sample of five million prompt J/ψ events generated with PYTHIA using the PYTHIA implementation of the colour-octet model. In order to increase the number of events at the higher end of the low- p_T region, this sample was supplemented with a sample of one million $pp \rightarrow b\bar{b}$ events also generated with PYTHIA, in which at least one J/ψ decaying into muons of $p_T > 2.5$ GeV was required in the b -quark decay chain.

The reconstruction efficiencies obtained from the analysis of the J/ψ Monte Carlo samples are shown in Fig. 5, as a function of p_T and η , for CB and CB+ST muons from chain 1. The most discernible features are the areas of lower efficiency at fixed η that result from the un-instrumented (‘crack’) region in the MS at $\eta \sim 0$ and from the barrel/end-cap transition regions where the chamber configuration ($1.1 < |\eta| < 1.3$) and the magnetic field ($1.1 < |\eta| < 1.7$) are rather non-

uniform. Also visible is the impact of the energy loss in the calorimeter on the efficiency, for muons with p_T of less than 2–5 GeV (depending on the η region), which are absorbed in the calorimeter. For $|\eta| < 2.0$, the CB+ST muon reconstruction starts to be efficient at p_T values lower than in the reconstruction of pure CB muons, since it includes muons reaching only the inner layer of MDT chambers. For $|\eta| > 2.0$ the CB and CB+ST efficiencies are very similar for chain 1, because cases with only one segment in the CSC chambers, corresponding to the inner layer of precision chambers in this region, are not considered for ST muons. Chain 2 does make use of these segments, and shows an improved CB+ST efficiency in this region (see Sect. 8.3). These detector features motivate the binning used for the determination of the p_T dependence of the reconstruction efficiency at low p_T .

For the $J/\psi \rightarrow \mu^+\mu^-$ analysis the measured efficiencies are separated into five pseudorapidity intervals according to the different MS regions:

- | | | |
|----------------------|------------------------------|-----|
| $ \eta < 0.1$ | the $\eta = 0$ crack region; | |
| $0.1 < \eta < 1.1$ | the barrel region; | |
| $1.1 < \eta < 1.3$ | the transition region | (1) |
| | between barrel and end-cap; | |
| $1.3 < \eta < 2.0$ | the end-cap region; | |
| $2.0 < \eta < 2.5$ | the forward region. | |

Muons from $Z \rightarrow \mu^+\mu^-$ decays were required to have $p_T > 20$ GeV. In contrast to the case of lower- p_T muons from J/ψ decays, the ϕ deflections of these muons by the magnetic fields in the detector are so small that one can use the muon directions of flight at the pp interaction point to associate them with specific (η, ϕ) regions of the MS. Ten different regions are defined, corresponding to ten different physical regions in the MS [3]. In each of these, the muon traverses a particular set of detector layers and encounters a different quality of detector alignment, a different amount of material or a different magnetic field configuration. The ten regions are described below (see also Fig. 1).

- *Barrel large*: the regions containing large barrel chambers only, which are mounted between the barrel toroid coils.
- *Barrel small*: the regions containing small barrel chambers only, which are mounted on the barrel toroid coils.
- *Barrel overlap*: the regions where small and large barrel chambers have slight overlaps in acceptance.
- *Feet*: the detector is supported by ‘feet’ on its bottom half, which results in a loss of acceptance due to missing chambers, making muon reconstruction more challenging.
- *Transition*: the region $1.1 < |\eta| < 1.3$, between the barrel and the end-cap wheels.
- *End-cap small*: the small end-cap sectors, consisting of MDT chambers.

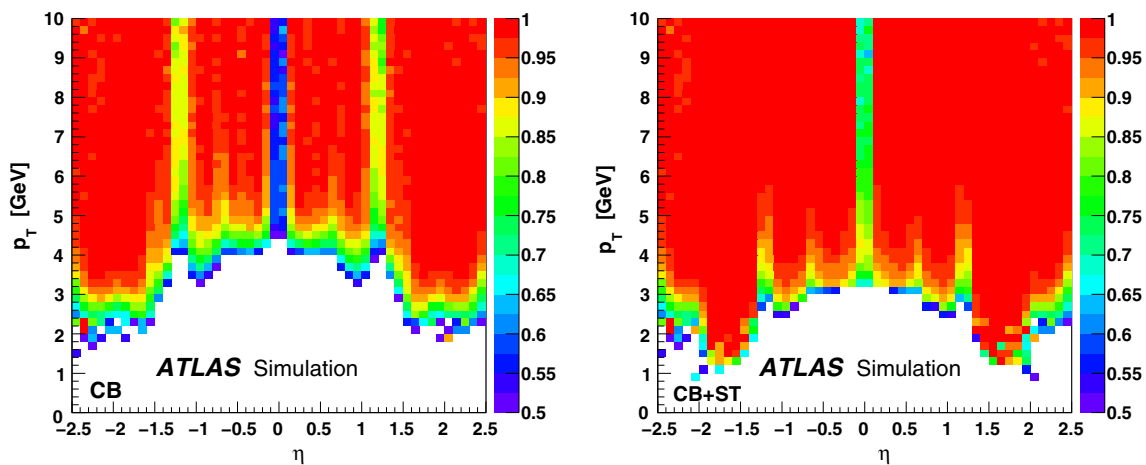


Fig. 5 The chain 1 muon reconstruction efficiency from simulated J/ψ decays for CB (left) and CB+ST (right) muons as a function of η and p_T for efficiency values above 50 %

- *End-cap large*: the large end-cap sectors, consisting of MDT chambers and which (in contrast to the *Barrel large* regions) contain the toroid coils.
- *BEE*: the regions containing barrel end-cap extra chambers, which are mounted on the end-cap toroid cryostats.
- *CSC small*: the end-cap sectors consisting of small CSC chambers.
- *CSC large*: the end-cap sectors consisting of large CSC chambers.

6 Selection of tag-and-probe pairs

6.1 Event selection

The events used for the efficiency measurements were selected online with a single-muon trigger. For the studies with $J/\psi \rightarrow \mu^+\mu^-$ decays, a combined muon is required, with minimum p_T thresholds of 4, 6, 10, or 13 GeV (as it was necessary to increase the thresholds during the year, in order to keep the trigger rate within limits). For the studies with $Z \rightarrow \mu^+\mu^-$ decays, events have to pass the lowest p_T threshold muon trigger that was unrescaled. The thresholds of the selected triggers range from 10 to 13 GeV, well below the transverse momentum threshold of the tag muon in the analysis. To suppress non-collision background events, a reconstructed collision vertex with at least three associated ID tracks is required.

6.2 Inner detector track selection

Tracks in the ID are required to satisfy conditions on the number of hits in the silicon detectors in order to qualify as a muon candidate. They must have at least two pixel hits, including at least one in the b-layer, and at least six SCT hits. In order to reduce inefficiencies due to known inoperative

sensors,³ the latter are counted as hits for tracks crossing them. Within $|\eta| < 1.9$, a good-quality extension of the muon trajectory into the TRT is enforced by requirements on the numbers of associated good TRT hits and TRT outliers.

The TRT outliers appear in two forms in the track reconstruction: as straw tubes with a signal from tracks other than the one in consideration, or as a set of TRT measurements in the extrapolation of a track which fail to form a smooth trajectory together with the pixel and SCT measurements. The latter case is typical of a hadron decay-in-flight, and can be rejected by requiring that the outlier fraction (the ratio of outliers to total TRT hits) is less than 90 %. In the region $|\eta| < 1.9$ the sum of the numbers of TRT hits and outliers is required to be greater than five, with an outlier fraction less than 90 %. At higher $|\eta|$ the requirement on the total number of TRT hits and outliers is not applied, but tracks which do pass it are also required to pass the cut on the outlier fraction. These quality cuts suppress fake tracks and discriminate against muons from π/K decays.

6.3 Tag selection

For each of the two reconstruction chains, tag muons are defined as CB muons from the interaction vertex. Different selection cuts are applied for the measurements using $J/\psi \rightarrow \mu^+\mu^-$ and $Z \rightarrow \mu^+\mu^-$ decays to account for the different kinematics and final-state topologies. For the studies with $J/\psi \rightarrow \mu^+\mu^-$ a tag muon has to pass the following requirements:

- the tag muon triggered the readout of the event;
- $p_T > 4$ GeV, $|\eta| < 2.5$;

³ The fraction of inoperative sensors was ≈ 3 % for the pixel detector and < 1 % for the SCT.

- the distance of closest approach of the muon to the primary vertex, in the transverse plane, has transverse coordinate $|d_0| < 0.3$ mm, and longitudinal coordinate $|z_0| < 1.5$ mm, and significances $|d_0|/\sigma(d_0) < 3$, $|z_0|/\sigma(z_0) < 3$, respectively.

For the studies with $Z \rightarrow \mu^+\mu^-$ decays an additional quantity is used, namely track isolation

$$T_{\text{isol}}^{\Delta R < 0.4} = \sum p_T(\Delta R < 0.4)/p_T(\text{tag}), \quad (2)$$

where the sum extends over all tracks with $p_T > 1$ GeV (excluding the track on which the tag was based), within a cone of $\Delta R \equiv \sqrt{(\Delta\eta)^2 + (\Delta\phi)^2} = 0.4$ around the tag. A tag muon must pass the following requirements:

- the tag muon triggered the readout of the event (restricting the tag muon to the trigger acceptance, $|\eta| < 2.4$);
- $p_T > 20$ GeV;
- $T_{\text{isol}}^{\Delta R < 0.4} < 0.2$.

6.4 Probe selection

Probes are either SA muons or ID tracks, depending on which efficiency measurement is being performed. They have to satisfy the following criteria for studies using $J/\psi \rightarrow \mu^+\mu^-$ decays:

- an ID track fulfilling the hit requirements described in Sect. 6.2 (SA muons are not used, as the ID efficiency is not measured using these decays);
- reconstructed momentum, $p > 3$ GeV, $|\eta| < 2.5$;
- the tag and the probe are oppositely charged;
- the tag and the probe must be associated with the same vertex;
- $\Delta R < 3.5$ between the tag and probe.
- the invariant mass of the tag-and-probe pair is within the range of $2 < m < 3.6$ GeV

Different cuts are applied in case of $Z \rightarrow \mu^+\mu^-$ decays:

- an ID track fulfilling the hit requirements or a SA muon with at least one ϕ measurement;
- $p_T > 20$ GeV, $|\eta| < 2.5$;
- the tag and the probe are oppositely charged;
- the tag and the probe are associated with the same vertex;
- azimuthal separation of the tag and the probe, $\Delta\phi > 2.0$;
- $T_{\text{isol}}^{\Delta R < 0.4} < 0.2$;
- the invariant mass of the tag-and-probe pair is within 10 GeV of m_Z .

6.5 Matching of probes to ID tracks and muons

After selecting all tag-and-probe pairs, an attempt is made to match probe tracks to the objects for which the efficiency is

to be measured, i.e. SA probe tracks to ID tracks in the case of the ID efficiency, or ID tracks to CB or CB+ST muons in the case where the reconstruction efficiencies for these two classes of muons are investigated. A match between an ID probe and a reconstructed muon is considered successful if they have the same charge and are close in (η, ϕ) space: $\Delta R \leq 0.01$. Similarly, a match between an SA probe and an ID track is considered successful if $\Delta R \leq 0.05$.

7 Low- p_T reconstruction efficiency measured with $J/\psi \rightarrow \mu^+\mu^-$ decays

Figures 6 and 7 show the reconstruction efficiencies for chain 1 and chain 2 with respect to ID tracks with momentum $p > 3$ GeV, as a function of the probe p_T , for the five bins in probe $|\eta|$ described in Sect. 5. Also shown are the Monte Carlo predictions, which agree with data within the statistical and systematic uncertainties of the measurements.

A number of checks were performed to study the dependence of the results on analysis details and assumptions.

1. Signal shapes: the means and the widths of the two (matched and unmatched) Gaussians in the fit were allowed to vary independently.
2. Background shape: a linear background function was used in the fit, instead of the quadratic parameterisation; in this case the fit was performed in the reduced mass range of 2.7–3.5 GeV (instead of 2.0–3.6 GeV).
3. Alternative fit: an independent fit to the matched and the total (matched + unmatched) distributions, rather than to matched and unmatched, was used and the efficiency estimated as the ratio of the signal normalisations in the two distributions. While this option does not provide for an easy propagation of the uncertainty from the background subtraction and does not directly account for the correlations between the two samples, it profits from a higher stability of the two simpler fits, whereas the default method needs some care in the choice of the initial conditions, in particular in cases of very high efficiency or small overall sample size.

The largest positive and negative variations obtained from any of the three checks were taken as systematic uncertainties and added in quadrature to the statistical uncertainty to obtain the total upper and lower uncertainties. The statistical uncertainties were found to be at the level of a few percent.

8 Intermediate- and high- p_T reconstruction efficiencies measured with $Z \rightarrow \mu^+\mu^-$ decays

For higher momentum muons, with $p_T > 20$ GeV, Z decays are used to measure the reconstruction efficiencies.

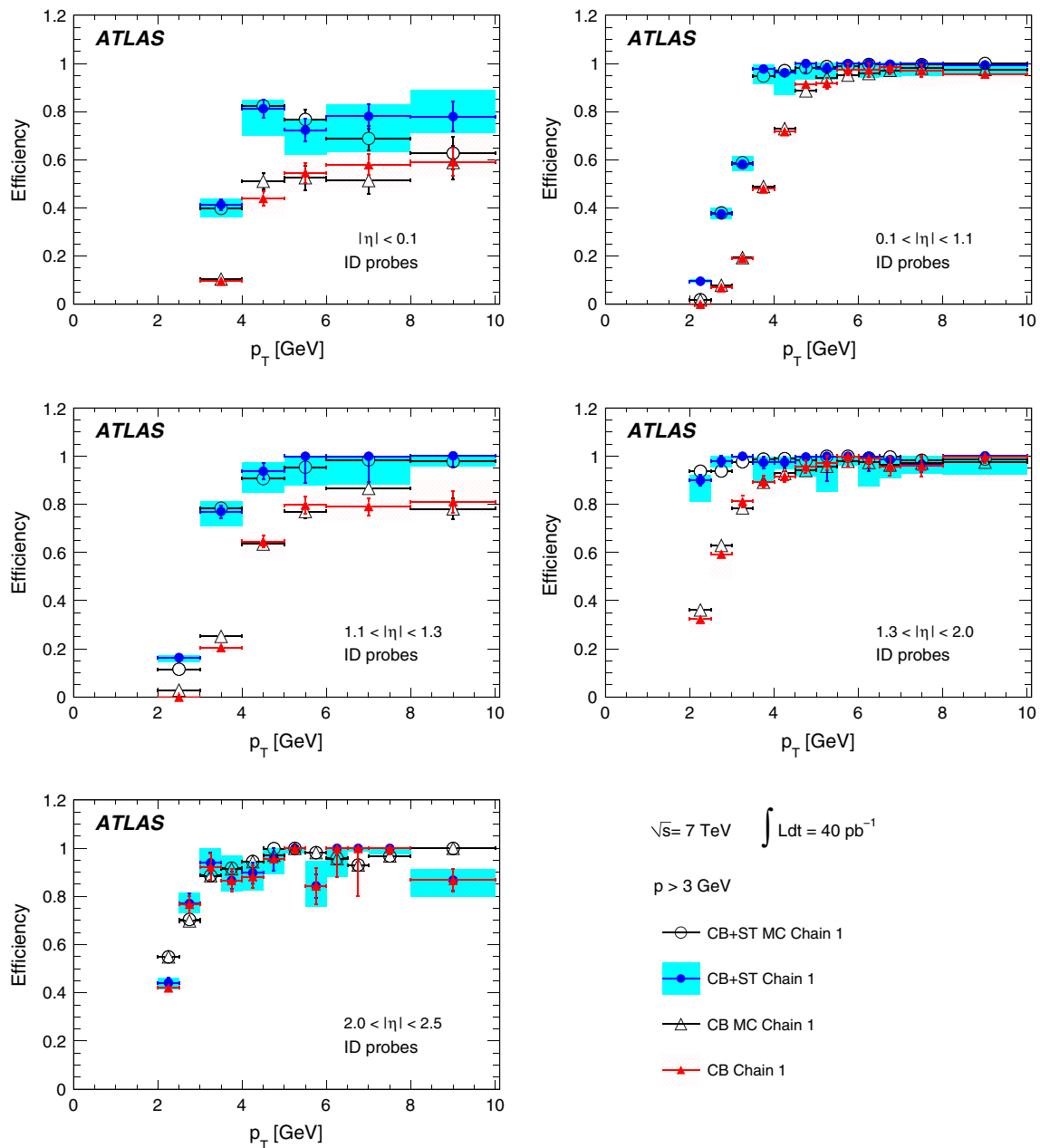


Fig. 6 Efficiency for chain 1 CB and CB+ST muons with momentum $p > 3$ GeV (from J/ψ decays), as a function of p_T , for five bins in $|\eta|$ as described in the legend, for data and MC events. The error bars

represent the statistical uncertainties while the bands around the data points represent the statistical and systematic uncertainties added in quadrature

8.1 Inner detector reconstruction and identification efficiency

Figure 8 shows the reconstruction and identification efficiency in the ID as a function of η , for data and simulation, as determined using SA probes. The simulation includes all considered backgrounds. The scale factors (SF), defined as the ratio of the data efficiency to the Monte Carlo efficiency, are displayed in the lower panel (the smallness of the back-

ground correction, as described in Sect. 4, means that its effect on the SF is negligible).

As discussed earlier, the efficiency for the combined reconstruction varies with the detector region, and with p_T in the range below 6 GeV. In contrast, the ID reconstruction efficiency is independent of ϕ and p_T [3], and shows only a slight dependence on η .

The slightly lower efficiencies at $\eta \sim 0$ and $|\eta| \sim 1$ are caused by the ID hit requirements for muon identification

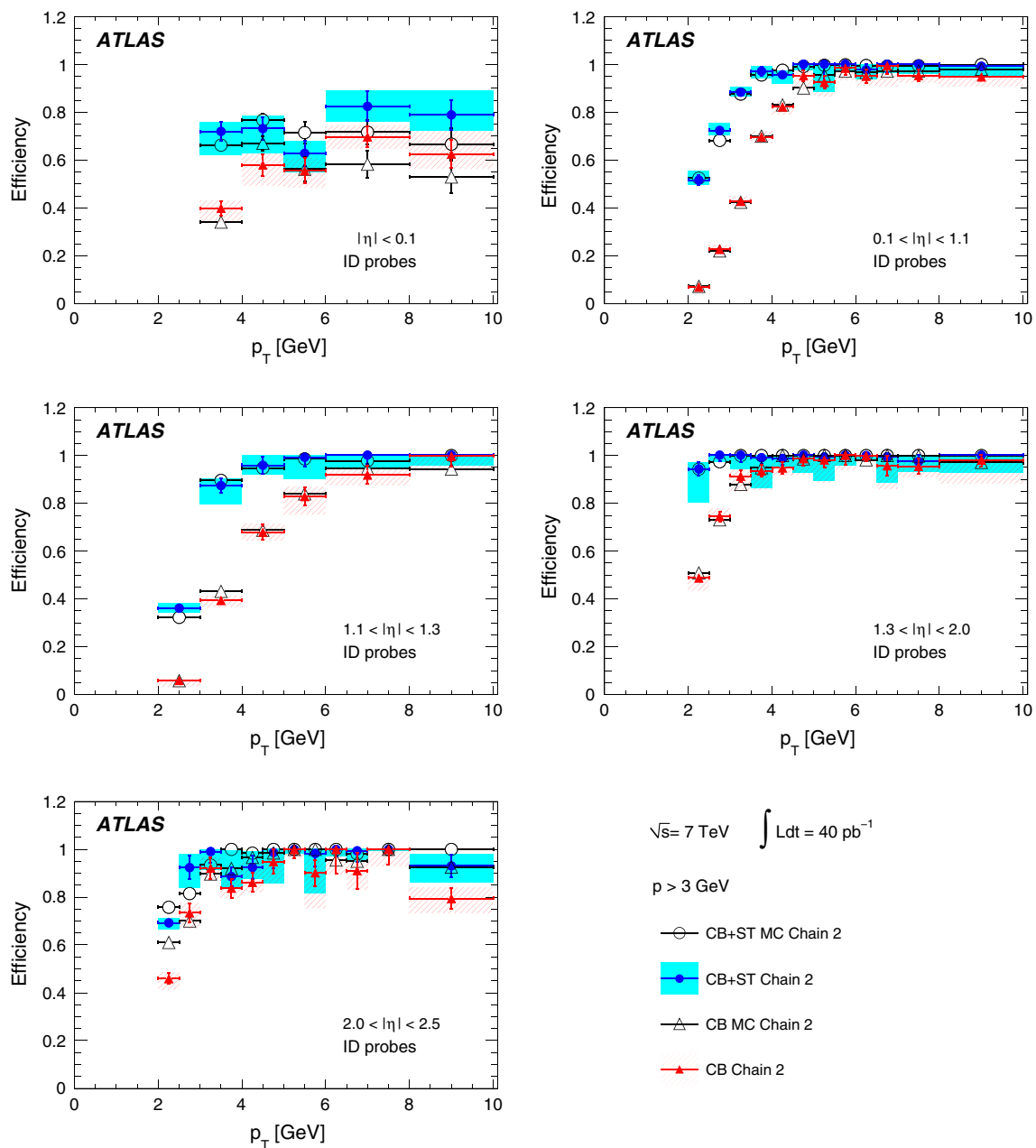


Fig. 7 Efficiency for chain 2 CB and CB+ST muons with momentum $p > 3$ GeV (from J/ψ decays), as a function of p_T , for five bins in $|\eta|$ as described in the legend, for data and MC events. The *error bars*

represent the statistical uncertainties while the band around the data points represents the statistical and systematic uncertainties added in quadrature

described in Sect. 6.2: at $\eta \sim 0$, ID tracks pass through an inactive region near the middle of the TRT barrel where straws produce no TRT hits; at $|\eta| \sim 1$, there is a small region in the transition between the barrel and the end-caps of the ID in which muons cross fewer than six SCT sensors [3]. The measured ID muon reconstruction and identification efficiencies agree with the Monte Carlo predictions within 1 %, and, for the most part, within the statistical uncertainties. The average ID efficiency is 0.991 ± 0.001 with the small loss being due to the hit requirements imposed on the ID muon tracks.

These results are independent of the choice of the algorithm chain for the stand-alone muon.

8.2 Reconstruction efficiencies for CB muons

Figure 9 shows the reconstruction efficiency (relative to the ID reconstruction efficiency) for CB muons as a function of the detector region, p_T and η , for data and simulation (with all considered backgrounds included). The scale factors are displayed in the lower panel of each plot.

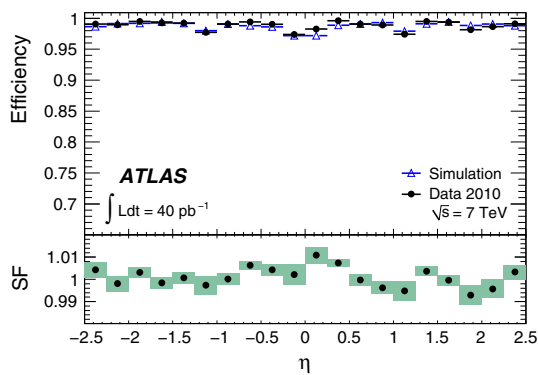


Fig. 8 Measured ID reconstruction and identification efficiency for muons (from Z decays), as a function of η , for data and Monte Carlo simulation. The scale factors (SF), defined as the ratio of the measured efficiency to the predicted efficiency, are shown in the lower panel of the plot. The uncertainties are statistical. The systematic uncertainty is discussed in Sect. 8.4

The mean value of the η -dependent scale factor is 0.989 ± 0.003 for chain 1 and 0.995 ± 0.002 for chain 2, where the errors are statistical. The 1 % deviation from unity in the overall efficiency scale factor of chain 1 is caused mainly by the data/MC disagreement in the transition region ($SF = 0.94$). The lower data efficiency in the transition region is attributed to the limited accuracy of the magnetic field map used in the reconstruction of the ATLAS data in this region, which leads to a small mis-measurement of the stand-alone muon momentum. This in turn may affect the combination of the MS and ID tracks, as their momenta may not be compatible. The transition region efficiency drop can be recovered, and the overall efficiency significantly increased by including ST muons, which are tagged by only one muon layer, as described in detail below.

The scale factors determined in bins of p_T agree, within 1.5 standard deviations, with the average scale factor for the algorithm in question.

The background-corrected efficiencies for CB muons are shown in Fig. 10. The background is estimated from Monte Carlo simulation, as described in Sect. 4, and is subtracted bin by bin. The average CB muon reconstruction efficiency is 0.928 ± 0.002 for chain 1 and 0.958 ± 0.001 for chain 2. The difference in efficiency between the two chains arises mainly from the more stringent requirements on the reconstructed MS tracks in chain 1. The ratios between data and MC efficiencies are almost identical to the SFs already discussed for Fig. 9 as a consequence of the smallness of the background correction.

8.3 Reconstruction efficiencies for CB+ST muons

The degree to which segment tagging can recover some muons, in particular in detector regions with only partial muon coverage, is studied by measuring the efficiency for

CB+ST muons. The same tag-and-probe method is used with the only difference being that the probe is matched to a CB or ST muon. Figure 11 shows the measured CB+ST muon efficiencies as functions of the detector region, p_T and η , in comparison with the corresponding CB muon efficiencies. The gains in efficiency when using ST muons in addition to the CB muons are presented in the lower panels of the plots. These are largest in the ATLAS Feet (13 %) and Transition (15 %) regions of the detector for chain 1. For chain 2 the largest gain is 3 % in the Feet and BEE regions. Figure 11 also shows that the two chains have similar overall efficiencies for CB+ST muons, 0.970 ± 0.001 for chain 1 and 0.980 ± 0.001 for chain 2.

In Fig. 12, the efficiency for CB+ST muons measured from data is compared to the Monte Carlo expectations and scale factors are presented. Remarkable agreement between the measured and predicted efficiencies is achieved. The scale factors for CB+ST muons are 1.003 ± 0.002 for chain 1 and 1.001 ± 0.002 for chain 2.

8.4 Systematic uncertainties

Uncertainties on the background contributions and on the resolution of the detector are considered as sources of systematic uncertainties. The uncertainty due to the description of the finite detector resolution is estimated by varying the selection cuts when determining the efficiencies from MC-simulated data. For CB muons, the cuts on the mass window around m_Z and the cut on the transverse momentum of the tag are each varied within $\pm 1\sigma$ of the $m_{\mu^+\mu^-}$ and p_T resolutions. Other cuts are varied by $\pm 10\%$. The resulting changes in the scale factors are quoted as systematic uncertainties. The normalisation of the background contribution inside the mass window is varied by $\pm 10\%$ and the resulting differences in the scale factors are considered as additional systematic uncertainties. The individual uncertainties are considered to be uncorrelated and are added in quadrature to estimate the total systematic uncertainty. For values which result from an upwards and downwards variation, the larger value is used. The largest contribution arises from the level of background contamination, which depends primarily on the choice of the mass window and the normalisation of the backgrounds. Another important contribution is due to the variation of the probe isolation criteria. The overall systematic uncertainty on the CB muon efficiency is 0.2 % for both chains.

As the same tag-and-probe selection is used for the measurements of the CB+ST muon efficiencies, the same systematic uncertainties are expected for the corresponding scale factors. The systematic uncertainties on the ID muon efficiency scale factors are substantially smaller, principally due to the high purity of the MS probe muons.

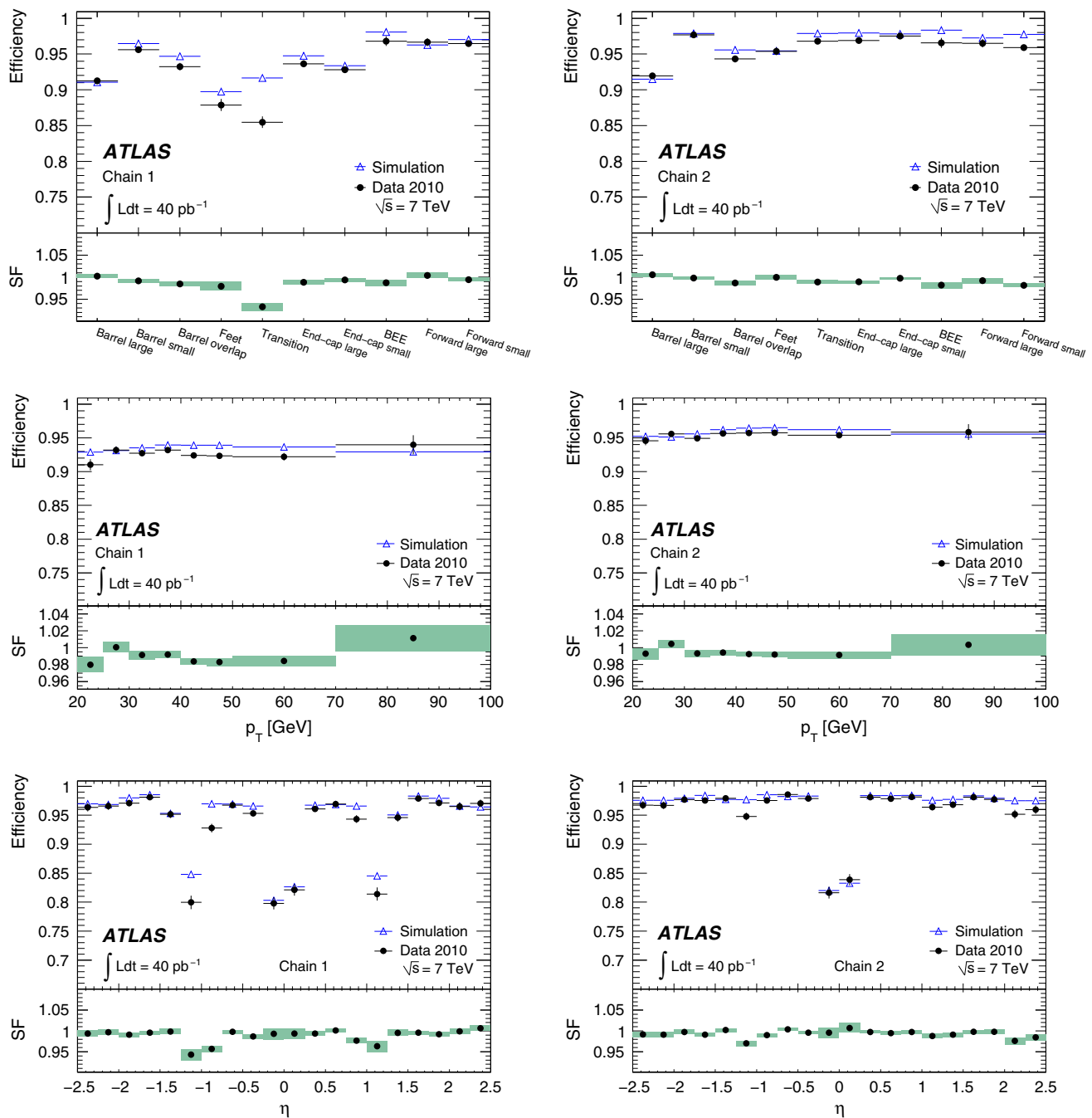


Fig. 9 Reconstruction efficiencies (relative to the ID efficiency) and scale factors for CB muons (from Z decays) as a function of detector region, muon p_T and muon η as indicated in the figure. The efficiencies for the two reconstruction chains, obtained from data (without

background correction) and Monte Carlo simulation (including backgrounds) are shown in the *upper part* of each figure. The corresponding scale factors are shown in the *lower panels*. The uncertainties are statistical only. The systematic uncertainties are discussed in Sect. 8.4

9 Measurement of the muon isolation efficiency

Muon isolation is a powerful tool for a high-purity event selection in many physics analyses, and is also used for rejecting muons from hadron decays in the Z decay tag-and-probe analyses presented here. It is therefore desirable to quantify the reliability of the Monte Carlo prediction of the isolation

efficiency (simulated using PYTHIA).⁴ This is studied using the same event selection that was used for the reconstruction efficiency measurements, up to and including the selection of the tag muon (the specific chain used is not shown, since the

⁴ The effects of pile-up are taken into account in the simulation as described in Sect. 5.

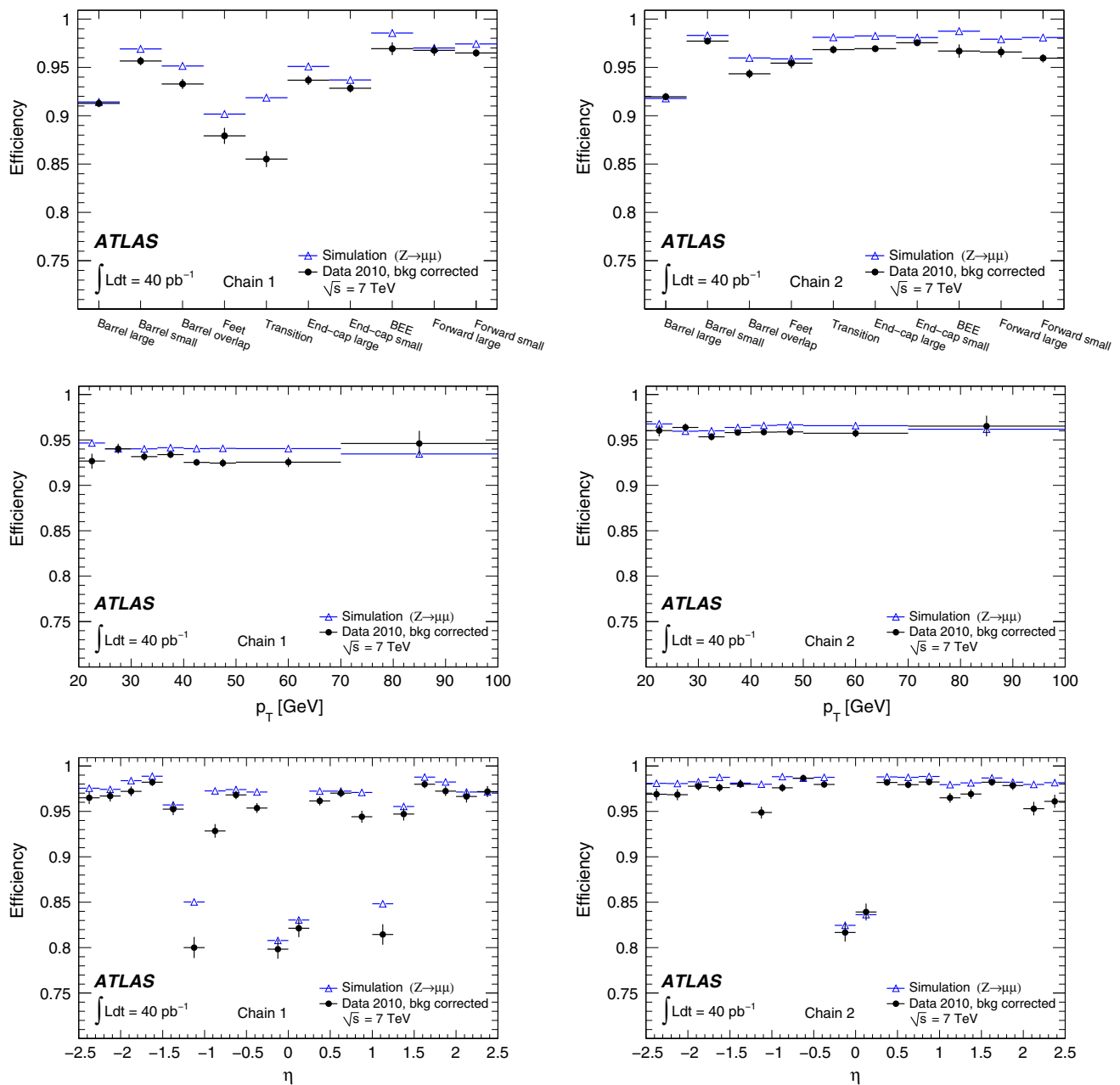


Fig. 10 Background-corrected efficiencies for CB muons (from Z decays) as a function of detector region, muon p_T and muon η as indicated in the figure, obtained from data and Monte Carlo simulation for

the two reconstruction chains. The uncertainties are statistical only. The systematic uncertainties are discussed in Sect. 8.4

performance is comparable for both). In this case, the probe muon is defined as a CB muon with $p_T > 20$ GeV that fulfils the ID hit requirements described in Sect. 6. We consider the following isolation variables:

- track isolation⁵—the summed p_T of tracks (excluding that of the muon) in cones of size $\Delta R = 0.3$ and $\Delta R = 0.4$ around the muon, divided by the p_T of the muon;

⁵ The track isolation, $T_{\text{isol}}^{\Delta R < 0.4}$, was defined in Sect. 6.3.

- calorimeter isolation—the transverse energy (E_T) deposition in the calorimeter in cones of size $\Delta R = 0.3$ and $\Delta R = 0.4$ around the muon (with the muon's energy loss subtracted [1, p. 194]), divided by the p_T of the muon.

The tag-and-probe selections, as described in Sect. 6, only make use of $T_{\text{isol}}^{\Delta R < 0.4} < 0.2$. However, the choice of isolation criteria depends on the analysis and this section presents the comparisons of data and Monte Carlo simulations for the following combinations of isolation variables:

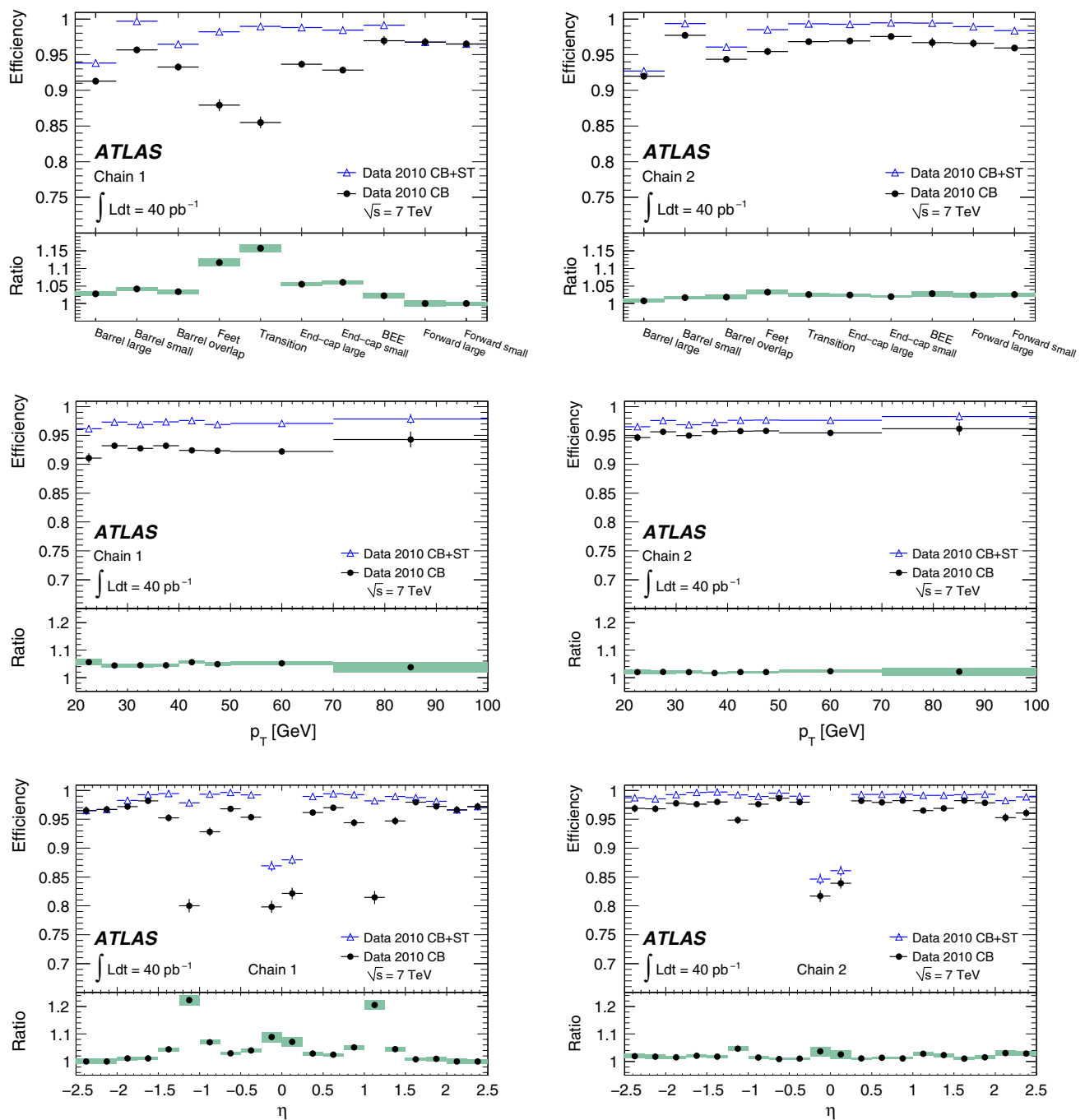


Fig. 11 Efficiencies for CB+ST muons (from Z decays) in comparison to those for CB muons only, for the two reconstruction chains and as a function of detector region, muon p_T and muon η as indicated in

- $T_{\text{isol}}^{\Delta R < 0.4} < 0.2$ and $E_T^{\Delta R < 0.4}/p_T(\mu) < 0.2$;
- $T_{\text{isol}}^{\Delta R < 0.4} < 0.1$ and $E_T^{\Delta R < 0.4}/p_T(\mu) < 0.1$;
- $T_{\text{isol}}^{\Delta R < 0.3} < 0.1$ and $E_T^{\Delta R < 0.3}/p_T(\mu) < 0.1$.

Figure 13 compares the distributions of the measured isolation variables for the probe muons with the Monte Carlo

the figure. The relative gain is shown in the *lower panel* of each figure. The uncertainties are statistical only. The systematic uncertainties are discussed in Sect. 8.4

predictions. The experimental and simulated distributions agree well, leading to a reliable prediction as a function of p_T , of the isolation efficiency, which is defined as the fraction of probe muons passing a given set of isolation cuts.

The measured isolation efficiencies and the corresponding Monte Carlo predictions are compared for chain 1 in Fig. 14; the results for chain 2 are consistent. Experimental and sim-

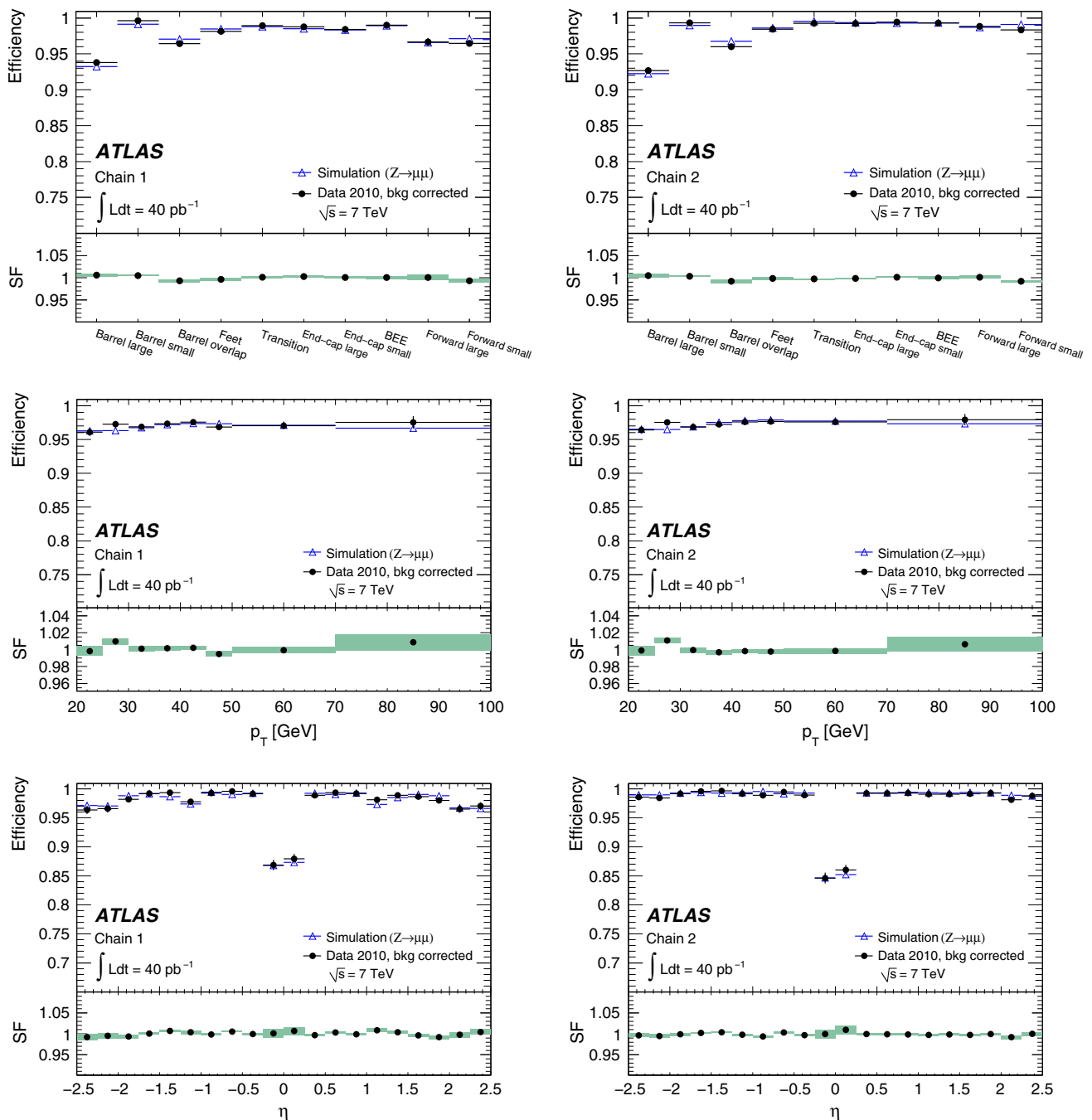


Fig. 12 Efficiencies for CB+ST muons (from Z decays), for the two reconstruction chains as a function of detector region, muon p_T and muon η as indicated in the figure. The efficiencies are obtained from data with background correction and from Monte Carlo simulation of

the signal. The corresponding scale factors are shown in the *lower panel* of each plot. The uncertainties are statistical only. The systematic uncertainty is discussed in Sect. 8.4

ulated data agree within uncertainties. The lower efficiencies at low p_T are mainly caused by the fact that the p_T and E_T sums, which depend only weakly on the muon p_T , are divided by this quantity, leading to isolation variables that rise with decreasing muon p_T . They are also partially due to the background, which is non-negligible in the low- p_T region.

10 Measurement of the muon momentum resolution

The muon momentum resolution of the ATLAS detector depends on the η , ϕ , and p_T of the muon [3]. In the ID, the p_T dependence of the relative momentum resolution can be parameterised to a good approximation [1] by the quadratic sum of two terms,

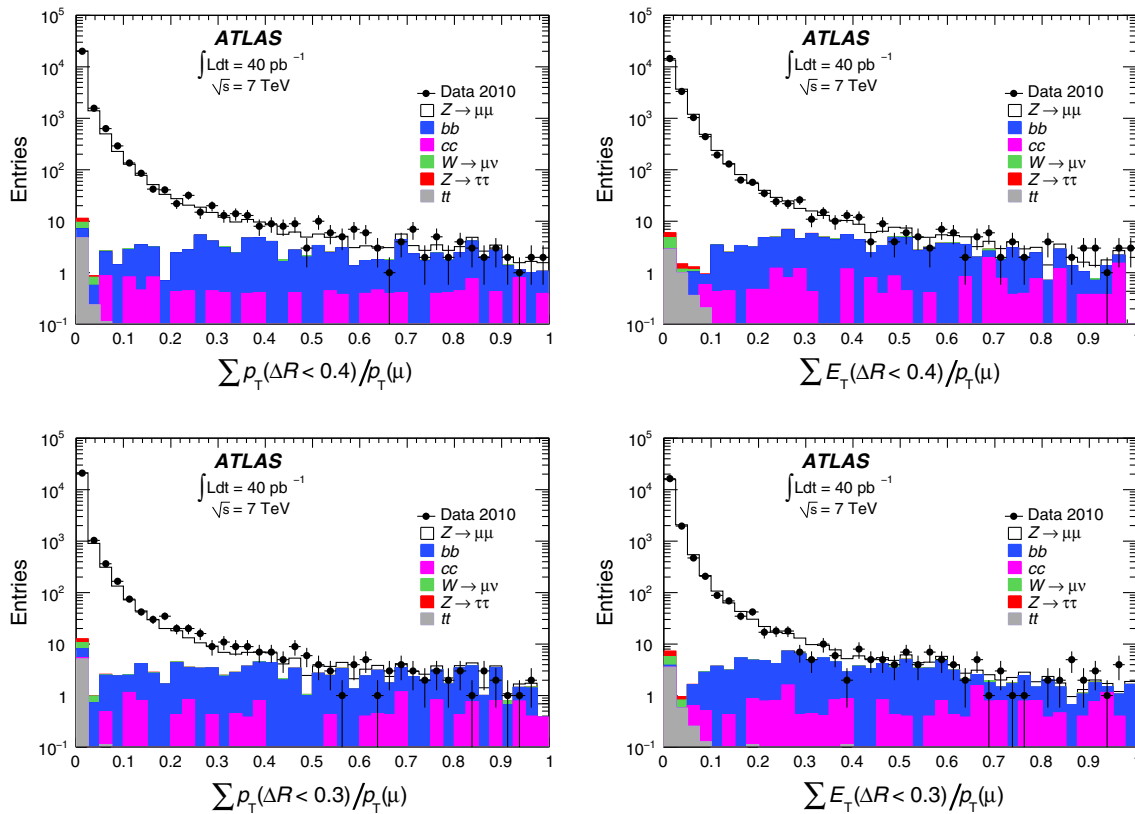


Fig. 13 Comparison of the measured track isolation (*left*) and calorimeter isolation (*right*) distributions of the probe muon (from Z decays) with the Monte Carlo predictions, for two different cone sizes using the isolation variables defined in the text. The *upper* and *lower*

plots correspond to $\Delta R = 0.4$ and $\Delta R = 0.3$, respectively. The simulation includes the effects of pile-up, as described in the text. The uncertainties are statistical

$$\begin{aligned} \frac{\sigma_{\text{ID}}(p_T)}{p_T} &= a_{\text{ID}}(\eta) \oplus b_{\text{ID}}(\eta) \cdot p_T \quad \text{for } 0 < |\eta| < 2.0; \\ \frac{\sigma_{\text{ID}}(p_T)}{p_T} &= a_{\text{ID}}(\eta) \oplus \frac{b_{\text{ID}}(\eta) \cdot p_T}{\tan^2(\theta)} \quad \text{for } 2.0 < |\eta| < 2.5. \end{aligned} \quad (3)$$

The first term describes the multiple scattering contribution, whilst the second term describes the intrinsic resolution caused by the imperfect knowledge of the magnetic field in the ID, by the spatial resolution of the detector components, and by any residual misalignment of the detector components. For $|\eta| > 2.0$, the best parameterisation of the second term is given by $b_{\text{ID}}(\eta) \cdot p_T / \tan^2(\theta)$. Measurements (from data) of the material distribution in the ID [11, 12] constrain $a_{\text{ID}}(\eta)$ to values which agree with the Monte Carlo prediction to within 5 % in the barrel and 10 % in the end-caps. The parameter $b_{\text{ID}}(\eta)$ is derived from the dimuon invariant mass resolution in $Z \rightarrow \mu^+ \mu^-$ decays.

The stand-alone muon resolution can be parameterised as follows:

$$\frac{\sigma_{\text{SA}}(p_T)}{p_T} = a_{\text{MS}}(\eta, \phi) \oplus b_{\text{MS}}(\eta, \phi) \cdot p_T \oplus \frac{c(\eta, \phi)}{p_T}, \quad (4)$$

where the first two terms parameterise the effect of the multiple scattering and the contribution of the intrinsic momentum resolution of the MS, respectively. The third term parameterises the effect of the fluctuations of the muon energy loss in the calorimeters, but this is small for the momentum range under consideration and is fixed to the value predicted by MC simulation.

A special data set, recorded in 2011, with no toroidal magnetic field in the MS, was used to simulate high-momentum (i.e. straight) tracks and estimate $b_{\text{MS}}(\eta, \phi)$, yielding $b_{\text{MS}}(\eta, \phi) \sim 0.2 \text{ TeV}^{-1}$ in the barrel and the MDT end-cap region (excluding the transition region) and $\sim 0.4 \text{ TeV}^{-1}$ in the CSC end-cap region, with a relative accuracy of about 10 % in both regions. This special data set made it possible to improve the alignment of the muon chambers, leading to $b_{\text{MS}}(\eta, \phi) \lesssim 0.2 \text{ TeV}^{-1}$ everywhere in the MS in 2011.

Figure 15 shows the dimuon invariant mass resolution of the ID in $Z \rightarrow \mu^+ \mu^-$ decays as a function of the pseudorapidity interval of the decay muons, where both are required to lie in the same interval. The mass resolution is the width of a Gaussian which, when convolved with the generator-

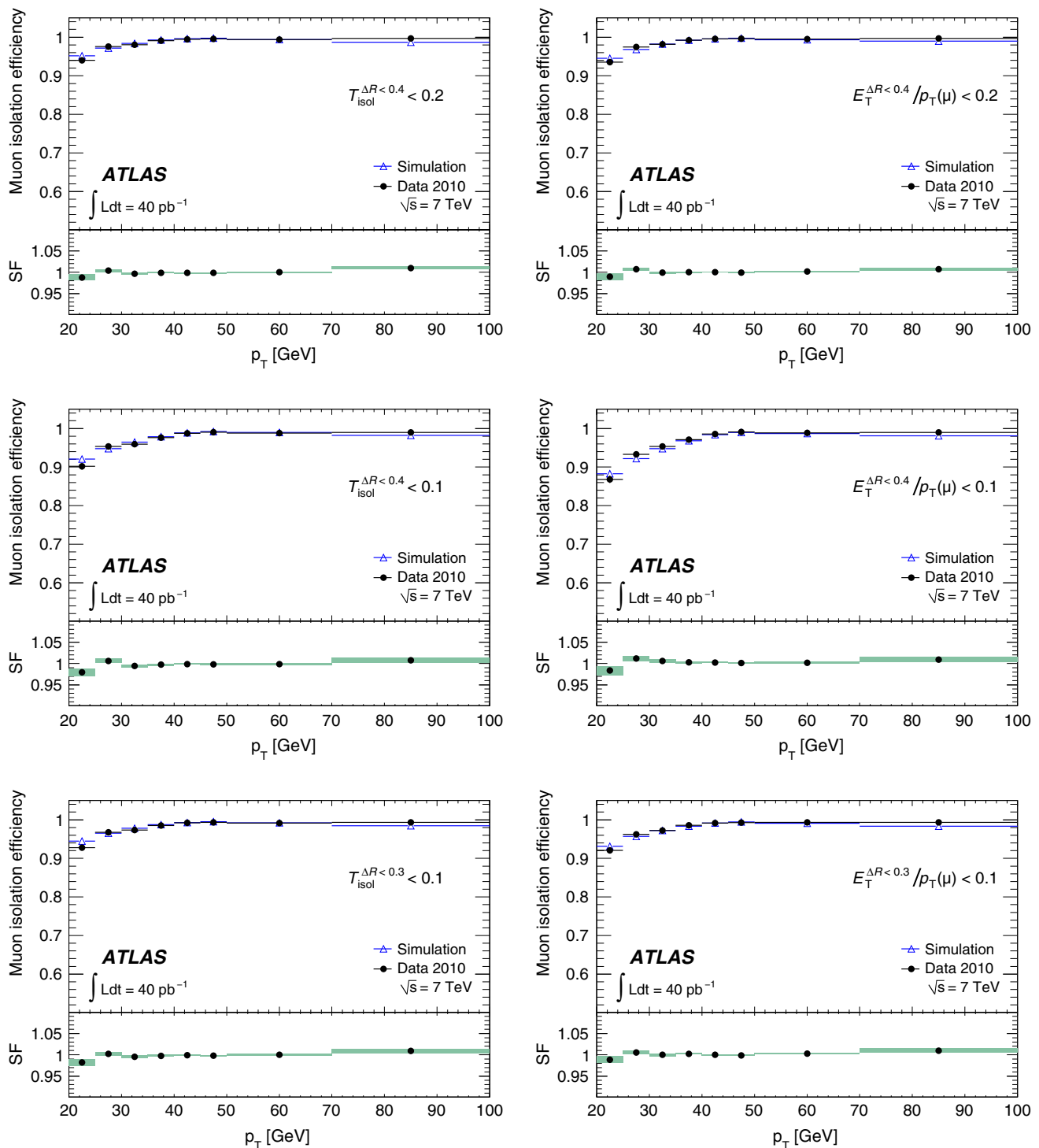


Fig. 14 Isolation efficiencies for muons from Z decays as a function of p_T , for track isolation (*left*) and calorimeter isolation (*right*) requirements with different isolation cone radii, ΔR , as described in the legend.

level dimuon invariant mass, reproduces the dimuon invariant mass distribution observed in data. The ID dimuon invariant mass resolution is best in the barrel, where it is about 2 GeV, is better than 3 GeV for $|\eta| < 2.0$ and degrades to

The Monte Carlo predictions include background processes as well as the Z signal. The uncertainties are statistical only

about 6 GeV for $2.0 < |\eta| < 2.5$. The degradation of the mass resolution with increasing $|\eta|$ is primarily caused by the fact that as $|\eta|$ increases there is a lower field integral per track. That the dimuon invariant mass resolution measured

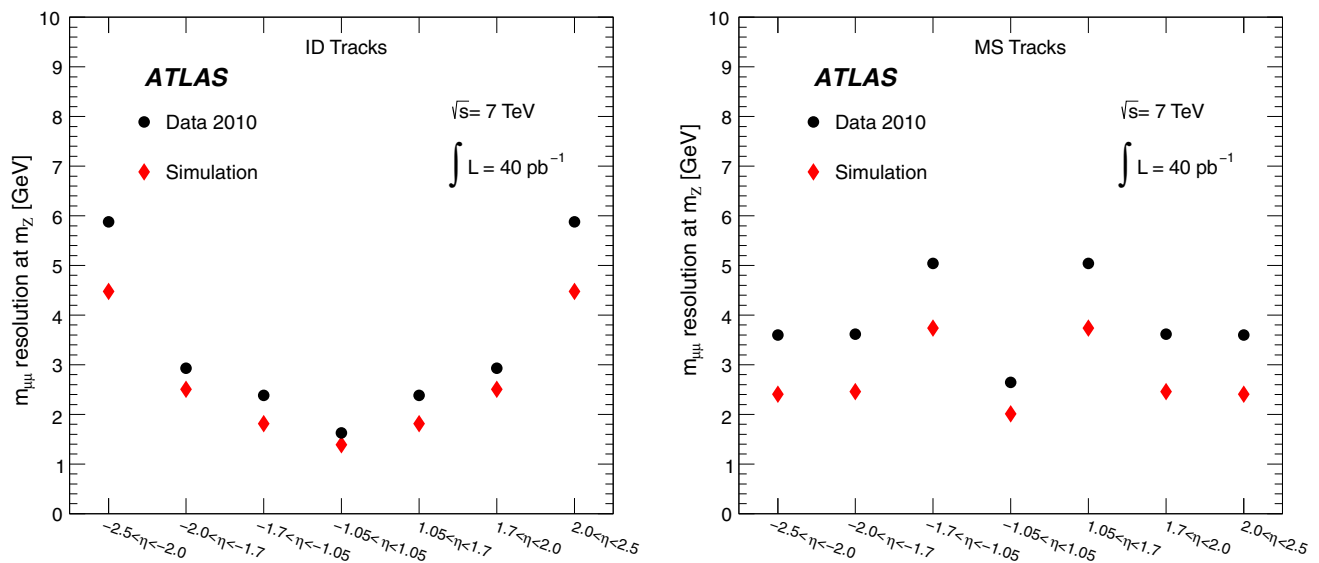


Fig. 15 The dimuon invariant mass ($m_{\mu\mu}$) resolutions in $Z \rightarrow \mu^+\mu^-$ decays in the data and in the MC as a function of η region with both decay muons in the same η region, for the ID (left) and MS (right). The simulation assumes a perfectly aligned ATLAS detector

in experimental data is worse than predicted (typically by about 30 %), is attributed to residual internal misalignments of the ID. The internal alignment of the ID was performed by minimising track residuals. This procedure has certain ambiguities which can be resolved by adding constraints such as the requirement that the energy/momentum ratio (E/p) distributions of electrons and positrons be the same. These constraints were only introduced into the alignment procedure for the 2011 data [13], in which a significantly improved dimuon invariant mass resolution is observed.

Due to the toroidal magnetic field, the relative momentum resolution of SA muons (and hence the corresponding dimuon invariant mass resolution—as shown in Fig. 15) is expected to be independent of the η of the decay muons, except in the magnet transition region ($1.05 < |\eta| < 1.7$) where the magnetic field in the MS is highly non-uniform, with a field integral approaching 0 in certain (η , ϕ) regions [3]. Furthermore, some chambers in the region $1.05 < |\eta| < 1.3$ were not yet installed,⁶ which means that the momentum measurement relies on only two layers of chambers, causing a significant degradation in the momentum resolution.

Figure 15 also shows that the MS dimuon invariant mass resolution is consistently worse in data than in simulation (typically between 30 and 50 % worse, depending on η region). Two sources for this effect were identified.

1. **Asymmetry of the magnetic field:** in the MC simulation, a perfectly aligned detector is assumed. In reality, the two end-cap toroid systems are not symmetric with

respect to the plane orthogonal to the major axis of the ID, and situated at the centre of the detector. This small asymmetry translates into an asymmetry of the magnetic field integrals, in particular in the transition regions. The reconstruction of the 2010 data with a corrected field map improves the dimuon invariant mass resolution in the transition region by 0.4 GeV.

2. **Residual misalignment of the muon chambers:** even after the MS alignment procedures are applied, residual misalignments remain, which limit the attainable momentum resolution. The analysis of a special set of 2011 data with no magnetic field in the MS was used to produce a Monte Carlo simulation of $Z \rightarrow \mu^+\mu^-$ events with the addition of a realistic residual misalignment of the MS. The results of this simulation are in agreement with the experimentally determined invariant mass resolutions.

The dimuon invariant mass resolution obtained with CB muons profits from the complementary momentum measurements of the ID and MS. As shown in Fig. 16, a dimuon invariant mass resolution between 1.4 and 2.5 GeV is achieved, with little dependence on η .

The measured dimuon invariant mass resolutions can be translated into muon momentum resolutions. This was done by smearing the generated muon momenta, according to Eqs. (3) and (4), by the amounts necessary to reproduce the measured dimuon invariant mass resolutions. Only the parameters $b_{\text{ID}}(\eta)$ and $a_{\text{MS}}(\eta, \phi)$ were varied during this procedure. The parameter $a_{\text{ID}}(\eta)$ was set to the Monte Carlo prediction and varied within its uncertainty (see above) to evaluate the impact on the result for $b_{\text{ID}}(\eta)$. The param-

⁶ This detector configuration was also used for the 2011 data taking.

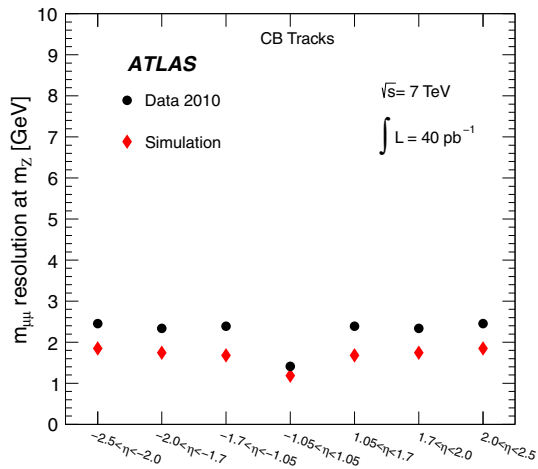


Fig. 16 Dimuon invariant mass ($m_{\mu\mu}$) resolution for combined muons in $Z \rightarrow \mu^+\mu^-$ decays in the data and in the MC as a function of η region with both decay muons in the same η region. The simulation assumes a perfectly aligned ATLAS detector

ter $b_{MS}(\eta, \phi)$ was set to the value derived from the special straight-track data set while $c(\eta, \phi)$ was set to its predicted value. In order to gain additional sensitivity to the momentum resolutions of the ID and MS, in addition to the dimuon mass spectrum of Z boson decays, the distributions of the differences between the ID and SA momenta of muons from $W \rightarrow \mu\nu_\mu$ decays were compared between the experimental and smeared MC data. The W boson selection and the MC samples for the analysis are the same as in Ref. [10]. As the use of W boson decays correlates the SA and ID resolutions, those are extracted simultaneously in the fit. The results are displayed for the different detector regions in Figs. 17 and 18, with the uncertainty of the curves computed from the uncertainties of the parameters in the resolution functions [Eqs. (3) and (4)]. Also shown is the expected resolution beyond the region in p_T probed by the Z -boson decays. As discussed earlier, the momentum resolution in experimental data is worse than in the Monte Carlo simulation, which is attributed, in part, to the residual misalignments of the ID and MS.

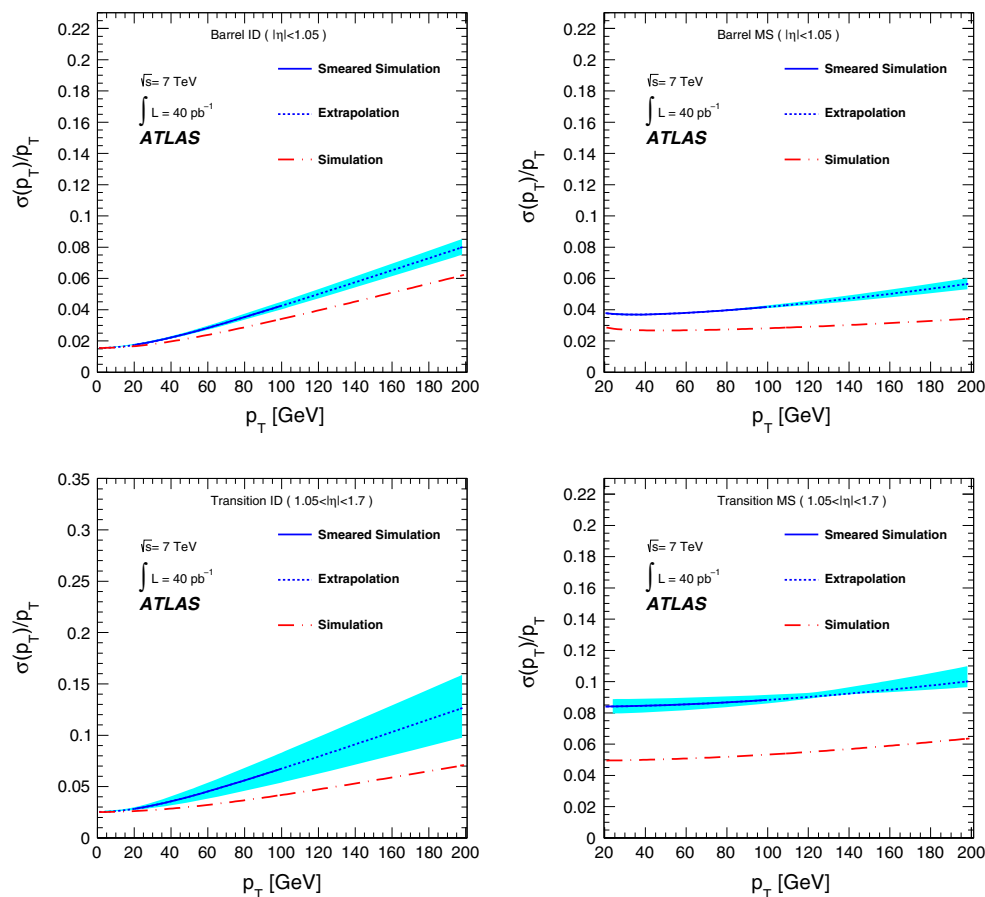


Fig. 17 Muon momentum resolution as a function of p_T for different barrel and transition $|\eta|$ regions as denoted in the legend. The dot-dash line is from a simulation which assumes perfect alignment of the ATLAS detector, whilst the solid/dotted line shows simulation smeared to reproduce the invariant mass resolution measured in data. The solid

section of the line shows the p_T range measured by Z and W decays, and the dotted section the 'extrapolation' regions. The shaded bands show the uncertainty of the curves, computed from the uncertainties of the parameters derived in the resolution functions shown in Eqs. (3) and (4)

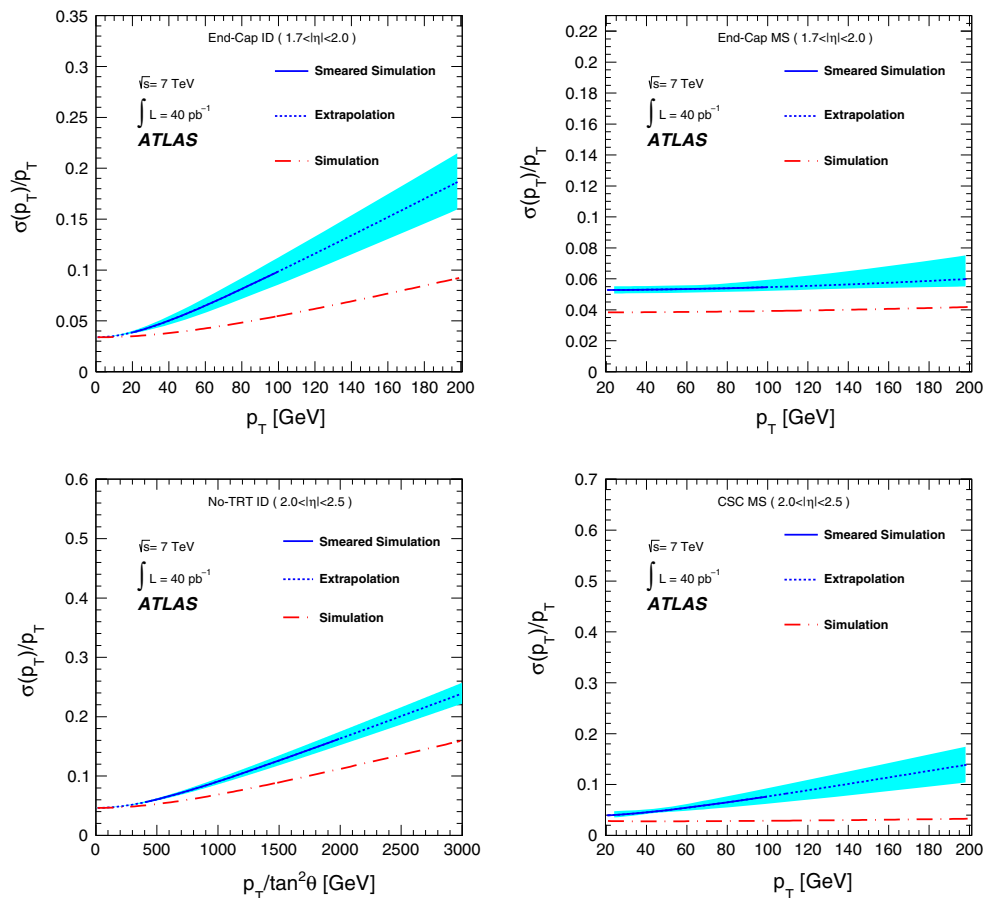


Fig. 18 Muon momentum resolutions as a function of p_T for different end-cap $|\eta|$ regions as denoted in the legend. For the ID region $|\eta| > 2.0$ (bottom-left), the best parameterisation of the resolution depends on $p_T/\tan^2(\theta)$ instead of p_T . The dot-dash line is simulation which assumes perfect alignment of the ATLAS detector, whilst the solid/dotted line shows simulation smeared to reproduce the invariant

mass resolution measured in data. The solid section of the line shows the p_T range measured by Z decays, and the dotted section the ‘extrapolation’ regions. The shaded bands show the uncertainty of the curves, which are computed from the uncertainties of the parameters in the resolution functions shown in Eqs. (3) and (4)

11 Summary

The ATLAS muon reconstruction efficiencies were studied with $J/\psi \rightarrow \mu^+\mu^-$ and $Z \rightarrow \mu^+\mu^-$ decays using 40 pb^{-1} of $\sqrt{s} = 7 \text{ TeV}$ pp LHC collision data recorded in 2010.

Samples of J/ψ and Z decays were used to access the transverse momentum regions of $p_T < 10 \text{ GeV}$ and $20 \text{ GeV} < p_T < 100 \text{ GeV}$ respectively. The muon reconstruction efficiency is found to be $>96\%$ and agrees with the MC prediction to better than 1% . The reconstructed quantities used to ensure muon isolation are shown to be well modelled in Monte Carlo simulations, and the corresponding muon isolation efficiencies are in excellent agreement with the MC predictions.

The muon momentum resolutions for $p_T > 20 \text{ GeV}$ are derived from the dimuon mass resolutions in $Z \rightarrow \mu^+\mu^-$ decays and from the differences between the ID and SA momenta of muons from $W \rightarrow \mu\nu_\mu$ decays. The resolutions

are worse in data than in simulation for the entire momentum range considered. For instance, at $p_T \approx 30 \text{ GeV}$ and $1.7 < |\eta| < 2.0$ the resolutions in experimental data are found to be about 30% worse than predicted by the simulation. These differences are attributed to mis-modelling of the magnetic field and residual misalignments of the inner detector and muon spectrometer. An improved magnetic field map was used from 2011 onwards, and there have since been several iterations of the alignment.

Acknowledgments We thank CERN for the very successful operation of the LHC, as well as the support staff from our institutions without whom ATLAS could not be operated efficiently. We acknowledge the support of ANPCyT, Argentina; YerPhI, Armenia; ARC, Australia; BMWF and FWF, Austria; ANAS, Azerbaijan; SSTC, Belarus; CNPq and FAPESP, Brazil; NSERC, NRC and CFI, Canada; CERN; CONICYT, Chile; CAS, MOST and NSFC, China; COLCIENCIAS, Colombia; MSMT CR, MPO CR and VSC CR, Czech Republic; DNRF DNSRC and Lundbeck Foundation, Denmark; EPLANET, ERC and NSRF, European Union; IN2P3-CNRS, CEA-DSM/IRFU, France;

GNSF, Georgia; BMBF, DFG, HGF, MPG and AvH Foundation, Germany; GSRT and NSRF, Greece; ISF, MINERVA, GIF, I-CORE and Benoziyo Center, Israel; INFN, Italy; MEXT and JSPS, Japan; CNRST, Morocco; FOM and NWO, Netherlands; BRF and RCN, Norway; MNiSW and NCN, Poland; GRICES and FCT, Portugal; MNE/IFA, Romania; MES of Russia and ROSATOM, Russian Federation; JINR; MSTD, Serbia; MSSR, Slovakia; ARRS and MIZŠ, Slovenia; DST/NRF, South Africa; MINECO, Spain; SRC and Wallenberg Foundation, Sweden; SER, SNSF and Cantons of Bern and Geneva, Switzerland; NSC, Taiwan; TAEK, Turkey; STFC, the Royal Society and Leverhulme Trust, United Kingdom; DOE and NSF, United States of America. The crucial computing support from all WLCG partners is acknowledged gratefully, in particular from CERN and the ATLAS Tier-1 facilities at TRIUMF (Canada), NDGF (Denmark, Norway, Sweden), CC-IN2P3 (France), KIT/GridKA (Germany), INFN-CNAF (Italy), NL-T1 (Netherlands), PIC (Spain), ASGC (Taiwan), RAL (UK) and BNL (USA) and in the Tier-2 facilities worldwide.

Open Access This article is distributed under the terms of the Creative Commons Attribution License which permits any use, distribution, and reproduction in any medium, provided the original author(s) and the source are credited.

Funded by SCOAP³ / License Version CC BY 4.0.

References

1. ATLAS Collaboration, Expected Performance of the ATLAS Experiment - Detector, Trigger and Physics. [arXiv:0901.0512](#) [hep-ex]
2. ATLAS Collaboration, Improved luminosity determination in pp collisions at $\sqrt{s} = 7$ TeV using the ATLAS detector at the LHC. *Eur. Phys. J. C* **73** 2518 (2013). [arXiv:1302.4393](#) [hep-ex]
3. ATLAS Collaboration, The ATLAS Experiment at the CERN Large Hadron Collider. *JINST* **3** S08003 (2008)
4. ATLAS Collaboration, The Optical Alignment System of the ATLAS Muon Spectrometer Endcaps. *JINST* **3** P11005 (2008)
5. ATLAS Collaboration, Measurement of the differential cross-sections of inclusive, prompt and non-prompt J/ψ production in p-p collisions at $\sqrt{s} = 7$ TeV. *Nucl. Phys. B* **850** 437 (2011). [arXiv:1104.3038](#) [hep-ex]
6. T. Sjostrand, S. Mrenna, P.Z. Skands, PYTHIA 6.4 Physics and Manual. *JHEP* **05**, 026 (2006)
7. ATLAS Collaboration, The ATLAS Simulation Infrastructure, *Eur. Phys. J. C* **70**, 823–874 (2010). [arXiv:1005.4568](#) [hep-ex]
8. Geant4 Collaboration, S. Agostinelli et al., Geant4: A simulation toolkit. *Nucl. Instrum. Meth. A* **506**, 250 (2003)
9. J. Allison et al., Geant4 developments and applications. *IEEE Trans. Nucl. Sci.* **53**(1), 270 (2006)
10. ATLAS Collaboration, Measurement of the inclusive W^\pm and Z/γ^* cross sections in the e and μ decay channels in pp collisions at $\sqrt{s} = 7$ TeV with the ATLAS detector. *Phys. Rev. D* **85** 072004 (2012). [arXiv:1109.5141](#) [hep-ex]
11. ATLAS Collaboration, Study of the Material Budget in the ATLAS Inner Detector with K_S^0 decays in collision data at $\sqrt{s} = 900$ GeV. ATLAS-CONF-2010-019 (2010). <http://cdsweb.cern.ch/record/1277651>
12. ATLAS Collaboration, Mapping the material in the ATLAS Inner Detector using secondary hadronic interactions in 7 TeV collisions. ATLAS-CONF-2010-058 (2010). <http://cdsweb.cern.ch/record/1281331>
13. ATLAS Collaboration, Study of alignment-related systematic effects on the ATLAS Inner Detector tracking, ATLAS-CONF-2012-141 (2012). <https://cds.cern.ch/record/1483518>

The ATLAS Collaboration

G. Aad⁴⁸, T. Abajyan²¹, B. Abbott¹¹², J. Abdallah¹², S. Abdel Khalek¹¹⁶, A. A. Abdelalim⁴⁹, O. Abidinov¹¹, R. Aben¹⁰⁶, B. Abi¹¹³, M. Abolins⁸⁹, O. S. AbouZeid¹⁵⁹, H. Abramowicz¹⁵⁴, H. Abreu¹³⁷, Y. Abulaiti^{147a,147b}, B. S. Acharya^{165a,165b,a}, L. Adamczyk^{38a}, D. L. Adams²⁵, T. N. Addy⁵⁶, J. Adelman¹⁷⁷, S. Adomeit⁹⁹, T. Adye¹³⁰, S. Aefsky²³, T. Agatonovic-Jovin^{13b}, J. A. Aguilar-Saavedra^{125b,b}, M. Agostoni¹⁷, S. P. Ahlen²², F. Ahles⁴⁸, A. Ahmad¹⁴⁹, M. Ahsan⁴¹, G. Aielli^{134a,134b}, T. P. A. Åkesson⁸⁰, G. Akimoto¹⁵⁶, A. V. Akimov⁹⁵, M. A. Alam⁷⁶, J. Albert¹⁷⁰, S. Albrand⁵⁵, M. J. Alconada Verzini⁷⁰, M. Aleksa³⁰, I. N. Aleksandrov⁶⁴, F. Alessandria^{90a}, C. Alexa^{26a}, G. Alexander¹⁵⁴, G. Alexandre⁴⁹, T. Alexopoulos¹⁰, M. Alhroob^{165a,165c}, M. Aliev¹⁶, G. Alimonti^{90a}, J. Alison³¹, B. M. M. Allbrooke¹⁸, L. J. Allison⁷¹, P. P. Allport⁷³, S. E. Allwood-Spiers⁵³, J. Almond⁸³, A. Aloisio^{103a,103b}, R. Alon¹⁷³, A. Alonso³⁶, F. Alonso⁷⁰, A. Altheimer³⁵, B. Alvarez Gonzalez⁸⁹, M. G. Alviggi^{103a,103b}, K. Amako⁶⁵, Y. Amaral Coutinho^{24a}, C. Amelung²³, V. V. Ammosov^{129,*}, S. P. Amor Dos Santos^{125a}, A. Amorim^{125a,c}, S. Amoroso⁴⁸, N. Amram¹⁵⁴, C. Anastopoulos³⁰, L. S. Ancu¹⁷, N. Andari³⁰, T. Andeen³⁵, C. F. Anders^{58b}, G. Anders^{58a}, K. J. Anderson³¹, A. Andreazza^{90a,90b}, V. Andrei^{58a}, X. S. Anduaga⁷⁰, S. Angelidakis⁹, P. Anger⁴⁴, A. Angerami³⁵, F. Anghinolfi³⁰, A. V. Anisenkov¹⁰⁸, N. Anjos^{125a}, A. Annovi⁴⁷, A. Antonaki⁹, M. Antonelli⁴⁷, A. Antonov⁹⁷, J. Antos^{145b}, F. Anulli^{133a}, M. Aoki¹⁰², L. Aperio Bella¹⁸, R. Apolle^{119,d}, G. Arabidze⁸⁹, I. Aracena¹⁴⁴, Y. Arai⁶⁵, A. T. H. Arce⁴⁵, S. Arfaoui¹⁴⁹, J-F. Arguin⁹⁴, S. Argyropoulos⁴², E. Arik^{19a,*}, M. Arik^{19a}, A. J. Armbruster⁸⁸, O. Arnaez⁸², V. Arnal⁸¹, A. Artamonov⁹⁶, G. Artoni^{133a,133b}, D. Arutinov²¹, S. Asai¹⁵⁶, N. Asbah⁹⁴, S. Ask²⁸, B. Åsman^{147a,147b}, L. Asquith⁶, K. Assamagan²⁵, R. Astalos^{145a}, A. Astbury¹⁷⁰, M. Atkinson¹⁶⁶, B. Auerbach⁶, E. Auge¹¹⁶, K. Augsten¹²⁷, M. Aurousseau^{146b}, G. Avolio³⁰, D. Axen¹⁶⁹, G. Azuelos^{94,e}, Y. Azuma¹⁵⁶, M. A. Baak³⁰, G. Baccaglioni^{90a}, C. Bacci^{135a,135b}, A. M. Bach¹⁵, H. Bachacou¹³⁷, K. Bachas¹⁵⁵, M. Backes⁴⁹, M. Backhaus²¹, J. Backus Mayes¹⁴⁴, E. Badescu^{26a}, P. Bagiacchi^{133a,133b}, P. Bagnaia^{133a,133b}, Y. Bai^{33a}, D. C. Bailey¹⁵⁹, T. Bain³⁵, J. T. Baines¹³⁰, O. K. Baker¹⁷⁷, S. Baker⁷⁷, P. Balek¹²⁸, F. Balli¹³⁷, E. Banas³⁹, P. Banerjee⁹⁴, Sw. Banerjee¹⁷⁴, D. Banfi³⁰, A. Bangert¹⁵¹, V. Bansal¹⁷⁰, H. S. Bansil¹⁸, L. Barak¹⁷³, S. P. Baranov⁹⁵, T. Barber⁴⁸, E. L. Barberio⁸⁷, D. Barberis^{50a,50b}, M. Barbero⁸⁴, D. Y. Bardin⁶⁴, T. Barillari¹⁰⁰, M. Barisonzi¹⁷⁶,

T. Barklow¹⁴⁴, N. Barlow²⁸, B. M. Barnett¹³⁰, R. M. Barnett¹⁵, A. Baroncelli^{135a}, G. Barone⁴⁹, A. J. Barr¹¹⁹, F. Barreiro⁸¹, J. Barreiro Guimarães da Costa⁵⁷, R. Bartoldus¹⁴⁴, A. E. Barton⁷¹, V. Bartsch¹⁵⁰, A. Basye¹⁶⁶, R. L. Bates⁵³, L. Batkova^{145a}, J. R. Batley²⁸, A. Battaglia¹⁷, M. Battistin³⁰, F. Bauer¹³⁷, H. S. Bawa^{144,f}, S. Beale⁹⁹, T. Beau⁷⁹, P. H. Beauchemin¹⁶², R. Beccherle^{50a}, P. Bechtel²¹, H. P. Beck¹⁷, K. Becker¹⁷⁶, S. Becker⁹⁹, M. Beckingham¹³⁹, K. H. Becks¹⁷⁶, A. J. Beddall^{19c}, A. Beddall^{19c}, S. Bedikian¹⁷⁷, V. A. Bednyakov⁶⁴, C. P. Bee⁸⁴, L. J. Beemster¹⁰⁶, T. A. Beermann¹⁷⁶, M. Begel²⁵, C. Belanger-Champagne⁸⁶, P. J. Bell⁴⁹, W. H. Bell⁴⁹, G. Bella¹⁵⁴, L. Bellagamba^{20a}, A. Bellerive²⁹, M. Bellomo³⁰, A. Belloni⁵⁷, O. L. Beloborodova^{108,g}, K. Belotskiy⁹⁷, O. Beltramello³⁰, O. Benary¹⁵⁴, D. Benchechroun^{136a}, K. Bendtz^{147a,147b}, N. Benekos¹⁶⁶, Y. Benhammou¹⁵⁴, E. Benhar Nocchioli⁴⁹, J. A. Benitez Garcia^{160b}, D. P. Benjamin⁴⁵, J. R. Bensinger²³, K. Benslama¹³¹, S. Bentvelsen¹⁰⁶, D. Berge³⁰, E. Bergeas Kuutmann¹⁶, N. Berger⁵, F. Berghaus¹⁷⁰, E. Berglund¹⁰⁶, J. Beringer¹⁵, P. Bernat⁷⁷, R. Bernhard⁴⁸, C. Bernius⁷⁸, F. U. Bernlochner¹⁷⁰, T. Berry⁷⁶, C. Bertella⁸⁴, F. Bertolucci^{123a,123b}, M. I. Besana^{90a,90b}, G. J. Besjes¹⁰⁵, N. Besson¹³⁷, S. Bethke¹⁰⁰, W. Bhimji⁴⁶, R. M. Bianchi¹²⁴, L. Bianchini²³, M. Bianco^{72a,72b}, O. Biebel⁹⁹, S. P. Bieniek⁷⁷, K. Bierwagen⁵⁴, J. Biesiada¹⁵, M. Biglietti^{135a}, H. Bilokon⁴⁷, M. Bindi^{20a,20b}, S. Binet¹¹⁶, A. Bingul^{19c}, C. Bini^{133a,133b}, B. Bittner¹⁰⁰, C. W. Black¹⁵¹, J. E. Black¹⁴⁴, K. M. Black²², D. Blackburn¹³⁹, R. E. Blair⁶, J.-B. Blanchard¹³⁷, T. Blazek^{145a}, I. Bloch⁴², C. Blocker²³, J. Blocki³⁹, W. Blum⁸², U. Blumenschein⁵⁴, G. J. Bobbink¹⁰⁶, V. S. Bobrovnikov¹⁰⁸, S. S. Bocchetta⁸⁰, A. Bocci⁴⁵, C. R. Boddy¹¹⁹, M. Boehler⁴⁸, J. Boek¹⁷⁶, T. T. Boek¹⁷⁶, N. Boelaert³⁶, J. A. Bogaerts³⁰, A. G. Bogdanchikov¹⁰⁸, A. Bogouch^{91,*}, C. Bohm^{147a}, J. Bohm¹²⁶, V. Boisvert⁷⁶, T. Bold^{38a}, V. Boldea^{26a}, N. M. Bolnet¹³⁷, M. Bomben⁷⁹, M. Bona⁷⁵, M. Boonekamp¹³⁷, S. Bordon⁷⁹, C. Borer¹⁷, A. Borisov¹²⁹, G. Borissov⁷¹, M. Borri⁸³, S. Borroni⁴², J. Bortfeldt⁹⁹, V. Bortolotto^{135a,135b}, K. Bos¹⁰⁶, D. Boscherini^{20a}, M. Bosman¹², H. Boterenbrood¹⁰⁶, J. Bouchami⁹⁴, J. Boudreau¹²⁴, E. V. Bouhova-Thacker⁷¹, D. Boumediene³⁴, C. Bourdarios¹¹⁶, N. Bousson⁸⁴, S. Boutouil^{136d}, A. Boveia³¹, J. Boyd³⁰, I. R. Boyko⁶⁴, I. Bozovic-Jelisavcic^{13b}, J. Bracinik¹⁸, P. Branchini^{135a}, A. Brandt⁸, G. Brandt¹⁵, O. Brandt⁵⁴, U. Bratzler¹⁵⁷, B. Brau⁸⁵, J. E. Brau¹¹⁵, H. M. Braun^{176,*}, S. F. Brazzale^{165a,165c}, B. Brelief¹⁵⁹, J. Bremer³⁰, K. Brendlinger¹²¹, R. Brenner¹⁶⁷, S. Bressler¹⁷³, T. M. Bristow⁴⁶, D. Britton⁵³, F. M. Brochu²⁸, I. Brock²¹, R. Brock⁸⁹, F. Broggi^{90a}, C. Bromberg⁸⁹, J. Bronner¹⁰⁰, G. Brooijmans³⁵, T. Brooks⁷⁶, W. K. Brooks^{32b}, G. Brown⁸³, P. A. Bruckman de Renstrom³⁹, D. Bruncko^{145b}, R. Brunelieri⁴⁸, S. Brunet⁶⁰, A. Bruni^{20a}, G. Bruni^{20a}, M. Bruschi^{20a}, L. Bryngemark⁸⁰, T. Buanes¹⁴, Q. Buat⁵⁵, F. Bucci⁴⁹, J. Buchanan¹¹⁹, P. Buchholz¹⁴², R. M. Buckingham¹¹⁹, A. G. Buckley⁴⁶, S. I. Buda^{26a}, I. A. Budagov⁶⁴, B. Budick¹⁰⁹, L. Bugge¹¹⁸, O. Bulekov⁹⁷, A. C. Bundock⁷³, M. Bunse⁴³, T. Buran^{118,*}, H. Burckhart³⁰, S. Burdin⁷³, T. Burgess¹⁴, S. Burke¹³⁰, E. Busato³⁴, V. Büscher⁸², P. Bussey⁵³, C. P. Buszello¹⁶⁷, B. Butler⁵⁷, J. M. Butler²², C. M. Buttar⁵³, J. M. Butterworth⁷⁷, W. Buttinger²⁸, M. Byszewski¹⁰, S. Cabrera Urbán¹⁶⁸, D. Caforio^{20a,20b}, O. Cakir^{4a}, P. Calafiura¹⁵, G. Calderini⁷⁹, P. Calfayan⁹⁹, R. Calkins¹⁰⁷, L. P. Caloba^{24a}, R. Caloi^{133a,133b}, D. Calvel³⁴, S. Calvel³⁴, R. Camacho Toro⁴⁹, P. Camarri^{134a,134b}, D. Cameron¹¹⁸, L. M. Caminada¹⁵, R. Caminal Armadans¹², S. Campana³⁰, M. Campanelli⁷⁷, V. Canale^{103a,103b}, F. Canelli³¹, A. Canepa^{160a}, J. Cantero⁸¹, R. Cantrill⁷⁶, T. Cao⁴⁰, M. D. M. Capeans Garrido³⁰, I. Caprini^{26a}, M. Caprini^{26a}, D. Capriotti¹⁰⁰, M. Capua^{37a,37b}, R. Caputo⁸², R. Cardarelli^{134a}, T. Carli³⁰, G. Carlino^{103a}, L. Carminati^{90a,90b}, S. Caron¹⁰⁵, E. Carquin^{32b}, G. D. Carrillo-Montoya^{146c}, A. A. Carter⁷⁵, J. R. Carter²⁸, J. Carvalho^{125a,h}, D. Casadei¹⁰⁹, M. P. Casado¹², M. Cascella^{123a,123b}, C. Caso^{50a,50b,*}, E. Castaneda-Miranda¹⁷⁴, A. Castelli¹⁰⁶, V. Castillo Gimenez¹⁶⁸, N. F. Castro^{125a}, G. Cataldi^{72a}, P. Catastini⁵⁷, A. Catinaccio³⁰, J. R. Catmore³⁰, A. Cattai³⁰, G. Cattani^{134a,134b}, S. Caughron⁸⁹, V. Cavaliere¹⁶⁶, D. Cavalli^{90a}, M. Cavalli-Sforza¹², V. Cavasinni^{123a,123b}, F. Ceradini^{135a,135b}, B. Cerio⁴⁵, A. S. Cerqueira^{24b}, A. Cerri¹⁵, L. Cerrito⁷⁵, F. Cerutti¹⁵, A. Cervelli¹⁷, S. A. Cetin^{19b}, A. Chafaq^{136a}, D. Chakraborty¹⁰⁷, I. Chalupkova¹²⁸, K. Chan³, P. Chang¹⁶⁶, B. Chapleau⁸⁶, J. D. Chapman²⁸, J. W. Chapman⁸⁸, D. G. Charlton¹⁸, V. Chavda⁸³, C. A. Chavez Barajas³⁰, S. Cheatham⁸⁶, S. Chekanov⁶, S. V. Chekulaev^{160a}, G. A. Chelkov⁶⁴, M. A. Chelstowska¹⁰⁵, C. Chen⁶³, H. Chen²⁵, S. Chen^{33c}, X. Chen¹⁷⁴, Y. Chen³⁵, Y. Cheng³¹, A. Cheplakov⁶⁴, R. Cherkaoui El Moursli^{136e}, V. Chernyatin²⁵, E. Cheu⁷, S. L. Cheung¹⁵⁹, L. Chevalier¹³⁷, V. Chiarella⁴⁷, G. Chiefari^{103a,103b}, J. T. Childers³⁰, A. Chilingarov⁷¹, G. Chiodini^{72a}, A. S. Chisholm¹⁸, R. T. Chislett⁷⁷, A. Chitan^{26a}, M. V. Chizhov⁶⁴, G. Choudalakis³¹, S. Chouridou⁹, B. K. B. Chow⁹⁹, I. A. Christidi⁷⁷, A. Christov⁴⁸, D. Chromek-Burckhart³⁰, M. L. Chu¹⁵², J. Chudoba¹²⁶, G. Ciapetti^{133a,133b}, A. K. Ciftci^{4a}, R. Ciftci^{4a}, D. Cinca⁶², V. Cindro⁷⁴, A. Ciocio¹⁵, M. Cirilli⁸⁸, P. Cirkovic^{13b}, Z. H. Citron¹⁷³, M. Citterio^{90a}, M. Ciubancan^{26a}, A. Clark⁴⁹, P. J. Clark⁴⁶, R. N. Clarke¹⁵, J. C. Clemens⁸⁴, B. Clement⁵⁵, C. Clement^{147a,147b}, Y. Coadou⁸⁴, M. Cobal^{165a,165c}, A. Coccaro¹³⁹, J. Cochran⁶³, S. Coelli^{90a}, L. Coffey²³, J. G. Cogan¹⁴⁴, J. Coggeshall¹⁶⁶, J. Colas⁵, S. Cole¹⁰⁷, A. P. Colijn¹⁰⁶, N. J. Collins¹⁸, C. Collins-Tooth⁵³, J. Collot⁵⁵, T. Colombo^{120a,120b}, G. Colon⁸⁵, G. Compostella¹⁰⁰, P. Conde Muiño^{125a}, E. Coniavitis¹⁶⁷, M. C. Conidi¹², S. M. Consonni^{90a,90b}, V. Consorti⁴⁸, S. Constantinescu^{26a}, C. Conta^{120a,120b}, G. Conti⁵⁷, F. Conventi^{103a,i}, M. Cooke¹⁵, B. D. Cooper⁷⁷, A. M. Cooper-Sarkar¹¹⁹, N. J. Cooper-Smith⁷⁶, K. Copic¹⁵, T. Cornelissen¹⁷⁶, M. Corradi^{20a}, F. Corriveau^{86j}, A. Corso-Radu¹⁶⁴, A. Cortes-Gonzalez¹⁶⁶, G. Cortiana¹⁰⁰, G. Costa^{90a}, M. J. Costa¹⁶⁸, D. Costanzo¹⁴⁰, D. Côté³⁰, G. Cottin^{32a}, L. Courneyea¹⁷⁰, G. Cowan⁷⁶, B. E. Cox⁸³, K. Cranmer¹⁰⁹, S. Crépe-Renaudin⁵⁵, F. Crescioli⁷⁹, M. Cristinziani²¹, G. Crosetti^{37a,37b}, C.-M. Cuciuc^{26a}, C. Cuenca Almenar¹⁷⁷, T. Cuhadar Donszelmann¹⁴⁰, J. Cummings¹⁷⁷, M. Curatolo⁴⁷, C. J. Curtis¹⁸, C. Cuthbert¹⁵¹, H. Czirr¹⁴², P. Czodrowski⁴⁴, Z. Czyczula¹⁷⁷, S. D'Auria⁵³, M.

- D'Onofrio⁷³, A. D'Orazio^{133a,133b}, M. J. Da Cunha Sargedas De Sousa^{125a}, C. Da Via⁸³, W. Dabrowski^{38a}, A. Dafinca¹¹⁹, T. Dai⁸⁸, F. Dallaire⁹⁴, C. Dallapiccola⁸⁵, M. Dam³⁶, D. S. Damiani¹³⁸, A. C. Daniells¹⁸, H. O. Danielsson³⁰, V. Dao¹⁰⁵, G. Darbo^{50a}, G. L. Darlea^{26b}, S. Darmora⁸, J. A. Dassoulas⁴², W. Davey²¹, T. Davidek¹²⁸, N. Davidson⁸⁷, E. Davies^{119,d}, M. Davies⁹⁴, O. Davignon⁷⁹, A. R. Davison⁷⁷, Y. Davygora^{58a}, E. Dawe¹⁴³, I. Dawson¹⁴⁰, R. K. Daya-Ishmukhametova²³, K. De⁸, R. de Asmundis^{103a}, S. De Castro^{20a,20b}, S. De Cecco⁷⁹, J. de Graat⁹⁹, N. De Groot¹⁰⁵, P. de Jong¹⁰⁶, C. De La Taille¹¹⁶, H. De la Torre⁸¹, F. De Lorenzi⁶³, L. De Nooij¹⁰⁶, D. De Pedis^{133a}, A. De Salvo^{133a}, U. De Sanctis^{165a,165c}, A. De Santo¹⁵⁰, J. B. De Vivie De Regie¹¹⁶, G. De Zorzi^{133a,133b}, W. J. Dearnaley⁷¹, R. Debbe²⁵, C. Debenedetti⁴⁶, B. Dechenaux⁵⁵, D. V. Dedovich⁶⁴, J. Degenhardt¹²¹, J. Del Peso⁸¹, T. Del Prete^{123a,123b}, T. Delemontex⁵⁵, M. Deliyergiyev⁷⁴, A. Dell'Acqua³⁰, L. Dell'Asta²², M. Della Pietra^{103a,i}, D. della Volpe^{103a,103b}, M. Delmastro⁵, P. A. Delsart⁵⁵, C. Deluca¹⁰⁶, S. Demers¹⁷⁷, M. Demichev⁶⁴, A. Demilly⁷⁹, B. Demirköz^{12,k}, S. P. Denisov¹²⁹, D. Derendarz³⁹, J. E. Derkaoui^{136d}, F. Derue⁷⁹, P. Dervan⁷³, K. Desch²¹, P. O. Deviveiros¹⁰⁶, A. Dewhurst¹³⁰, B. DeWilde¹⁴⁹, S. Dhaliwal¹⁰⁶, R. Dhullipudi^{78,1}, A. Di Ciaccio^{134a,134b}, L. Di Ciaccio⁵, C. Di Donato^{103a,103b}, A. Di Girolamo³⁰, B. Di Girolamo³⁰, S. Di Luise^{135a,135b}, A. Di Mattia¹⁵³, B. Di Micco^{135a,135b}, R. Di Nardo⁴⁷, A. Di Simone^{134a,134b}, R. Di Sipio^{20a,20b}, M. A. Diaz^{32a}, E. B. Diehl⁸⁸, J. Dietrich⁴², T. A. Dietzsch^{58a}, S. Diglio⁸⁷, K. Dindar Yagci⁴⁰, J. Dingfelder²¹, F. Dinut^{26a}, C. Dionisi^{133a,133b}, P. Dita^{26a}, S. Dita^{26a}, F. Dittus³⁰, F. Djama⁸⁴, T. Djobava^{51b}, M. A. B. do Vale^{24c}, A. Do Valle Wemans^{125a,m}, T. K. O. Doan⁵, D. Dobos³⁰, E. Dobson⁷⁷, J. Dodd³⁵, C. Doglioni⁴⁹, T. Doherty⁵³, T. Dohmae¹⁵⁶, Y. Doi^{65,*}, J. Dolejsi¹²⁸, Z. Dolezal¹²⁸, B. A. Dolgoshein^{97,*}, M. Donadelli^{24d}, J. Donini³⁴, J. Dopke³⁰, A. Doria^{103a}, A. Dos Anjos¹⁷⁴, A. Dotti^{123a,123b}, M. T. Dova⁷⁰, A. T. Doyle⁵³, M. Dris¹⁰, J. Dubbert⁸⁸, S. Dube¹⁵, E. Dubreuil³⁴, E. Duchovni¹⁷³, G. Duckeck⁹⁹, D. Duda¹⁷⁶, A. Dudarev³⁰, F. Dudziak⁶³, L. Duflo¹¹⁶, M.-A. Dufour⁸⁶, L. Duguid⁷⁶, M. Dührssen³⁰, M. Dunford^{58a}, H. Duran Yildiz^{4a}, M. Düren⁵², M. Dwuznik^{38a}, J. Ebke⁹⁹, S. Eckweiler⁸², W. Edson², C. A. Edwards⁷⁶, N. C. Edwards⁵³, W. Ehrenfeld²¹, T. Eifert¹⁴⁴, G. Eigen¹⁴, K. Einsweiler¹⁵, E. Eisenhandler⁷⁵, T. Ekelof¹⁶⁷, M. El Kacimi^{136c}, M. Ellert¹⁶⁷, S. Elles⁵, F. Ellinghaus⁸², K. Ellis⁷⁵, N. Ellis³⁰, J. Elmsheuser⁹⁹, M. Elsing³⁰, D. Emelianov¹³⁰, Y. Enari¹⁵⁶, O. C. Endner⁸², R. Engelmann¹⁴⁹, A. Engl⁹⁹, J. Erdmann¹⁷⁷, A. Ereditato¹⁷, D. Eriksson^{147a}, J. Ernst², M. Ernst²⁵, J. Ernwein¹³⁷, D. Errede¹⁶⁶, S. Errede¹⁶⁶, E. Ertel⁸², M. Escalier¹¹⁶, H. Esch⁴³, C. Escobar¹²⁴, X. Espinal Curull¹², B. Esposito⁴⁷, F. Etienne⁸⁴, A. I. Etiennevire¹³⁷, E. Etzion¹⁵⁴, D. Evangelakou⁵⁴, H. Evans⁶⁰, L. Fabbri^{20a,20b}, C. Fabre³⁰, G. Facini³⁰, R. M. Fakhruddinov¹²⁹, S. Falciano^{133a}, Y. Fang^{33a}, M. Fanti^{90a,90b}, A. Farbin⁸, A. Farilla^{135a}, T. Farooque¹⁵⁹, S. Farrell¹⁶⁴, S. M. Farrington¹⁷¹, P. Farthouat³⁰, F. Fassi¹⁶⁸, P. Fassnacht³⁰, D. Fassoulitis⁹, B. Fathollahzadeh¹⁵⁹, A. Favareto^{90a,90b}, L. Fayard¹¹⁶, P. Federic^{145a}, O. L. Fedin¹²², W. Fedorko¹⁶⁹, M. Fehling-Kaschek⁴⁸, L. Feligioni⁸⁴, C. Feng^{33d}, E. J. Feng⁶, H. Feng⁸⁸, A. B. Fenyuk¹²⁹, J. Ferencei^{145b}, W. Fernando⁶, S. Ferrag⁵³, J. Ferrando⁵³, V. Ferrara⁴², A. Ferrari¹⁶⁷, P. Ferrari¹⁰⁶, R. Ferrari^{120a}, D. E. Ferreira de Lima⁵³, A. Ferrel¹⁶⁸, D. Ferrere⁴⁹, C. Ferretti⁸⁸, A. Ferretto Parodi^{50a,50b}, M. Fiascaris³¹, F. Fiedler⁸², A. Filipčič⁷⁴, F. Filthaut¹⁰⁵, M. Fincke-Keeler¹⁷⁰, K. D. Finelli⁴⁵, M. C. N. Fiolhais^{125a,h}, L. Fiorini¹⁶⁸, A. Firan⁴⁰, J. Fischer¹⁷⁶, M. J. Fisher¹¹⁰, E. A. Fitzgerald²³, M. Flechl⁴⁸, I. Fleck¹⁴², P. Fleischmann¹⁷⁵, S. Fleischmann¹⁷⁶, G. T. Fletcher¹⁴⁰, G. Fletcher⁷⁵, T. Flick¹⁷⁶, A. Floderus⁸⁰, L. R. Flores Castillo¹⁷⁴, A. C. Florez Bustos^{160b}, M. J. Flowerdew¹⁰⁰, T. Fonseca Martin¹⁷, A. Formica¹³⁷, A. Forti⁸³, D. Fortin^{160a}, D. Fournier¹¹⁶, H. Fox⁷¹, P. Francavilla¹², M. Franchini^{20a,20b}, S. Franchino³⁰, D. Francis³⁰, M. Franklin⁵⁷, S. Franz³⁰, M. Fraternali^{120a,120b}, S. Fratina¹²¹, S. T. French²⁸, C. Friedrich⁴², F. Friedrich⁴⁴, D. Froidevaux³⁰, J. A. Frost²⁸, C. Fukunaga¹⁵⁷, E. Fullana Torregrosa¹²⁸, B. G. Fulson¹⁴⁴, J. Fuster¹⁶⁸, C. Gabaldon³⁰, O. Gabizon¹⁷³, A. Gabrielli^{20a,20b}, A. Gabrielli^{133a,133b}, S. Gadatsch¹⁰⁶, T. Gadfort²⁵, S. Gadomski⁴⁹, G. Gagliardi^{50a,50b}, P. Gagnon⁶⁰, C. Galea⁹⁹, B. Galhardo^{125a}, E. J. Gallas¹¹⁹, V. Gallo¹⁷, B. J. Gallop¹³⁰, P. Gallus¹²⁷, K. K. Gan¹¹⁰, R. P. Gandrajula⁶², Y. S. Gao^{144,f}, A. Gaponenko¹⁵, F. M. Garay Walls⁴⁶, F. Garbersen¹⁷⁷, C. García¹⁶⁸, J. E. García Navarro¹⁶⁸, M. Garcia-Sciveres¹⁵, R. W. Gardner³¹, N. Garelli¹⁴⁴, V. Garonne³⁰, C. Gatti⁴⁷, G. Gaudio^{120a}, B. Gaur¹⁴², L. Gauthier⁹⁴, P. Gauzzi^{133a,133b}, I. L. Gavrilenko⁹⁵, C. Gay¹⁶⁹, G. Gaycken²¹, E. N. Gazis¹⁰, P. Ge^{33d,n}, Z. Gece¹⁶⁹, C. N. P. Gee¹³⁰, D. A. A. Geerts¹⁰⁶, Ch. Geich-Gimbel²¹, K. Gellerstedt^{147a,147b}, C. Gemme^{50a}, A. Gemmell⁵³, M. H. Genest⁵⁵, S. Gentile^{133a,133b}, M. George⁵⁴, S. George⁷⁶, D. Gerbaudo¹⁶⁴, A. Gershon¹⁵⁴, H. Ghazlane^{136b}, N. Ghodbane³⁴, B. Giacobbe^{20a}, S. Giagu^{133a,133b}, V. Giangiobbe¹², F. Gianotti³⁰, B. Gibbard²⁵, A. Gibson¹⁵⁹, S. M. Gibson⁷⁶, M. Gilchriese¹⁵, T. P. S. Gillam²⁸, D. Gillberg³⁰, A. R. Gillman¹³⁰, D. M. Gingrich^{3,e}, N. Giokaris⁹, M. P. Giordani^{165c}, R. Giordano^{103a,103b}, F. M. Giorgi¹⁶, P. Giovannini¹⁰⁰, P. F. Giraud¹³⁷, D. Giugni^{90a}, C. Giuliani⁴⁸, M. Giunta⁹⁴, B. K. Gjelsten¹¹⁸, I. Gkialas^{155,o}, L. K. Gladilin⁹⁸, C. Glasman⁸¹, J. Glatzer²¹, A. Glazov⁴², G. L. Glonti⁶⁴, M. Goblirsch-Kolb¹⁰⁰, J. R. Goddard⁷⁵, J. Godfrey¹⁴³, J. Godlewski³⁰, M. Goebel⁴², C. Goeringer⁸², S. Goldfarb⁸⁸, T. Golling¹⁷⁷, D. Golubkov¹²⁹, A. Gomes^{125a,c}, L. S. Gomez Fajardo⁴², R. Gonçalves⁷⁶, J. Goncalves Pinto Firmino Da Costa⁴², L. Gonella²¹, S. González de la Hoz¹⁶⁸, G. Gonzalez Parra¹², M. L. Gonzalez Silva²⁷, S. Gonzalez-Sevilla⁴⁹, J. J. Goodson¹⁴⁹, L. Goossens³⁰, P. A. Gorbounov⁹⁶, H. A. Gordon²⁵, I. Gorelov¹⁰⁴, G. Gorfine¹⁷⁶, B. Gorini³⁰, E. Gorini^{72a,72b}, A. Gorišek⁷⁴, E. Gornicki³⁹, A. T. Goshaw⁶, C. Gössling⁴³, M. I. Gostkin⁶⁴, I. Gough Eschrich¹⁶⁴, M. Goughri^{136a}, D. Goujdami^{136c}, M. P. Goulette⁴⁹, A. G. Goussiou¹³⁹, C. Goy⁵, S. Gozpinar²³, L. Graber⁵⁴, I. Grabowska-Bold^{38a}, P. Grafström^{20a,20b}, K.-J. Grahn⁴², E. Gramstad¹¹⁸, F. Grancagnolo^{72a}, S. Grancagnolo¹⁶, V. Grassi¹⁴⁹, V. Gratchev¹²², H. M. Gray³⁰, J. A. Gray¹⁴⁹,

E. Graziani^{135a}, O. G. Grebenyuk¹²², T. Greenshaw⁷³, Z. D. Greenwood^{78,1}, K. Gregersen³⁶, I. M. Gregor⁴², P. Grenier¹⁴⁴, J. Griffiths⁸, N. Grigalashvili⁶⁴, A. A. Grillo¹³⁸, K. Grimm⁷¹, S. Grinstein^{12,p}, Ph. Gris³⁴, Y. V. Grishkevich⁹⁸, J.-F. Grivaz¹¹⁶, J. P. Grohs⁴⁴, A. Grohsjean⁴², E. Gross¹⁷³, J. Grosse-Knetter⁵⁴, J. Groth-Jensen¹⁷³, K. Grybel¹⁴², F. Guescini⁴⁹, D. Guest¹⁷⁷, O. Gueta¹⁵⁴, C. Guicheney³⁴, E. Guido^{50a,50b}, T. Guillemin¹¹⁶, S. Guindon², U. Gul⁵³, J. Gunther¹²⁷, J. Guo³⁵, P. Gutierrez¹¹², N. Guttman¹⁵⁴, O. Gutzwiller¹⁷⁴, C. Guyot¹³⁷, C. Gwenlan¹¹⁹, C. B. Gwilliam⁷³, A. Haas¹⁰⁹, S. Haas³⁰, C. Haber¹⁵, H. K. Hadavand⁸, P. Haefner²¹, Z. Hajduk³⁹, H. Hakobyan¹⁷⁸, D. Hall¹¹⁹, G. Halladjian⁶², K. Hamacher¹⁷⁶, P. Hamal¹¹⁴, K. Hamano⁸⁷, M. Hamer⁵⁴, A. Hamilton^{146a,q}, S. Hamilton¹⁶², L. Han^{33b}, K. Hanagaki¹¹⁷, K. Hanawa¹⁶¹, M. Hance¹⁵, C. Handel⁸², P. Hanke^{58a}, J. R. Hansen³⁶, J. B. Hansen³⁶, J. D. Hansen³⁶, P. H. Hansen³⁶, P. Hansson¹⁴⁴, K. Hara¹⁶¹, A. S. Hard¹⁷⁴, T. Harenberg¹⁷⁶, S. Harkusha⁹¹, D. Harper⁸⁸, R. D. Harrington⁴⁶, O. M. Harris¹³⁹, J. Hartert⁴⁸, F. Hartjes¹⁰⁶, T. Haruyama⁶⁵, A. Harvey⁵⁶, S. Hasegawa¹⁰², Y. Hasegawa¹⁴¹, S. Hassani¹³⁷, S. Haug¹⁷, M. Hauschild³⁰, R. Hauser⁸⁹, M. Havranek²¹, C. M. Hawkes¹⁸, R. J. Hawkins³⁰, A. D. Hawkins⁸⁰, T. Hayakawa⁶⁶, T. Hayashi¹⁶¹, D. Hayden⁷⁶, C. P. Hays¹¹⁹, H. S. Hayward⁷³, S. J. Haywood¹³⁰, S. J. Head¹⁸, T. Heck⁸², V. Hedberg⁸⁰, L. Heelan⁸, S. Heim¹²¹, B. Heinemann¹⁵, S. Heisterkamp³⁶, J. Hejbal¹²⁶, L. Helary²², C. Heller⁹⁹, M. Heller³⁰, S. Hellman^{147a,147b}, D. Hellmich²¹, C. Helsens³⁰, J. Henderson¹¹⁹, R. C. W. Henderson⁷¹, M. Henke^{58a}, A. Henrichs¹⁷⁷, A. M. Henriques Correia³⁰, S. Henrot-Versille¹¹⁶, C. Hensel⁵⁴, G. H. Herbert¹⁶, C. M. Hernandez⁸, Y. Hernández Jiménez¹⁶⁸, R. Herrberg-Schubert¹⁶, G. Herten⁴⁸, R. Hertenberger⁹⁹, L. Hervas³⁰, G. G. Hesketh⁷⁷, N. P. Hessey¹⁰⁶, R. Hickling⁷⁵, E. Higón-Rodríguez¹⁶⁸, J. C. Hill²⁸, K. H. Hiller⁴², S. Hillert²¹, S. J. Hillier¹⁸, I. Hinchliffe¹⁵, E. Hines¹²¹, M. Hirose¹¹⁷, D. Hirschbuehl¹⁷⁶, J. Hobbs¹⁴⁹, N. Hod¹⁰⁶, M. C. Hodgkinson¹⁴⁰, P. Hodgson¹⁴⁰, A. Hoecker³⁰, M. R. Hoferkamp¹⁰⁴, J. Hoffman⁴⁰, D. Hoffmann⁸⁴, J. I. Hofmann^{58a}, M. Hohlfeld⁸², S. O. Holmgren^{147a}, J. L. Holzbauer⁸⁹, T. M. Hong¹²¹, L. Hooft van Huysduynen¹⁰⁹, J.-Y. Hostachy⁵⁵, S. Hou¹⁵², A. Hoummada^{136a}, J. Howard¹¹⁹, J. Howarth⁸³, M. Hrabovsky¹¹⁴, I. Hristova¹⁶, J. Hrivnac¹¹⁶, T. Hryn'ova⁵, P. J. Hsu⁸², S.-C. Hsu¹³⁹, D. Hu³⁵, X. Hu²⁵, Z. Hubacek³⁰, F. Hubaut⁸⁴, F. Huegging²¹, A. Huettmann⁴², T. B. Huffman¹¹⁹, E. W. Hughes³⁵, G. Hughes⁷¹, M. Huhtinen³⁰, T. A. Hülsing⁸², M. Hurwitz¹⁵, N. Huseynov^{64,r}, J. Huston⁸⁹, J. Huth⁵⁷, G. Iacobucci⁴⁹, G. Iakovidis¹⁰, I. Ibragimov¹⁴², L. Iconomidou-Fayard¹¹⁶, J. Idarraga¹¹⁶, P. Iengo^{103a}, O. Igonkina¹⁰⁶, Y. Ikegami⁶⁵, K. Ikematsu¹⁴², M. Ikeno⁶⁵, D. Iliadis¹⁵⁵, N. Ilic¹⁵⁹, T. Ince¹⁰⁰, P. Ioannou⁹, M. Iodice^{135a}, K. Iordanidou⁹, V. Ippolito^{133a,133b}, A. Irlles Quiles¹⁶⁸, C. Isaksson¹⁶⁷, M. Ishino⁶⁷, M. Ishitsuka¹⁵⁸, R. Ishmukhametov¹¹⁰, C. Issever¹¹⁹, S. Istin^{19a}, A. V. Ivashin¹²⁹, W. Iwanski³⁹, H. Iwasaki⁶⁵, J. M. Izen⁴¹, V. Izzo^{103a}, B. Jackson¹²¹, J. N. Jackson⁷³, P. Jackson¹, M. R. Jaekel³⁰, V. Jain², K. Jakobs⁴⁸, S. Jakobsen³⁶, T. Jakoubek¹²⁶, J. Jakubek¹²⁷, D. O. Jamin¹⁵², D. K. Jana¹¹², E. Jansen⁷⁷, H. Jansen³⁰, J. Janssen²¹, A. Jantsch¹⁰⁰, M. Janus⁴⁸, R. C. Jared¹⁷⁴, G. Jarlskog⁸⁰, L. Jeanty⁵⁷, G.-Y. Jeng¹⁵¹, I. Jen-La Plante³¹, D. Jennens⁸⁷, P. Jenni³⁰, J. Jentsch⁴³, C. Jeske¹⁷¹, P. Jež³⁶, S. Jézéquel⁵, M. K. Jha^{20a}, H. Ji¹⁷⁴, W. Ji⁸², J. Jia¹⁴⁹, Y. Jiang^{33b}, M. Jimenez Belenguer⁴², S. Jin^{33a}, O. Jinnouchi¹⁵⁸, M. D. Joergensen³⁶, D. Joffe⁴⁰, M. Johansen^{147a,147b}, K. E. Johansson^{147a}, P. Johansson¹⁴⁰, S. Johnert⁴², K. A. Johns⁷, K. Jon-And^{147a,147b}, G. Jones¹⁷¹, R. W. L. Jones⁷¹, T. J. Jones⁷³, P. M. Jorge^{125a}, K. D. Joshi⁸³, J. Jovicevic¹⁴⁸, X. Ju¹⁷⁴, C. A. Jung⁴³, R. M. Jungst³⁰, P. Jussel⁶¹, A. Juste Rozas^{12,p}, S. Kabana¹⁷, M. Kaci¹⁶⁸, A. Kaczmarzka³⁹, P. Kadlecik³⁶, M. Kado¹¹⁶, H. Kagan¹¹⁰, M. Kagan¹⁴⁴, E. Kajomovitz¹⁵³, S. Kalinin¹⁷⁶, S. Kama⁴⁰, N. Kanaya¹⁵⁶, M. Kaneda³⁰, S. Kaneti²⁸, T. Kanno¹⁵⁸, V. A. Kantserov⁹⁷, J. Kanzaki⁶⁵, B. Kaplan¹⁰⁹, A. Kapliy³¹, D. Kar⁵³, K. Karakostas¹⁰, M. Karnevskiy⁸², V. Kartvelishvili⁷¹, A. N. Karyukhin¹²⁹, L. Kashif¹⁷⁴, G. Kasieczka^{58b}, R. D. Kass¹¹⁰, A. Kastanas¹⁴, Y. Kataoka¹⁵⁶, J. Katzy⁴², V. Kaushik⁷, K. Kawagoe⁶⁹, T. Kawamoto¹⁵⁶, G. Kawamura⁵⁴, S. Kazama¹⁵⁶, V. F. Kazanin¹⁰⁸, M. Y. Kazarinov⁶⁴, R. Keeler¹⁷⁰, P. T. Keener¹²¹, R. Kehoe⁴⁰, M. Keil⁵⁴, J. S. Keller¹³⁹, H. Keoshkerian⁵, O. Kepka¹²⁶, B. P. Kerševan⁷⁴, S. Kersten¹⁷⁶, K. Kessoku¹⁵⁶, J. Keung¹⁵⁹, F. Khalil-zada¹¹, H. Khandanyan^{147a,147b}, A. Khanov¹¹³, D. Kharchenko⁶⁴, A. Khodinov⁹⁷, A. Khomich^{58a}, T. J. Khoo²⁸, G. Khorialui²¹, A. Khoroshilov¹⁷⁶, V. Khovanskiy⁹⁶, E. Khramov⁶⁴, J. Khubua^{51b}, H. Kim^{147a,147b}, S. H. Kim¹⁶¹, N. Kimura¹⁷², O. Kind¹⁶, B. T. King⁷³, M. King⁶⁶, R. S. B. King¹¹⁹, S. B. King¹⁶⁹, J. Kirk¹³⁰, A. E. Kiryunin¹⁰⁰, T. Kishimoto⁶⁶, D. Kisielevska^{38a}, T. Kitamura⁶⁶, T. Kittelmann¹²⁴, K. Kiuchi¹⁶¹, E. Kladiva^{145b}, M. Klein⁷³, U. Klein⁷³, K. Kleinknecht⁸², M. Klemetti⁸⁶, A. Klier¹⁷³, P. Klimek^{147a,147b}, A. Klimentov²⁵, R. Klingenberg⁴³, J. A. Klinger⁸³, E. B. Klinkby³⁶, T. Klioutchnikova³⁰, P. F. Klok¹⁰⁵, E.-E. Kluge^{58a}, P. Kluit¹⁰⁶, S. Kluth¹⁰⁰, E. Kneringer⁶¹, E. B. F. G. Knoop⁸⁴, A. Knue⁵⁴, B. R. Ko⁴⁵, T. Kobayashi¹⁵⁶, M. Kobel⁴⁴, M. Kocian¹⁴⁴, P. Kodys¹²⁸, S. Koenig⁸², F. Koetsveld¹⁰⁵, P. Koevesarki²¹, T. Koffas²⁹, E. Koffeman¹⁰⁶, L. A. Kogan¹¹⁹, S. Kohlmann¹⁷⁶, F. Kohn⁵⁴, Z. Kohout¹²⁷, T. Kohriki⁶⁵, T. Koi¹⁴⁴, H. Kolanoski¹⁶, I. Koletsou^{90a}, J. Koll⁸⁹, A. A. Komar⁹⁵, Y. Komori¹⁵⁶, T. Kondo⁶⁵, K. Köneke³⁰, A. C. König¹⁰⁵, T. Kono^{65,s}, A. I. Kononov⁴⁸, R. Konoplich^{109,t}, N. Konstantinidis⁷⁷, R. Kopeliansky¹⁵³, S. Koperny^{38a}, L. Köpke⁸², A. K. Kopp⁴⁸, K. Korcyl³⁹, K. Kordas¹⁵⁵, A. Korn⁴⁶, A. A. Korol¹⁰⁸, I. Korolkov¹², E. V. Korolkova¹⁴⁰, V. A. Korotkov¹²⁹, O. Kortner¹⁰⁰, S. Kortner¹⁰⁰, V. V. Kostyukhin²¹, S. Kotov¹⁰⁰, V. M. Kotov⁶⁴, A. Kotwal⁴⁵, C. Kourkoumelis⁹, V. Kouskoura¹⁵⁵, A. Koutsman^{160a}, R. Kowalewski¹⁷⁰, T. Z. Kowalski^{38a}, W. Kozanecki¹³⁷, A. S. Kozhin¹²⁹, V. Kral¹²⁷, V. A. Kramarenko⁹⁸, G. Kramberger⁷⁴, M. W. Krasny⁷⁹, A. Krasznahorkay¹⁰⁹, J. K. Kraus²¹, A. Kravchenko²⁵, S. Kreiss¹⁰⁹, J. Kretzschmar⁷³, K. Kreutzfeldt⁵², N. Krieger⁵⁴, P. Krieger¹⁵⁹, K. Kroeninger⁵⁴, H. Kroha¹⁰⁰, J. Kroll¹²¹, J. Kroseberg²¹, J. Krstic^{13a}, U. Kruchonak⁶⁴, H. Krüger²¹, T. Kruker¹⁷, N. Krumnack⁶³, Z. V. Krumshcheyn⁶⁴, A. Kruse¹⁷⁴, M. C. Kruse⁴⁵, T. Kubota⁸⁷, S.

Kuday^{4a}, S. Kuehn⁴⁸, A. Kugel^{58c}, T. Kuhl⁴², V. Kukhtin⁶⁴, Y. Kulchitsky⁹¹, S. Kuleshov^{32b}, M. Kuna⁷⁹, J. Kunkle¹²¹, A. Kupco¹²⁶, H. Kurashige⁶⁶, M. Kurata¹⁶¹, Y. A. Kurochkin⁹¹, V. Kus¹²⁶, E. S. Kuwertz¹⁴⁸, M. Kuze¹⁵⁸, J. Kvita¹⁴³, R. Kwee¹⁶, A. La Rosa⁴⁹, L. La Rotonda^{37a,37b}, L. Labarga⁸¹, S. Lablak^{136a}, C. Lacasta¹⁶⁸, F. Lacava^{133a,133b}, J. Lacey²⁹, H. Lacker¹⁶, D. Lacour⁷⁹, V. R. Lacuesta¹⁶⁸, E. Ladygin⁶⁴, R. Lafaye⁵, B. Laforge⁷⁹, T. Lagouri¹⁷⁷, S. Lai⁴⁸, H. Laier^{58a}, E. Laisne⁵⁵, L. Lambourne⁷⁷, C. L. Lampen⁷, W. Lampl⁷, E. Lançon¹³⁷, U. Landgraf⁴⁸, M. P. J. Landon⁷⁵, V. S. Lang^{58a}, C. Lange⁴², A. J. Lankford¹⁶⁴, F. Lanni²⁵, K. Lantzsch³⁰, A. Lanza^{120a}, S. Laplace⁷⁹, C. Lapoire²¹, J. F. Laporte¹³⁷, T. Lari^{90a}, A. Larnier¹¹⁹, M. Lassnig³⁰, P. Laurelli⁴⁷, V. Lavorini^{37a,37b}, W. Lavrijsen¹⁵, P. Laycock⁷³, O. Le Dortz⁷⁹, E. Le Guirriec⁸⁴, E. Le Menedeu¹², T. LeCompte⁶, F. Ledroit-Guillon⁵⁵, H. Lee¹⁰⁶, J. S. H. Lee¹¹⁷, S. C. Lee¹⁵², L. Lee¹⁷⁷, G. Lefebvre⁷⁹, M. Lefebvre¹⁷⁰, M. Legendre¹³⁷, F. Legger⁹⁹, C. Leggett¹⁵, M. Lehmacher²¹, G. Lehmann Miotto³⁰, A. G. Leister¹⁷⁷, M. A. L. Leite^{24d}, R. Leitner¹²⁸, D. Lellouch¹⁷³, B. Lemmer⁵⁴, V. Lendermann^{58a}, K. J. C. Leney^{146c}, T. Lenz¹⁰⁶, G. Lenzen¹⁷⁶, B. Lenzi³⁰, K. Leonhardt⁴⁴, S. Leontsinis¹⁰, F. Lepold^{58a}, C. Leroy⁹⁴, J.-R. Lessard¹⁷⁰, C. G. Lester²⁸, C. M. Lester¹²¹, J. Levêque⁵, D. Levin⁸⁸, L. J. Levinson¹⁷³, A. Lewis¹¹⁹, G. H. Lewis¹⁰⁹, A. M. Leyko²¹, M. Leyton¹⁶, B. Li^{33b,u}, B. Li⁸⁴, H. Li¹⁴⁹, H. L. Li³¹, S. Li⁴⁵, X. Li⁸⁸, Z. Liang^{119,v}, H. Liao³⁴, B. Liberti^{134a}, P. Lichard³⁰, K. Lie¹⁶⁶, J. Liebal²¹, W. Liebig¹⁴, C. Limbach²¹, A. Limosani⁸⁷, M. Limper⁶², S. C. Lin^{152,w}, F. Linde¹⁰⁶, B. E. Lindquist¹⁴⁹, J. T. Linnemann⁸⁹, E. Lipeles¹²¹, A. Lipniacka¹⁴, M. Lisovyi⁴², T. M. Liss¹⁶⁶, D. Lissauer²⁵, A. Lister¹⁶⁹, A. M. Litke¹³⁸, D. Liu¹⁵², J. B. Liu^{33b}, K. Liu^{33b,x}, L. Liu⁸⁸, M. Liu⁴⁵, M. Liu^{33b}, Y. Liu^{33b}, M. Livan^{120a,120b}, S. S. A. Livermore¹¹⁹, A. Lleres⁵⁵, J. Llorente Merino⁸¹, S. L. Lloyd⁷⁵, F. Lo Sterzo^{133a,133b}, E. Lobodzinska⁴², P. Loch⁷, W. S. Lockman¹³⁸, T. Lodenkoetter²¹, F. K. Loebinger⁸³, A. E. Loevschall-Jensen³⁶, A. Loginov¹⁷⁷, C. W. Loh¹⁶⁹, T. Lohse¹⁶, K. Lohwasser⁴⁸, M. Lokajicek¹²⁶, V. P. Lombardo⁵, R. E. Long⁷¹, L. Lopes^{125a}, D. Lopez Mateos⁵⁷, J. Lorenz⁹⁹, N. Lorenzo Martinez¹¹⁶, M. Losada¹⁶³, P. Loscutoff¹⁵, M. J. Losty^{160a,*}, X. Lou⁴¹, A. Lounis¹¹⁶, K. F. Loureiro¹⁶³, J. Love⁶, P. A. Love⁷¹, A. J. Lowe^{144,f}, F. Lu^{33a}, H. J. Lubatti¹³⁹, C. Luci^{133a,133b}, A. Lucotte⁵⁵, D. Ludwig⁴², I. Ludwig⁴⁸, J. Ludwig⁴⁸, F. Luehring⁶⁰, W. Lukas⁶¹, L. Luminari^{133a}, E. Lund¹¹⁸, J. Lundberg^{147a,147b}, O. Lundberg^{147a,147b}, B. Lund-Jensen¹⁴⁸, J. Lundquist³⁶, M. Lungwitz⁸², D. Lynn²⁵, R. Lysak¹²⁶, E. Lytken⁸⁰, H. Ma²⁵, L. L. Ma¹⁷⁴, G. Maccarrone⁴⁷, A. Macchiolo¹⁰⁰, B. Maček⁷⁴, J. Machado Miguens^{125a}, D. Macina³⁰, R. Mackeprang³⁶, R. Madar⁴⁸, R. J. Madaras¹⁵, H. J. Maddocks⁷¹, W. F. Mader⁴⁴, A. Madsen¹⁶⁷, M. Maeno⁵, T. Maeno²⁵, L. Magnoni¹⁶⁴, E. Magradze⁵⁴, K. Mahboubi⁴⁸, J. Mahlstedt¹⁰⁶, S. Mahmoud⁷³, G. Mahout¹⁸, C. Maiani¹³⁷, C. Maidantchik^{24a}, A. Maio^{125a,c}, S. Majewski¹¹⁵, Y. Makida⁶⁵, N. Makovec¹¹⁶, P. Mal^{137,y}, B. Malaescu⁷⁹, Pa. Malecki³⁹, P. Malecki³⁹, V. P. Maleev¹²², F. Malek⁵⁵, U. Mallik⁶², D. Malon⁶, C. Malone¹⁴⁴, S. Maltezos¹⁰, V. M. Malyshev¹⁰⁸, S. Malyukov³⁰, J. Mamuzic^{13b}, L. Mandelli^{90a}, I. Mandić⁷⁴, R. Mandrysch⁶², J. Maneira^{125a}, A. Manfredini¹⁰⁰, L. Manhaes de Andrade Filho^{24b}, J. A. Manjarres Ramos¹³⁷, A. Mann⁹⁹, P. M. Manning¹³⁸, A. Manousakis-Katsikakis⁹, B. Mansoulie¹³⁷, R. Mantifel⁸⁶, L. Mapelli³⁰, L. March¹⁶⁸, J. F. Marchand²⁹, F. Marchese^{134a,134b}, G. Marchiori⁷⁹, M. Marcisovsky¹²⁶, C. P. Marino¹⁷⁰, C. N. Marques^{125a}, F. Marroquim^{24a}, Z. Marshall¹²¹, L. F. Marti¹⁷, S. Marti-Garcia¹⁶⁸, B. Martin³⁰, B. Martin⁸⁹, J. P. Martin⁹⁴, T. A. Martin¹⁷¹, V. J. Martin⁴⁶, B. Martin dit Latour⁴⁹, H. Martinez¹³⁷, M. Martinez^{12,p}, S. Martin-Haugh¹⁵⁰, A. C. Martyniuk¹⁷⁰, M. Marx⁸³, F. Marzano^{133a}, A. Marzin¹¹², L. Masetti⁸², T. Mashimo¹⁵⁶, R. Mashinistov⁹⁵, J. Masik⁸³, A. L. Maslennikov¹⁰⁸, I. Massa^{20a,20b}, N. Massol⁵, P. Mastrandrea¹⁴⁹, A. Mastroberardino^{37a,37b}, T. Masubuchi¹⁵⁶, H. Matsunaga¹⁵⁶, T. Matsushita⁶⁶, P. Mättig¹⁷⁶, S. Mättig⁴², C. Mattraversi^{119,d}, J. Maurer⁸⁴, S. J. Maxfield⁷³, D. A. Maximov^{108,g}, R. Mazini¹⁵², M. Mazur²¹, L. Mazzaferro^{134a,134b}, M. Mazzanti^{90a}, S. P. Mc Kee⁸⁸, A. McCarn¹⁶⁶, R. L. McCarthy¹⁴⁹, T. G. McCarthy²⁹, N. A. McCubbin¹³⁰, K. W. McFarlane^{56,*}, J. A. Mcfayden¹⁴⁰, G. Mchedlidze^{51b}, T. McLaughlan¹⁸, S. J. McMahon¹³⁰, R. A. McPherson^{170,j}, A. Meade⁸⁵, J. Mechnich¹⁰⁶, M. Mechtel¹⁷⁶, M. Medinnis⁴², S. Meehan³¹, R. Meera-Lebbai¹¹², T. Meguro¹¹⁷, S. Mehlhase³⁶, A. Mehta⁷³, K. Meier^{58a}, C. Meineck⁹⁹, B. Meirose⁸⁰, C. Melachrinou³¹, B. R. Mellado Garcia^{146c}, F. Meloni^{90a,90b}, L. Mendoza Navas¹⁶³, A. Mengarelli^{20a,20b}, S. Menke¹⁰⁰, E. Meoni¹⁶², K. M. Mercurio⁵⁷, N. Meric¹³⁷, P. Mermod⁴⁹, L. Merola^{103a,103b}, C. Meroni^{90a}, F. S. Merritt³¹, H. Merritt¹¹⁰, A. Messina^{30,z}, J. Metcalfe²⁵, A. S. Mete¹⁶⁴, C. Meyer⁸², C. Meyer³¹, J.-P. Meyer¹³⁷, J. Meyer³⁰, J. Meyer⁵⁴, S. Michal³⁰, R. P. Middleton¹³⁰, S. Migas⁷³, L. Mijović¹³⁷, G. Mikenberg¹⁷³, M. Mikestikova¹²⁶, M. Mikuž⁷⁴, D. W. Miller³¹, W. J. Mills¹⁶⁹, C. Mills⁵⁷, A. Milov¹⁷³, D. A. Milstead^{147a,147b}, D. Milstein¹⁷³, A. A. Minaenko¹²⁹, M. Miñano Moya¹⁶⁸, I. A. Minashvili⁶⁴, A. I. Mincer¹⁰⁹, B. Mindur^{38a}, M. Mineev⁶⁴, Y. Ming¹⁷⁴, L. M. Mir¹², G. Mirabelli^{133a}, J. Mitrevski¹³⁸, V. A. Mitsou¹⁶⁸, S. Mitsui⁶⁵, P. S. Miyagawa¹⁴⁰, J. U. Mjörnmark⁸⁰, T. Moa^{147a,147b}, V. Moeller²⁸, S. Mohapatra¹⁴⁹, W. Mohr⁴⁸, R. Moles-Valls¹⁶⁸, A. Molfetas³⁰, K. Mönig⁴², C. Monini⁵⁵, J. Monk³⁶, E. Monnier⁸⁴, J. Montejo Berlingen¹², F. Monticelli⁷⁰, S. Monzani^{20a,20b}, R. W. Moore³, C. Mora Herrera⁴⁹, A. Moraes⁵³, N. Morange⁶², J. Morel⁵⁴, D. Moreno⁸², M. Moreno Llácer¹⁶⁸, P. Morettini^{50a}, M. Morgenstern⁴⁴, M. Morii⁵⁷, S. Moritz⁸², A. K. Morley³⁰, G. Mornacchi³⁰, J. D. Morris⁷⁵, L. Morvaj¹⁰², N. Möser²¹, H. G. Moser¹⁰⁰, M. Mosidze^{51b}, J. Moss¹¹⁰, R. Mount¹⁴⁴, E. Mountricha^{10,aa}, S. V. Mouraviev^{95,*}, E. J. W. Moyses⁸⁵, R. D. Mudd¹⁸, F. Mueller^{58a}, J. Mueller¹²⁴, K. Mueller²¹, T. Mueller²⁸, T. Mueller⁸², D. Muenstermann³⁰, Y. Munwes¹⁵⁴, J. A. Murillo Quijada¹⁸, W. J. Murray¹³⁰, I. Mussche¹⁰⁶, E. Musto¹⁵³, A. G. Myagkov^{129,ab}, M. Myska¹²⁶, O. Nackenhorst⁵⁴, J. Nadal¹², K. Nagai¹⁶¹, R. Nagai¹⁵⁸, Y. Nagai⁸⁴, K. Nagano⁶⁵, A. Nagarkar¹¹⁰, Y. Nagasaka⁵⁹, M. Nagel¹⁰⁰, A. M. Nairz³⁰, Y. Nakahama³⁰, K. Nakamura⁶⁵, T. Nakamura¹⁵⁶,

I. Nakano¹¹¹, H. Namasivayam⁴¹, G. Nanava²¹, A. Napier¹⁶², R. Narayan^{58b}, M. Nash^{77,d}, T. Nattermann²¹, T. Naumann⁴², G. Navarro¹⁶³, H. A. Neal⁸⁸, P. Yu. Nechaeva⁹⁵, T. J. Neep⁸³, A. Negri^{120a,120b}, G. Negri³⁰, M. Negri^{20a}, S. Nektarijevic⁴⁹, A. Nelson¹⁶⁴, T. K. Nelson¹⁴⁴, S. Nemecek¹²⁶, P. Nemethy¹⁰⁹, A. A. Nepomuceno^{24a}, M. Nessi^{30,ac}, M. S. Neubauer¹⁶⁶, M. Neumann¹⁷⁶, A. Neusiedl⁸², R. M. Neves¹⁰⁹, P. Nevski²⁵, F. M. Newcomer¹²¹, P. R. Newman¹⁸, D. H. Nguyen⁶, V. Nguyen Thi Hong¹³⁷, R. B. Nickerson¹¹⁹, R. Nicolaidou¹³⁷, B. Nicquevert³⁰, F. Niedercorn¹¹⁶, J. Nielsen¹³⁸, N. Nikiporou³⁵, A. Nikiporov¹⁶, V. Nikolaenko^{129,ab}, I. Nikolic-Audit⁷⁹, K. Nikolics⁴⁹, K. Nikolopoulos¹⁸, P. Nilsson⁸, Y. Ninomiya¹⁵⁶, A. Nisati^{133a}, R. Nisius¹⁰⁰, T. Nobe¹⁵⁸, L. Nodulman⁶, M. Nomachi¹¹⁷, I. Nomidis¹⁵⁵, S. Norberg¹¹², M. Nordberg³⁰, J. Novakova¹²⁸, M. Nozaki⁶⁵, L. Nozka¹¹⁴, A.-E. Nuncio-Quiroz²¹, G. Nunes Hanninger⁸⁷, T. Nunnemann⁹⁹, E. Nurse⁷⁷, B. J. O'Brien⁴⁶, D. C. O'Neil¹⁴³, V. O'Shea⁵³, L. B. Oakes⁹⁹, F. G. Oakham^{29,e}, H. Oberlack¹⁰⁰, J. Ocariz⁷⁹, A. Ochi⁶⁶, M. I. Ochoa⁷⁷, S. Oda⁶⁹, S. Odaka⁶⁵, J. Odier⁸⁴, H. Ogren⁶⁰, A. Oh⁸³, S. H. Oh⁴⁵, C. C. Ohm³⁰, T. Ohshima¹⁰², W. Okamura¹¹⁷, H. Okawa²⁵, Y. Okumura³¹, T. Okuyama¹⁵⁶, A. Olariu^{26a}, A. G. Olchevski⁶⁴, S. A. Olivares Pino⁴⁶, M. Oliveira^{125a,h}, D. Oliveira Damazio²⁵, E. Oliver Garcia¹⁶⁸, D. Olivito¹²¹, A. Olszewski³⁹, J. Olszowska³⁹, A. Onofre^{125a,ad}, P. U. E. Onyisi^{31,ae}, C. J. Oram^{160a}, M. J. Oreglia³¹, Y. Oren¹⁵⁴, D. Orestano^{135a,135b}, N. Orlando^{72a,72b}, C. Oropeza Barrera⁵³, R. S. Orr¹⁵⁹, B. Osculati^{50a,50b}, R. Ospanov¹²¹, G. Otero y Garzon²⁷, J. P. Ottersbach¹⁰⁶, M. Ouchrif^{136d}, E. A. Ouellette¹⁷⁰, F. Ould-Saada¹¹⁸, A. Ouraou¹³⁷, Q. Ouyang^{33a}, A. Ovcharova¹⁵, M. Owen⁸³, S. Owen¹⁴⁰, V. E. Ozcan^{19a}, N. Ozturk⁸, A. Pacheco Pages¹², C. Padilla Aranda¹², S. Pagan Griso¹⁵, E. Paganis¹⁴⁰, C. Pahl¹⁰⁰, F. Paige²⁵, P. Pais⁸⁵, K. Pajchel¹¹⁸, G. Palacino^{160b}, C. P. Paleari⁷, S. Palestini³⁰, D. Pallin³⁴, A. Palma^{125a}, J. D. Palmer¹⁸, Y. B. Pan¹⁷⁴, E. Panagiotopoulou¹⁰, J. G. Panduro Vazquez⁷⁶, P. Pani¹⁰⁶, N. Panikashvili⁸⁸, S. Panitkin²⁵, D. Pantea^{26a}, A. Papadelis^{147a}, Th. D. Papadopoulos¹⁰, K. Papageorgiou^{155,o}, A. Paramonov⁶, D. Paredes Hernandez³⁴, W. Park^{25,af}, M. A. Parker²⁸, F. Parodi^{50a,50b}, J. A. Parsons³⁵, U. Parzefall⁴⁸, S. Pashapour⁵⁴, E. Pasqualucci^{133a}, S. Passaggio^{50a}, A. Passeri^{135a}, F. Pastore^{135a,135b,*}, Fr. Pastore⁷⁶, G. Pásztor^{49,ag}, S. Pataria¹⁷⁶, N. D. Patel¹⁵¹, J. R. Pater⁸³, S. Patricelli^{103a,103b}, T. Pauly³⁰, J. Pearce¹⁷⁰, M. Pedersen¹¹⁸, S. Pedraza Lopez¹⁶⁸, M. I. Pedraza Morales¹⁷⁴, S. V. Peleganchuk¹⁰⁸, D. Pelikan¹⁶⁷, H. Peng^{33b}, B. Penning³¹, A. Penson³⁵, J. Penwell⁶⁰, T. Perez Cavalcanti⁴², E. Perez Codina^{160a}, M. T. Pérez García-Estañ¹⁶⁸, V. Perez Reale³⁵, L. Perini^{90a,90b}, H. Pernegger³⁰, R. Perrino^{72a}, P. Perrodo⁵, V. D. Peshekhonov⁶⁴, K. Peters³⁰, R. F. Y. Peters^{54,ah}, B. A. Petersen³⁰, J. Petersen³⁰, T. C. Petersen³⁶, E. Petit⁵, A. Petridis^{147a,147b}, C. Petridou¹⁵⁵, E. Petrolu^{133a}, F. Petrucci^{135a,135b}, D. Petschull⁴², M. Petti¹⁴³, R. Pezoa^{32b}, A. Phan⁸⁷, P. W. Phillips¹³⁰, G. Piacquadio¹⁴⁴, E. Pianori¹⁷¹, A. Picazio⁴⁹, E. Piccaro⁷⁵, M. Piccinini^{20a,20b}, S. M. Piec⁴², R. Piegai²⁷, D. T. Pignotti¹¹⁰, J. E. Pilcher³¹, A. D. Pilkington⁷⁷, J. Pina^{125a,c}, M. Pinamonti^{165a,165c,ai}, A. Pinder¹¹⁹, J. L. Pinfold³, A. Pingel³⁶, B. Pinto^{125a}, C. Pizio^{90a,90b}, M.-A. Pleier²⁵, V. Pleskot¹²⁸, E. Plotnikova⁶⁴, P. Plucinski^{147a,147b}, A. Poblaguev²⁵, S. Poddar^{58a}, F. Podlyski³⁴, R. Poettgen⁸², L. Poggioli¹¹⁶, D. Pohl²¹, M. Pohl⁴⁹, G. Polesello^{120a}, A. Policicchio^{37a,37b}, R. Polifka¹⁵⁹, A. Polini^{20a}, V. Polychronakos²⁵, D. Pomeroy²³, K. Pommès³⁰, L. Pontecorvo^{133a}, B. G. Pope⁸⁹, G. A. Popeneciu^{26a}, D. S. Popovic^{13a}, A. Poppleton³⁰, X. Portell Bueso¹², G. E. Pospelov¹⁰⁰, S. Pospisil¹²⁷, I. N. Potrap⁶⁴, C. J. Potter¹⁵⁰, C. T. Potter¹¹⁵, G. Poulard³⁰, J. Poveda⁶⁰, V. Pozdnyakov⁶⁴, R. Prabhu⁷⁷, P. Pralavorio⁸⁴, A. Pranko¹⁵, S. Prasad³⁰, R. Pravahan²⁵, S. Prell⁶³, K. Pretzl¹⁷, D. Price⁶⁰, J. Price⁷³, L. E. Price⁶, D. Prieur¹²⁴, M. Primavera^{72a}, M. Proissl⁴⁶, K. Prokofiev¹⁰⁹, F. Prokoshin^{32b}, E. Protopapadaki¹³⁷, S. Protopopescu²⁵, J. Proudfoot⁶, X. Prudent⁴⁴, M. Przybycien^{38a}, H. Przysiezniak⁵, S. Psoroulas²¹, E. Ptacek¹¹⁵, E. Pueschel⁸⁵, D. Puldon¹⁴⁹, M. Purohit^{25,af}, P. Puzo¹¹⁶, Y. Pylypchenko⁶², J. Qian⁸⁸, A. Quadri⁵⁴, D. R. Quarrie¹⁵, W. B. Quayle¹⁷⁴, D. Quilty⁵³, M. Raas¹⁰⁵, V. Radeka²⁵, V. Radescu⁴², P. Radloff¹¹⁵, F. Ragusa^{90a,90b}, G. Rahal¹⁷⁹, S. Rajagopalan²⁵, M. Rammensee⁴⁸, M. Rammes¹⁴², A. S. Randle-Conde⁴⁰, K. Randrianarivony²⁹, C. Rangel-Smith⁷⁹, K. Rao¹⁶⁴, F. Rauscher⁹⁹, T. C. Rave⁴⁸, T. Ravenscroft⁵³, M. Raymond³⁰, A. L. Read¹¹⁸, D. M. Rebuzzi^{120a,120b}, A. Redelbach¹⁷⁵, G. Redlinger²⁵, R. Reece¹²¹, K. Reeves⁴¹, A. Reinsch¹¹⁵, I. Reisinger⁴³, M. Relich¹⁶⁴, C. Rembser³⁰, Z. L. Ren¹⁵², A. Renaud¹¹⁶, M. Rescigno^{133a}, S. Resconi^{90a}, B. Resende¹³⁷, P. Reznicek⁹⁹, R. Rezvani⁹⁴, R. Richter¹⁰⁰, E. Richter-Was^{38b}, M. Ridet⁷⁹, P. Rieck¹⁶, M. Rijssenbeek¹⁴⁹, A. Rimoldi^{120a,120b}, L. Rinaldi^{20a}, R. R. Rios⁴⁰, E. Ritsch⁶¹, I. Riu¹², G. Rivoltella^{90a,90b}, F. Rizatdinova¹¹³, E. Rizvi⁷⁵, S. H. Robertson^{86,j}, A. Robichaud-Veronneau¹¹⁹, D. Robinson²⁸, J. E. M. Robinson⁸³, A. Robson⁵³, J. G. Rocha de Lima¹⁰⁷, C. Roda^{123a,123b}, D. Roda Dos Santos³⁰, A. Roe⁵⁴, S. Roe³⁰, O. Røhne¹¹⁸, S. Rolli¹⁶², A. Romaniouk⁹⁷, M. Romano^{20a,20b}, G. Romeo²⁷, E. Romero Adam¹⁶⁸, N. Rompotis¹³⁹, L. Roos⁷⁹, E. Ros¹⁶⁸, S. Rosati^{133a}, K. Rosbach⁴⁹, A. Rose¹⁵⁰, M. Rose⁷⁶, G. A. Rosenbaum¹⁵⁹, P. L. Rosendahl¹⁴, O. Rosenthal¹⁴², V. Rossetti¹², E. Rossi^{133a,133b}, L. P. Rossi^{50a}, M. Rotaru^{26a}, I. Roth¹⁷³, J. Rothberg¹³⁹, D. Rousseau¹¹⁶, C. R. Royon¹³⁷, A. Rozanov⁸⁴, Y. Rozen¹⁵³, X. Ruan^{33a,aj}, F. Rubbo¹², I. Rubinskiy⁴², N. Ruckstuhl¹⁰⁶, V. I. Rud⁹⁸, C. Rudolph⁴⁴, M. S. Rudolph¹⁵⁹, F. Rühr⁷, A. Ruiz-Martinez⁶³, L. Rummyantsev⁶⁴, Z. Rurikova⁴⁸, N. A. Rusakovich⁶⁴, A. Ruschke⁹⁹, J. P. Rutherford⁷, N. Ruthmann⁴⁸, P. Ruzicka¹²⁶, Y. F. Ryabov¹²², M. Rybar¹²⁸, G. Rybkin¹¹⁶, N. C. Ryder¹¹⁹, A. F. Saavedra¹⁵¹, A. Saddique³, I. Sadeh¹⁵⁴, H. F.-W. Sadrozinski¹³⁸, R. Sadykov⁶⁴, F. Safai Tehrani^{133a}, H. Sakamoto¹⁵⁶, G. Salamanna⁷⁵, A. Salamon^{134a}, M. Saleem¹¹², D. Salek³⁰, D. Salihagic¹⁰⁰, A. Salnikov¹⁴⁴, J. Salt¹⁶⁸, B. M. Salvachua Ferrando⁶, D. Salvatore^{37a,37b}, F. Salvatore¹⁵⁰, A. Salvucci¹⁰⁵, A. Salzburger³⁰, D. Sampsonidis¹⁵⁵, A. Sanchez^{103a,103b}, J. Sánchez¹⁶⁸, V. Sanchez Martinez¹⁶⁸, H. Sandaker¹⁴, H. G. Sander⁸², M. P. Sanders⁹⁹, M. Sandhoff¹⁷⁶, T. Sandoval²⁸,

C. Sandoval¹⁶³, R. Sandstroem¹⁰⁰, D. P. C. Sankey¹³⁰, A. Sansoni⁴⁷, C. Santoni³⁴, R. Santonico^{134a,134b}, H. Santos^{125a}, I. Santoyo Castillo¹⁵⁰, K. Sapp¹²⁴, J. G. Saraiva^{125a}, T. Sarangi¹⁷⁴, E. Sarkisyan-Grinbaum⁸, B. Sarrazin²¹, F. Sarri^{123a,123b}, G. Sartisohn¹⁷⁶, O. Sasaki⁶⁵, Y. Sasaki¹⁵⁶, N. Sasao⁶⁷, I. Satsounkevitch⁹¹, G. Sauvage^{5,*}, E. Sauvan⁵, J. B. Sauvan¹¹⁶, P. Savard^{159,e}, V. Savinov¹²⁴, D. O. Savu³⁰, C. Sawyer¹¹⁹, L. Sawyer^{78,1}, D. H. Saxon⁵³, J. Saxon¹²¹, C. Sbarra^{20a}, A. Sbrizzi³, D. A. Scannicchio¹⁶⁴, M. Scarcella¹⁵¹, J. Schaarschmidt¹¹⁶, P. Schacht¹⁰⁰, D. Schaefer¹²¹, A. Schaelicke⁴⁶, S. Schaepe²¹, S. Schaetzel^{58b}, U. Schäfer⁸², A. C. Schaffer¹¹⁶, D. Schaile⁹⁹, R. D. Schamberger¹⁴⁹, V. Scharf^{58a}, V. A. Schegelsky¹²², D. Scheirich⁸⁸, M. Schernau¹⁶⁴, M. I. Scherzer³⁵, C. Schiavi^{50a,50b}, J. Schieck⁹⁹, C. Schillo⁴⁸, M. Schioppa^{37a,37b}, S. Schlenker³⁰, E. Schmidt⁴⁸, K. Schmieden³⁰, C. Schmitt⁸², C. Schmitt⁹⁹, S. Schmitt^{58b}, B. Schneider¹⁷, Y. J. Schnellbach⁷³, U. Schnoor⁴⁴, L. Schoeffel¹³⁷, A. Schoening^{58b}, A. L. S. Schorlemmer⁵⁴, M. Schott⁸², D. Schouten^{160a}, J. Schovancova¹²⁶, M. Schram⁸⁶, C. Schroeder⁸², N. Schuh⁸², N. Schroer^{58c}, M. J. Schultens²¹, H.-C. Schultz-Coulon^{58a}, H. Schulz¹⁶, M. Schumacher⁴⁸, B. A. Schumm¹³⁸, Ph. Schune¹³⁷, A. Schwartzman¹⁴⁴, Ph. Schwegler¹⁰⁰, Ph. Schwemling¹³⁷, R. Schvienhorst⁸⁹, J. Schwindling¹³⁷, T. Schwindt²¹, M. Schwoerer⁵, F. G. Sciaccia¹⁷, E. Scifo¹¹⁶, G. Sciolla²³, W. G. Scott¹³⁰, F. Scutti²¹, J. Searcy⁸⁸, G. Sedov⁴², E. Sedykh¹²², S. C. Seidel¹⁰⁴, A. Seiden¹³⁸, F. Seifert⁴⁴, J. M. Seixas^{24a}, G. Sekhniaidze^{103a}, S. J. Sekula⁴⁰, K. E. Selbach⁴⁶, D. M. Seliverstov¹²², G. Sellers⁷³, M. Seman^{145b}, N. Semprini-Cesari^{20a,20b}, C. Serfon³⁰, L. Serin¹¹⁶, L. Serkin⁵⁴, T. Serre⁸⁴, R. Seuster^{160a}, H. Severini¹¹², A. Sfyrla³⁰, E. Shabalina⁵⁴, M. Shamim¹¹⁵, L. Y. Shan^{33a}, J. T. Shank²², Q. T. Shao⁸⁷, M. Shapiro¹⁵, P. B. Shatalov⁹⁶, K. Shaw^{165a,165c}, P. Sherwood⁷⁷, S. Shimizu¹⁰², M. Shimojima¹⁰¹, T. Shin⁵⁶, M. Shiyakova⁶⁴, A. Shmeleva⁹⁵, M. J. Shochet³¹, D. Short¹¹⁹, S. Shrestha⁶³, E. Shulga⁹⁷, M. A. Shupe⁷, P. Sicho¹²⁶, A. Sidoti^{133a}, F. Siegert⁴⁸, Dj. Sijacki^{13a}, O. Silbert¹⁷³, J. Silva^{125a}, Y. Silver¹⁵⁴, D. Silverstein¹⁴⁴, S. B. Silverstein^{147a}, V. Simak¹²⁷, O. Simard⁵, Lj. Simic^{13a}, S. Simion¹¹⁶, E. Simioni⁸², B. Simmons⁷⁷, R. Simoniello^{90a,90b}, M. Simonyan³⁶, P. Sinervo¹⁵⁹, N. B. Sinev¹¹⁵, V. Sipica¹⁴², G. Siragusa¹⁷⁵, A. Sircar⁷⁸, A. N. Sisakyan^{64,*}, S. Yu. Sivoklov⁹⁸, J. Sjölin^{147a,147b}, T. B. Sjusen¹⁴, L. A. Skinnari¹⁵, H. P. Skottowe⁵⁷, K. Yu. Skovpen¹⁰⁸, P. Skubic¹¹², M. Slater¹⁸, T. Slavicek¹²⁷, K. Sliwa¹⁶², V. Smakhtin¹⁷³, B. H. Smart⁴⁶, L. Smestad¹¹⁸, S. Yu. Smirnov⁹⁷, Y. Smirnov⁹⁷, L. N. Smirnova^{98,ak}, O. Smirnova⁸⁰, K. M. Smith⁵³, M. Smizanska⁷¹, K. Smolek¹²⁷, A. A. Snesarev⁹⁵, G. Snidero⁷⁵, J. Snow¹¹², S. Snyder²⁵, R. Sobie^{170,j}, J. Sodomka¹²⁷, A. Soffer¹⁵⁴, D. A. Soh^{152,v}, C. A. Solans³⁰, M. Solar¹²⁷, J. Solc¹²⁷, E. Yu. Soldatov⁹⁷, U. Soldevila¹⁶⁸, E. Solfaroli Camillocci^{133a,133b}, A. A. Solodkov¹²⁹, O. V. Solovyanov¹²⁹, V. Solovyev¹²², N. Soni¹, A. Sood¹⁵, V. Sopko¹²⁷, B. Sopko¹²⁷, M. Sosebee⁸, R. Soualah^{165a,165c}, P. Soueid⁹⁴, A. M. Soukharev¹⁰⁸, D. South⁴², S. Spagnolo^{72a,72b}, F. Spanò⁷⁶, R. Spighi^{20a}, G. Spigo³⁰, R. Spiwoks³⁰, M. Spousta^{128,al}, T. Spreitzer¹⁵⁹, B. Spurlock⁸, R. D. St. Denis⁵³, J. Stahlman¹²¹, R. Stamen^{58a}, E. Stanecka³⁹, R. W. Stanek⁶, C. Stanescu^{135a}, M. Stanescu-Bellu⁴², M. M. Stanitzki⁴², S. Stapnes¹¹⁸, E. A. Starchenko¹²⁹, J. Stark⁵⁵, P. Staroba¹²⁶, P. Starovoitov⁴², R. Staszewski³⁹, A. Staude⁹⁹, P. Stavina^{145a,*}, G. Steele⁵³, P. Steinbach⁴⁴, P. Steinberg²⁵, I. Stekl¹²⁷, B. Stelzer¹⁴³, H. J. Stelzer⁸⁹, O. Stelzer-Chilton^{160a}, H. Stenzel⁵², S. Stern¹⁰⁰, G. A. Stewart³⁰, J. A. Stillings²¹, M. C. Stockton⁸⁶, M. Stoebe⁸⁶, K. Stoerig⁴⁸, G. Stoica^{26a}, S. Stonjek¹⁰⁰, A. R. Stradling⁸, A. Straessner⁴⁴, J. Strandberg¹⁴⁸, S. Strandberg^{147a,147b}, A. Strandlie¹¹⁸, M. Strang¹¹⁰, E. Strauss¹⁴⁴, M. Strauss¹¹², P. Strizenec^{145b}, R. Ströhmer¹⁷⁵, D. M. Strom¹¹⁵, J. A. Strong^{76,*}, R. Stroynowski⁴⁰, B. Stugu¹⁴, I. Stumer^{25,*}, J. Stupak¹⁴⁹, P. Sturm¹⁷⁶, N. A. Styles⁴², D. Su¹⁴⁴, HS. Subramania³, R. Subramaniam⁷⁸, A. Succurro¹², Y. Sugaya¹¹⁷, C. Suhr¹⁰⁷, M. Suk¹²⁷, V. V. Sulin⁹⁵, S. Sultansoy^{4c}, T. Sumida⁶⁷, X. Sun⁵⁵, J. E. Sundermann⁴⁸, K. Suruliz¹⁴⁰, G. Susinno^{37a,37b}, M. R. Sutton¹⁵⁰, Y. Suzuki⁶⁵, Y. Suzuki⁶⁶, M. Svatos¹²⁶, S. Swedish¹⁶⁹, M. Swiatlowski¹⁴⁴, I. Sykora^{145a}, T. Sykora¹²⁸, D. Ta¹⁰⁶, K. Tackmann⁴², A. Taffard¹⁶⁴, R. Tafirout^{160a}, N. Taiblum¹⁵⁴, Y. Takahashi¹⁰², H. Takai²⁵, R. Takashima⁶⁸, H. Takeda⁶⁶, T. Takeshita¹⁴¹, Y. Takubo⁶⁵, M. Talby⁸⁴, A. A. Talyshev^{108,g}, J. Y. C. Tam¹⁷⁵, M. C. Tamsett^{78,am}, K. G. Tan⁸⁷, J. Tanaka¹⁵⁶, R. Tanaka¹¹⁶, S. Tanaka¹³², S. Tanaka⁶⁵, A. J. Tanasijczuk¹⁴³, K. Tani⁶⁶, N. Tannoury⁸⁴, S. Tapprogge⁸², D. Tardif¹⁵⁹, S. Tarem¹⁵³, F. Tarrade²⁹, G. F. Tartarelli^{90a}, P. Tas¹²⁸, M. Tasevsky¹²⁶, T. Tashiro⁶⁷, E. Tassi^{37a,37b}, Y. Tayalati^{136d}, C. Taylor⁷⁷, F. E. Taylor⁹³, G. N. Taylor⁸⁷, W. Taylor^{160b}, M. Teinturier¹¹⁶, F. A. Teischinger³⁰, M. Teixeira Dias Castanheira⁷⁵, P. Teixeira-Dias⁷⁶, K. K. Temming⁴⁸, H. Ten Kate³⁰, P. K. Teng¹⁵², S. Terada⁶⁵, K. Terashi¹⁵⁶, J. Terron⁸¹, M. Testa⁴⁷, R. J. Teuscher^{159,j}, J. Therhaag²¹, T. Theveneaux-Pelzer³⁴, S. Thoma⁴⁸, J. P. Thomas¹⁸, E. N. Thompson³⁵, P. D. Thompson¹⁸, P. D. Thompson¹⁵⁹, A. S. Thompson⁵³, L. A. Thomsen³⁶, E. Thomson¹²¹, M. Thomson²⁸, W. M. Thong⁸⁷, R. P. Thun^{88,*}, F. Tian³⁵, M. J. Tibbetts¹⁵, T. Tic¹²⁶, V. O. Tikhomirov^{95,an}, Yu. A. Tikhonov^{108,g}, S. Timoshenko⁹⁷, E. Tiouchichine⁸⁴, P. Tipton¹⁷⁷, S. Tisserant⁸⁴, T. Todorov⁵, S. Todorova-Nova¹⁶², B. Toggerson¹⁶⁴, J. Tojo⁶⁹, S. Tokár^{145a}, K. Tokushuku⁶⁵, K. Tollefson⁸⁹, L. Tomlinson⁸³, M. Tomoto¹⁰², L. Tompkins³¹, K. Toms¹⁰⁴, A. Tonoyan¹⁴, C. Topfel¹⁷, N. D. Topilin⁶⁴, E. Torrence¹¹⁵, H. Torres⁷⁹, E. Torró Pastor¹⁶⁸, J. Toth^{84,ag}, F. Touchard⁸⁴, D. R. Tovey¹⁴⁰, H. L. Tran¹¹⁶, T. Trefzger¹⁷⁵, L. Tremblet³⁰, A. Tricoli³⁰, I. M. Trigger^{160a}, S. Trincas-Duvold⁷⁹, M. F. Tripania⁷⁰, N. Triplett²⁵, W. Trischuk¹⁵⁹, B. Trocme⁵⁵, C. Troncon^{90a}, M. Trottier-McDonald¹⁴³, M. Trovatelli^{135a,135b}, P. True⁸⁹, M. Trzebinski³⁹, A. Trzupek³⁹, C. Tsarouchas³⁰, J. C.-L. Tseng¹¹⁹, M. Tsiakiris¹⁰⁶, P. V. Tsiareshka⁹¹, D. Tsionou¹³⁷, G. Tsipolitis¹⁰, S. Tsiskaridze¹², V. Tsiskaridze⁴⁸, E. G. Tskhadadze^{51a}, I. I. Tsukerman⁹⁶, V. Tsulaia¹⁵, J.-W. Tsung²¹, S. Tsuno⁶⁵, D. Tsybychev¹⁴⁹, A. Tua¹⁴⁰, A. Tudorache^{26a}, V. Tudorache^{26a}, J. M. Tuggle³¹, A. N. Tuna¹²¹, M. Turala³⁹, D. Turecek¹²⁷, I. Turk Cakir^{4d}, R. Turra^{90a,90b}, P. M. Tuts³⁵, A. Tykhonov⁷⁴,

M. Tylmad^{147a,147b}, M. Tyndel¹³⁰, K. Uchida²¹, I. Ueda¹⁵⁶, R. Ueno²⁹, M. Ughetto⁸⁴, M. Ugland¹⁴, M. Uhlenbrock²¹, F. Ukegawa¹⁶¹, G. Unal³⁰, A. Undrus²⁵, G. Unel¹⁶⁴, F. C. Ungaro⁴⁸, Y. Unno⁶⁵, D. Urbaniec³⁵, P. Urquijo²¹, G. Usai⁸, L. Vacavant⁸⁴, V. Vacek¹²⁷, B. Vachon⁸⁶, S. Vahsen¹⁵, N. Valencic¹⁰⁶, S. Valentinetti^{20a,20b}, A. Valero¹⁶⁸, L. Valery³⁴, S. Valkar¹²⁸, E. Valladolid Gallego¹⁶⁸, S. Vallecorsa¹⁵³, J. A. Valls Ferrer¹⁶⁸, R. Van Berg¹²¹, P. C. Van Der Deijl¹⁰⁶, R. van der Geer¹⁰⁶, H. van der Graaf¹⁰⁶, R. Van Der Leeuw¹⁰⁶, D. van der Ster³⁰, N. van Eldik³⁰, P. van Gemmeren⁶, J. Van Nieuwkoop¹⁴³, I. van Vulpen¹⁰⁶, M. Vanadia¹⁰⁰, W. Vandelli³⁰, A. Vaniachine⁶, P. Vankov⁴², F. Vannucci⁷⁹, R. Vari^{133a}, E. W. Varnes⁷, T. Varol⁸⁵, D. Varouchas¹⁵, A. Vartapetian⁸, K. E. Varvell¹⁵¹, V. I. Vassilakopoulos⁵⁶, F. Vazeille³⁴, T. Vazquez Schroeder⁵⁴, F. Veloso^{125a}, S. Veneziano^{133a}, A. Ventura^{72a,72b}, D. Ventura⁸⁵, M. Venturi⁴⁸, N. Venturi¹⁵⁹, V. Vercesi^{120a}, M. Verducci¹³⁹, W. Verkerke¹⁰⁶, J. C. Vermeulen¹⁰⁶, A. Vest⁴⁴, M. C. Vetterli^{143,e}, I. Vichou¹⁶⁶, T. Vickey^{146c,ao}, O. E. Vickey Boeriu^{146c}, G. H. A. Viehhauser¹¹⁹, S. Viel¹⁶⁹, M. Villa^{20a,20b}, M. Villaplana Perez¹⁶⁸, E. Vilucchi⁴⁷, M. G. Vinciter²⁹, V. B. Vinogradov⁶⁴, J. Virzi¹⁵, O. Vitells¹⁷³, M. Viti⁴², I. Vivarelli⁴⁸, F. Vives Vaque³, S. Vlachos¹⁰, D. Vladoiu⁹⁹, M. Vlasak¹²⁷, A. Vogel²¹, P. Vokac¹²⁷, G. Volpi⁴⁷, M. Volpi⁸⁷, G. Volpini^{90a}, H. von der Schmitt¹⁰⁰, H. von Radziewski⁴⁸, E. von Toerne²¹, V. Vorobel¹²⁸, M. Vos¹⁶⁸, R. Voss³⁰, J. H. Vossebeld⁷³, N. Vranjes¹³⁷, M. Vranjes Milosavljevic¹⁰⁶, V. Vrba¹²⁶, M. Vreeswijk¹⁰⁶, T. Vu Anh⁴⁸, R. Vuillermet³⁰, I. Vukotic³¹, Z. Vykydal¹²⁷, W. Wagner¹⁷⁶, P. Wagner²¹, S. Wahrmond⁴⁴, J. Wakabayashi¹⁰², S. Walch⁸⁸, J. Walder⁷¹, R. Walker⁹⁹, W. Walkowiak¹⁴², R. Wall¹⁷⁷, P. Waller⁷³, B. Walsh¹⁷⁷, C. Wang⁴⁵, H. Wang¹⁷⁴, H. Wang⁴⁰, J. Wang¹⁵², J. Wang^{33a}, K. Wang⁸⁶, R. Wang¹⁰⁴, S. M. Wang¹⁵², T. Wang²¹, X. Wang¹⁷⁷, A. Warburton⁸⁶, C. P. Ward²⁸, D. R. Wardrope⁷⁷, M. Warsinsky⁴⁸, A. Washbrook⁴⁶, C. Wasicki⁴², I. Watanabe⁶⁶, P. M. Watkins¹⁸, A. T. Watson¹⁸, I. J. Watson¹⁵¹, M. F. Watson¹⁸, G. Watts¹³⁹, S. Watts⁸³, A. T. Waugh¹⁵¹, B. M. Waugh⁷⁷, M. S. Weber¹⁷, J. S. Webster³¹, A. R. Weidberg¹¹⁹, P. Weigell¹⁰⁰, J. Weingarten⁵⁴, C. Weiser⁴⁸, P. S. Wells³⁰, T. Wenaus²⁵, D. Wendland¹⁶, Z. Weng^{152,v}, T. Wengler³⁰, S. Wenig³⁰, N. Wermes²¹, M. Werner⁴⁸, P. Werner³⁰, M. Werth¹⁶⁴, M. Wessels^{58a}, J. Wetter¹⁶², K. Whalen²⁹, A. White⁸, M. J. White⁸⁷, R. White^{32b}, S. White^{123a,123b}, S. R. Whitehead¹¹⁹, D. Whiteson¹⁶⁴, D. Whittington⁶⁰, D. Wicke¹⁷⁶, F. J. Wickens¹³⁰, W. Wiedenmann¹⁷⁴, M. Wielers^{80,d}, P. Wienemann²¹, C. Wiglesworth³⁶, L. A. M. Wiik-Fuchs²¹, P. A. Wijeratne⁷⁷, A. Wildauer¹⁰⁰, M. A. Wildt^{42,ap}, I. Wilhelm¹²⁸, H. G. Wilkens³⁰, J. Z. Will⁹⁹, E. Williams³⁵, H. H. Williams¹²¹, S. Williams²⁸, W. Willis^{35,*}, S. Willocq⁸⁵, J. A. Wilson¹⁸, A. Wilson⁸⁸, I. Wingerter-Seez⁵, S. Winkelmann⁴⁸, F. Winklmeier³⁰, M. Wittgen¹⁴⁴, T. Wittig⁴³, J. Wittkowski⁹⁹, S. J. Wollstadt⁸², M. W. Wolter³⁹, H. Wolters^{125a,h}, W. C. Wong⁴¹, G. Wooden⁸⁸, B. K. Wosiek³⁹, J. Wotschack³⁰, M. J. Woudstra⁸³, K. W. Wozniak³⁹, K. Wraight⁵³, M. Wright⁵³, B. Wrona⁷³, S. L. Wu¹⁷⁴, X. Wu⁴⁹, Y. Wu⁸⁸, E. Wulf³⁵, B. M. Wynne⁴⁶, S. Xella³⁶, M. Xiao¹³⁷, S. Xie⁴⁸, C. Xu^{33b,aa}, D. Xu^{33a}, L. Xu^{33b,aq}, B. Yabsley¹⁵¹, S. Yacoub^{146b,ar}, M. Yamada⁶⁵, H. Yamaguchi¹⁵⁶, Y. Yamaguchi¹⁵⁶, A. Yamamoto⁶⁵, K. Yamamoto⁶³, S. Yamamoto¹⁵⁶, T. Yamamura¹⁵⁶, T. Yamanaka¹⁵⁶, K. Yamauchi¹⁰², T. Yamazaki¹⁵⁶, Y. Yamazaki⁶⁶, Z. Yan²², H. Yang^{33e}, H. Yang¹⁷⁴, U. K. Yang⁸³, Y. Yang¹¹⁰, Z. Yang^{147a,147b}, S. Yanush⁹², L. Yao^{33a}, Y. Yasu⁶⁵, E. Yatsenko⁴², K. H. Yau Wong²¹, J. Ye⁴⁰, S. Ye²⁵, A. L. Yen⁵⁷, E. Yildirim⁴², M. Yilmaz^{4b}, R. Yoosoofmiya¹²⁴, K. Yorita¹⁷², R. Yoshida⁶, K. Yoshihara¹⁵⁶, C. Young¹⁴⁴, C. J. S. Young¹¹⁹, S. Youssef²², D. Yu²⁵, D. R. Yu¹⁵, J. Yu⁸, J. Yu¹¹³, L. Yuan⁶⁶, A. Yurkewicz¹⁰⁷, B. Zabinski³⁹, R. Zaidan⁶², A. M. Zaitsev^{129,ab}, S. Zambito²³, L. Zanello^{133a,133b}, D. Zanzi¹⁰⁰, A. Zaytsev²⁵, C. Zeitnitz¹⁷⁶, M. Zeman¹²⁷, A. Zemla³⁹, O. Zenin¹²⁹, T. Ženiš^{145a}, D. Zerwas¹¹⁶, G. Zevi della Porta⁵⁷, D. Zhang⁸⁸, H. Zhang⁸⁹, J. Zhang⁶, L. Zhang¹⁵², X. Zhang^{33d}, Z. Zhang¹¹⁶, Z. Zhao^{33b}, A. Zhemchugov⁶⁴, J. Zhong¹¹⁹, B. Zhou⁸⁸, N. Zhou¹⁶⁴, Y. Zhou¹⁵², C. G. Zhu^{33d}, H. Zhu⁴², J. Zhu⁸⁸, Y. Zhu^{33b}, X. Zhuang^{33a}, A. Zibell⁹⁹, D. Zieminska⁶⁰, N. I. Zimin⁶⁴, C. Zimmermann⁸², R. Zimmermann²¹, S. Zimmermann²¹, S. Zimmermann⁴⁸, Z. Zinonos^{123a,123b}, M. Ziolkowski¹⁴², R. Zitoun⁵, L. Živković³⁵, V. Zmouchko^{129,*}, G. Zobernig¹⁷⁴, A. Zoccoli^{20a,20b}, M. zur Nedden¹⁶, V. Zutshi¹⁰⁷, L. Zwalinski³⁰

¹ School of Chemistry and Physics, University of Adelaide, Adelaide, Australia

² Physics Department, SUNY Albany, Albany, NY, USA

³ Department of Physics, University of Alberta, Edmonton, AB, Canada

⁴ (a) Department of Physics, Ankara University, Ankara, Turkey; (b) Department of Physics, Gazi University, Ankara, Turkey; (c) Division of Physics, TOBB University of Economics and Technology, Ankara, Turkey; (d) Turkish Atomic Energy Authority, Ankara, Turkey

⁵ LAPP, CNRS/IN2P3 and Université de Savoie, Annecy-le-Vieux, France

⁶ High Energy Physics Division, Argonne National Laboratory, Argonne, IL, USA

⁷ Department of Physics, University of Arizona, Tucson, AZ, USA

⁸ Department of Physics, The University of Texas at Arlington, Arlington, TX, USA

⁹ Physics Department, University of Athens, Athens, Greece

¹⁰ Physics Department, National Technical University of Athens, Zografou, Greece

¹¹ Institute of Physics, Azerbaijan Academy of Sciences, Baku, Azerbaijan

¹² Institut de Física d'Altes Energies and Departament de Física de la Universitat Autònoma de Barcelona, Barcelona, Spain

- ¹³ (a) Institute of Physics, University of Belgrade, Belgrade, Serbia; (b) Vinca Institute of Nuclear Sciences, University of Belgrade, Belgrade, Serbia
- ¹⁴ Department for Physics and Technology, University of Bergen, Bergen, Norway
- ¹⁵ Physics Division, Lawrence Berkeley National Laboratory and University of California, Berkeley, CA, USA
- ¹⁶ Department of Physics, Humboldt University, Berlin, Germany
- ¹⁷ Albert Einstein Center for Fundamental Physics and Laboratory for High Energy Physics, University of Bern, Bern, Switzerland
- ¹⁸ School of Physics and Astronomy, University of Birmingham, Birmingham, UK
- ¹⁹ (a) Department of Physics, Bogazici University, Istanbul, Turkey; (b) Department of Physics, Dogus University, Istanbul, Turkey; (c) Department of Physics Engineering, Gaziantep University, Gaziantep, Turkey
- ²⁰ (a) INFN Sezione di Bologna, Bologna, Italy; (b) Dipartimento di Fisica e Astronomia, Università di Bologna, Bologna, Italy
- ²¹ Physikalisches Institut, University of Bonn, Bonn, Germany
- ²² Department of Physics, Boston University, Boston, MA, USA
- ²³ Department of Physics, Brandeis University, Waltham, MA, USA
- ²⁴ (a) Universidade Federal do Rio De Janeiro COPPE/EE/IF, Rio de Janeiro, Brazil; (b) Federal University of Juiz de Fora (UFJF), Juiz de Fora, Brazil; (c) Federal University of Sao Joao del Rei (UFSJ), Sao Joao del Rei, Brazil; (d) Instituto de Fisica, Universidade de Sao Paulo, Sao Paulo, Brazil
- ²⁵ Physics Department, Brookhaven National Laboratory, Upton, NY, USA
- ²⁶ (a) National Institute of Physics and Nuclear Engineering, Bucharest, Romania; (b) University Politehnica Bucharest, Bucharest, Romania; (c) West University in Timisoara, Timisoara, Romania
- ²⁷ Departamento de Física, Universidad de Buenos Aires, Buenos Aires, Argentina
- ²⁸ Cavendish Laboratory, University of Cambridge, Cambridge, UK
- ²⁹ Department of Physics, Carleton University, Ottawa, ON, Canada
- ³⁰ CERN, Geneva, Switzerland
- ³¹ Enrico Fermi Institute, University of Chicago, Chicago, IL, USA
- ³² (a) Departamento de Física, Pontificia Universidad Católica de Chile, Santiago, Chile; (b) Departamento de Física, Universidad Técnica Federico Santa María, Valparaíso, Chile
- ³³ (a) Institute of High Energy Physics, Chinese Academy of Sciences, Beijing, China; (b) Department of Modern Physics, University of Science and Technology of China, Hefei, Anhui, China; (c) Department of Physics, Nanjing University, Nanjing, Jiangsu, China; (d) School of Physics, Shandong University, Jinan, Shandong, China; (e) Physics Department, Shanghai Jiao Tong University, Shanghai, China
- ³⁴ Laboratoire de Physique Corpusculaire, Clermont Université and Université Blaise Pascal and CNRS/IN2P3, Clermont-Ferrand, France
- ³⁵ Nevis Laboratory, Columbia University, Irvington, NY, USA
- ³⁶ Niels Bohr Institute, University of Copenhagen, Copenhagen, Denmark
- ³⁷ (a) INFN Gruppo Collegato di Cosenza; (b) Dipartimento di Fisica, Università della Calabria, Rende, Italy
- ³⁸ (a) Faculty of Physics and Applied Computer Science, AGH University of Science and Technology, Kraków, Poland; (b) Marian Smoluchowski Institute of Physics, Jagiellonian University, Kraków, Poland
- ³⁹ The Henryk Niewodniczanski Institute of Nuclear Physics, Polish Academy of Sciences, Kraków, Poland
- ⁴⁰ Physics Department, Southern Methodist University, Dallas, TX, USA
- ⁴¹ Physics Department, University of Texas at Dallas, Richardson, TX, USA
- ⁴² DESY, Hamburg and Zeuthen, Germany
- ⁴³ Institut für Experimentelle Physik IV, Technische Universität Dortmund, Dortmund, Germany
- ⁴⁴ Institut für Kern- und Teilchenphysik, Technische Universität Dresden, Dresden, Germany
- ⁴⁵ Department of Physics, Duke University, Durham, NC, USA
- ⁴⁶ SUPA-School of Physics and Astronomy, University of Edinburgh, Edinburgh, UK
- ⁴⁷ INFN Laboratori Nazionali di Frascati, Frascati, Italy
- ⁴⁸ Fakultät für Mathematik und Physik, Albert-Ludwigs-Universität, Freiburg, Germany
- ⁴⁹ Section de Physique, Université de Genève, Geneva, Switzerland
- ⁵⁰ (a) INFN Sezione di Genova, Genoa, Italy; (b) Dipartimento di Fisica, Università di Genova, Genoa, Italy
- ⁵¹ (a) E. Andronikashvili Institute of Physics, Iv. Javakishvili Tbilisi State University, Tbilisi, Georgia; (b) High Energy Physics Institute, Tbilisi State University, Tbilisi, Georgia

- ⁵² II Physikalisches Institut, Justus-Liebig-Universität Giessen, Giessen, Germany
- ⁵³ SUPA-School of Physics and Astronomy, University of Glasgow, Glasgow, UK
- ⁵⁴ II Physikalisches Institut, Georg-August-Universität, Göttingen, Germany
- ⁵⁵ Laboratoire de Physique Subatomique et de Cosmologie, Université Joseph Fourier and CNRS/IN2P3 and Institut National Polytechnique de Grenoble, Grenoble, France
- ⁵⁶ Department of Physics, Hampton University, Hampton, VA, USA
- ⁵⁷ Laboratory for Particle Physics and Cosmology, Harvard University, Cambridge, MA, USA
- ⁵⁸ ^(a) Kirchhoff-Institut für Physik, Ruprecht-Karls-Universität Heidelberg, Heidelberg, Germany; ^(b) Physikalisches Institut, Ruprecht-Karls-Universität Heidelberg, Heidelberg, Germany; ^(c) ZITI Institut für technische Informatik, Ruprecht-Karls-Universität Heidelberg, Mannheim, Germany
- ⁵⁹ Faculty of Applied Information Science, Hiroshima Institute of Technology, Hiroshima, Japan
- ⁶⁰ Department of Physics, Indiana University, Bloomington, IN, USA
- ⁶¹ Institut für Astro- und Teilchenphysik, Leopold-Franzens-Universität, Innsbruck, Austria
- ⁶² University of Iowa, Iowa City, IA, USA
- ⁶³ Department of Physics and Astronomy, Iowa State University, Ames, IA, USA
- ⁶⁴ Joint Institute for Nuclear Research, JINR Dubna, Dubna, Russia
- ⁶⁵ KEK, High Energy Accelerator Research Organization, Tsukuba, Japan
- ⁶⁶ Graduate School of Science, Kobe University, Kobe, Japan
- ⁶⁷ Faculty of Science, Kyoto University, Kyoto, Japan
- ⁶⁸ Kyoto University of Education, Kyoto, Japan
- ⁶⁹ Department of Physics, Kyushu University, Fukuoka, Japan
- ⁷⁰ Instituto de Física La Plata, Universidad Nacional de La Plata and CONICET, La Plata, Argentina
- ⁷¹ Physics Department, Lancaster University, Lancaster, UK
- ⁷² ^(a) INFN Sezione di Lecce, Lecce, Italy; ^(b) Dipartimento di Matematica e Fisica, Università del Salento, Lecce, Italy
- ⁷³ Oliver Lodge Laboratory, University of Liverpool, Liverpool, UK
- ⁷⁴ Department of Physics, Jožef Stefan Institute and University of Ljubljana, Ljubljana, Slovenia
- ⁷⁵ School of Physics and Astronomy, Queen Mary University of London, London, UK
- ⁷⁶ Department of Physics, Royal Holloway University of London, Surrey, UK
- ⁷⁷ Department of Physics and Astronomy, University College London, London, UK
- ⁷⁸ Louisiana Tech University, Ruston, LA, USA
- ⁷⁹ Laboratoire de Physique Nucléaire et de Hautes Energies, UPMC and Université Paris-Diderot and CNRS/IN2P3, Paris, France
- ⁸⁰ Fysiska institutionen, Lunds universitet, Lund, Sweden
- ⁸¹ Departamento de Física Teórica C-15, Universidad Autónoma de Madrid, Madrid, Spain
- ⁸² Institut für Physik, Universität Mainz, Mainz, Germany
- ⁸³ School of Physics and Astronomy, University of Manchester, Manchester, UK
- ⁸⁴ CPPM, Aix-Marseille Université and CNRS/IN2P3, Marseille, France
- ⁸⁵ Department of Physics, University of Massachusetts, Amherst, MA, USA
- ⁸⁶ Department of Physics, McGill University, Montreal, QC, Canada
- ⁸⁷ School of Physics, University of Melbourne, Parkville, VIC, Australia
- ⁸⁸ Department of Physics, The University of Michigan, Ann Arbor, MI, USA
- ⁸⁹ Department of Physics and Astronomy, Michigan State University, East Lansing, MI, USA
- ⁹⁰ ^(a) INFN Sezione di Milano, Milan, Italy; ^(b) Dipartimento di Fisica, Università di Milano, Milan, Italy
- ⁹¹ B.I. Stepanov Institute of Physics, National Academy of Sciences of Belarus, Minsk, Republic of Belarus
- ⁹² National Scientific and Educational Centre for Particle and High Energy Physics, Minsk, Republic of Belarus
- ⁹³ Department of Physics, Massachusetts Institute of Technology, Cambridge, MA, USA
- ⁹⁴ Group of Particle Physics, University of Montreal, Montreal, QC, Canada
- ⁹⁵ P.N. Lebedev Institute of Physics, Academy of Sciences, Moscow, Russia
- ⁹⁶ Institute for Theoretical and Experimental Physics (ITEP), Moscow, Russia
- ⁹⁷ Moscow Engineering and Physics Institute (MEPhI), Moscow, Russia
- ⁹⁸ D.V. Skobeltsyn Institute of Nuclear Physics, M.V. Lomonosov Moscow State University, Moscow, Russia
- ⁹⁹ Fakultät für Physik, Ludwig-Maximilians-Universität München, Munich, Germany
- ¹⁰⁰ Max-Planck-Institut für Physik (Werner-Heisenberg-Institut), Munich, Germany

- ¹⁰¹ Nagasaki Institute of Applied Science, Nagasaki, Japan
- ¹⁰² Graduate School of Science and Kobayashi-Maskawa Institute, Nagoya University, Nagoya, Japan
- ¹⁰³ (a) INFN Sezione di Napoli; (b) Dipartimento di Scienze Fisiche, Università di Napoli, Napoli, Italy
- ¹⁰⁴ Department of Physics and Astronomy, University of New Mexico, Albuquerque, NM, USA
- ¹⁰⁵ Institute for Mathematics, Astrophysics and Particle Physics, Radboud University Nijmegen/Nikhef, Nijmegen, The Netherlands
- ¹⁰⁶ Nikhef National Institute for Subatomic Physics and University of Amsterdam, Amsterdam, The Netherlands
- ¹⁰⁷ Department of Physics, Northern Illinois University, DeKalb, IL, USA
- ¹⁰⁸ Budker Institute of Nuclear Physics, SB RAS, Novosibirsk, Russia
- ¹⁰⁹ Department of Physics, New York University, New York, NY, USA
- ¹¹⁰ Ohio State University, Columbus, OH, USA
- ¹¹¹ Faculty of Science, Okayama University, Okayama, Japan
- ¹¹² Homer L. Dodge Department of Physics and Astronomy, University of Oklahoma, Norman, OK, USA
- ¹¹³ Department of Physics, Oklahoma State University, Stillwater, OK, USA
- ¹¹⁴ Palacký University, RCPTM, Olomouc, Czech Republic
- ¹¹⁵ Center for High Energy Physics, University of Oregon, Eugene, OR, USA
- ¹¹⁶ LAL, Université Paris-Sud and CNRS/IN2P3, Orsay, France
- ¹¹⁷ Graduate School of Science, Osaka University, Osaka, Japan
- ¹¹⁸ Department of Physics, University of Oslo, Oslo, Norway
- ¹¹⁹ Department of Physics, Oxford University, Oxford, UK
- ¹²⁰ (a) INFN Sezione di Pavia, Pavia, Italy; (b) Dipartimento di Fisica, Università di Pavia, Pavia, Italy
- ¹²¹ Department of Physics, University of Pennsylvania, Philadelphia, PA, USA
- ¹²² Petersburg Nuclear Physics Institute, Gatchina, Russia
- ¹²³ (a) INFN Sezione di Pisa, Pisa, Italy; (b) Dipartimento di Fisica E. Fermi, Università di Pisa, Pisa, Italy
- ¹²⁴ Department of Physics and Astronomy, University of Pittsburgh, Pittsburgh, PA, USA
- ¹²⁵ (a) Laboratório de Instrumentação e Física Experimental de Partículas-LIP, Lisbon, Portugal; (b) Departamento de Física Teórica y del Cosmos and CAFPE, Universidad de Granada, Granada, Spain
- ¹²⁶ Institute of Physics, Academy of Sciences of the Czech Republic, Prague, Czech Republic
- ¹²⁷ Czech Technical University in Prague, Prague, Czech Republic
- ¹²⁸ Faculty of Mathematics and Physics, Charles University in Prague, Prague, Czech Republic
- ¹²⁹ State Research Center Institute for High Energy Physics, Protvino, Russia
- ¹³⁰ Particle Physics Department, Rutherford Appleton Laboratory, Didcot, UK
- ¹³¹ Physics Department, University of Regina, Regina, SK, Canada
- ¹³² Ritsumeikan University, Kusatsu, Shiga, Japan
- ¹³³ (a) INFN Sezione di Roma I, Rome, Italy; (b) Dipartimento di Fisica, Università La Sapienza, Rome, Italy
- ¹³⁴ (a) INFN Sezione di Roma Tor Vergata, Rome, Italy; (b) Dipartimento di Fisica, Università di Roma Tor Vergata, Rome, Italy
- ¹³⁵ (a) INFN Sezione di Roma Tre, Rome, Italy; (b) Dipartimento di Matematica e Fisica, Università Roma Tre, Rome, Italy
- ¹³⁶ (a) Faculté des Sciences Ain Chock, Réseau Universitaire de Physique des Hautes Energies-Université Hassan II, Casablanca, Morocco; (b) Centre National de l'Energie des Sciences Techniques Nucleaires, Rabat, Morocco; (c) Faculté des Sciences Semlalia, Université Cadi Ayyad, LPHEA-Marrakech, Marrakech, Morocco; (d) Faculté des Sciences, Université Mohamed Premier and LTPM, Oujda, Morocco; (e) Faculté des Sciences, Université Mohammed V-Agdal, Rabat, Morocco
- ¹³⁷ DSM/IRFU (Institut de Recherches sur les Lois Fondamentales de l'Univers), CEA Saclay (Commissariat à l'Energie Atomique et aux Energies Alternatives), Gif-sur-Yvette, France
- ¹³⁸ Santa Cruz Institute for Particle Physics, University of California Santa Cruz, Santa Cruz, CA, USA
- ¹³⁹ Department of Physics, University of Washington, Seattle, WA, USA
- ¹⁴⁰ Department of Physics and Astronomy, University of Sheffield, Sheffield, UK
- ¹⁴¹ Department of Physics, Shinshu University, Nagano, Japan
- ¹⁴² Fachbereich Physik, Universität Siegen, Siegen, Germany
- ¹⁴³ Department of Physics, Simon Fraser University, Burnaby, BC, Canada
- ¹⁴⁴ SLAC National Accelerator Laboratory, Stanford, CA, USA

- ¹⁴⁵ (a) Faculty of Mathematics, Physics and Informatics, Comenius University, Bratislava, Slovak Republic; (b) Department of Subnuclear Physics, Institute of Experimental Physics of the Slovak Academy of Sciences, Kosice, Slovak Republic
- ¹⁴⁶ (a) Department of Physics, University of Cape Town, Cape Town, South Africa; (b) Department of Physics, University of Johannesburg, Johannesburg, South Africa; (c) School of Physics, University of the Witwatersrand, Johannesburg, South Africa
- ¹⁴⁷ (a) Department of Physics, Stockholm University, Stockholm, Sweden; (b) The Oskar Klein Centre, Stockholm, Sweden
- ¹⁴⁸ Physics Department, Royal Institute of Technology, Stockholm, Sweden
- ¹⁴⁹ Departments of Physics and Astronomy and Chemistry, Stony Brook University, Stony Brook, NY, USA
- ¹⁵⁰ Department of Physics and Astronomy, University of Sussex, Brighton, UK
- ¹⁵¹ School of Physics, University of Sydney, Sydney, Australia
- ¹⁵² Institute of Physics, Academia Sinica, Taipei, Taiwan
- ¹⁵³ Department of Physics, Technion: Israel Institute of Technology, Haifa, Israel
- ¹⁵⁴ Raymond and Beverly Sackler School of Physics and Astronomy, Tel Aviv University, Tel Aviv, Israel
- ¹⁵⁵ Department of Physics, Aristotle University of Thessaloniki, Thessaloniki, Greece
- ¹⁵⁶ International Center for Elementary Particle Physics and Department of Physics, The University of Tokyo, Tokyo, Japan
- ¹⁵⁷ Graduate School of Science and Technology, Tokyo Metropolitan University, Tokyo, Japan
- ¹⁵⁸ Department of Physics, Tokyo Institute of Technology, Tokyo, Japan
- ¹⁵⁹ Department of Physics, University of Toronto, Toronto, ON, Canada
- ¹⁶⁰ (a) TRIUMF, Vancouver, BC, Canada; (b) Department of Physics and Astronomy, York University, Toronto, ON, Canada
- ¹⁶¹ Faculty of Pure and Applied Sciences, University of Tsukuba, Tsukuba, Japan
- ¹⁶² Department of Physics and Astronomy, Tufts University, Medford, MA, USA
- ¹⁶³ Centro de Investigaciones, Universidad Antonio Narino, Bogotá, Colombia
- ¹⁶⁴ Department of Physics and Astronomy, University of California Irvine, Irvine, CA, USA
- ¹⁶⁵ (a) INFN Gruppo Collegato di Udine, Italy; (b) ICTP, Trieste, Italy; (c) Dipartimento di Chimica, Fisica e Ambiente, Università di Udine, Udine, Italy
- ¹⁶⁶ Department of Physics, University of Illinois, Urbana, IL, USA
- ¹⁶⁷ Department of Physics and Astronomy, University of Uppsala, Uppsala, Sweden
- ¹⁶⁸ Instituto de Física Corpuscular (IFIC) and Departamento de Física Atómica, Molecular y Nuclear and Departamento de Ingeniería Electrónica and Instituto de Microelectrónica de Barcelona (IMB-CNM), University of Valencia and CSIC, Valencia, Spain
- ¹⁶⁹ Department of Physics, University of British Columbia, Vancouver, BC, Canada
- ¹⁷⁰ Department of Physics and Astronomy, University of Victoria, Victoria, BC, Canada
- ¹⁷¹ Department of Physics, University of Warwick, Coventry, UK
- ¹⁷² Waseda University, Tokyo, Japan
- ¹⁷³ Department of Particle Physics, The Weizmann Institute of Science, Rehovot, Israel
- ¹⁷⁴ Department of Physics, University of Wisconsin, Madison, WI, USA
- ¹⁷⁵ Fakultät für Physik und Astronomie, Julius-Maximilians-Universität, Würzburg, Germany
- ¹⁷⁶ Fachbereich C Physik, Bergische Universität Wuppertal, Wuppertal, Germany
- ¹⁷⁷ Department of Physics, Yale University, New Haven, CT, USA
- ¹⁷⁸ Yerevan Physics Institute, Yerevan, Armenia
- ¹⁷⁹ Centre de Calcul de l'Institut National de Physique Nucléaire et de Physique des Particules (IN2P3), Villeurbanne, France
- ^a Also at Department of Physics, King's College London, London, UK
- ^b Also at Laboratorio de Instrumentacao e Fisica Experimental de Particulas-LIP, Lisbon, Portugal
- ^c Also at Faculdade de Ciencias and CFNUL, Universidade de Lisboa, Lisbon, Portugal
- ^d Also at Particle Physics Department, Rutherford Appleton Laboratory, Didcot, UK
- ^e Also at TRIUMF, Vancouver, BC, Canada
- ^f Also at Department of Physics, California State University, Fresno, CA, USA
- ^g Also at Novosibirsk State University, Novosibirsk, Russia
- ^h Also at Department of Physics, University of Coimbra, Coimbra, Portugal
- ⁱ Also at Università di Napoli Parthenope, Naples, Italy
- ^j Also at Institute of Particle Physics (IPP), Canada

- ^k Also at Department of Physics, Middle East Technical University, Ankara, Turkey
- ^l Also at Louisiana Tech University, Ruston, LA, USA
- ^m Also at Dep Fisica and CEFITEC of Faculdade de Ciencias e Tecnologia, Universidade Nova de Lisboa, Caparica, Portugal
- ⁿ Also at Department of Physics and Astronomy, Michigan State University, East Lansing, MI, USA
- ^o Also at Department of Financial and Management Engineering, University of the Aegean, Chios, Greece
- ^p Also at Institutio Catalana de Recerca i Estudis Avancats, ICREA, Barcelona, Spain
- ^q Also at Department of Physics, University of Cape Town, Cape Town, South Africa
- ^r Also at Institute of Physics, Azerbaijan Academy of Sciences, Baku, Azerbaijan
- ^s Also at Ochadai Academic Production, Ochanomizu University, Tokyo, Japan
- ^t Also at Manhattan College, New York, NY, USA
- ^u Also at Institute of Physics, Academia Sinica, Taipei, Taiwan
- ^v Also at School of Physics and Engineering, Sun Yat-sen University, Guangzhou, China
- ^w Also at Academia Sinica Grid Computing, Institute of Physics, Academia Sinica, Taipei, Taiwan
- ^x Also at Laboratoire de Physique Nucléaire et de Hautes Energies, UPMC and Université Paris-Diderot and CNRS/IN2P3, Paris, France
- ^y Also at School of Physical Sciences, National Institute of Science Education and Research, Bhubaneswar, India
- ^z Also at Dipartimento di Fisica, Università La Sapienza, Rome, Italy
- ^{aa} Also at DSM/IRFU (Institut de Recherches sur les Lois Fondamentales de l'Univers), CEA Saclay (Commissariat à l'Energie Atomique et aux Energies Alternatives), Gif-sur-Yvette, France
- ^{ab} Also at Moscow Institute of Physics and Technology State University, Dolgoprudny, Russia
- ^{ac} Also at Section de Physique, Université de Genève, Geneva, Switzerland
- ^{ad} Also at Departamento de Fisica, Universidade de Minho, Braga, Portugal
- ^{ae} Also at Department of Physics, The University of Texas at Austin, Austin, TX, USA
- ^{af} Also at Department of Physics and Astronomy, University of South Carolina, Columbia, SC, USA
- ^{ag} Also at Institute for Particle and Nuclear Physics, Wigner Research Centre for Physics, Budapest, Hungary
- ^{ah} Also at DESY, Hamburg and Zeuthen, Germany
- ^{ai} Also at International School for Advanced Studies (SISSA), Trieste, Italy
- ^{aj} Also at LAL, Université Paris-Sud and CNRS/IN2P3, Orsay, France
- ^{ak} Also at Faculty of Physics, M.V.Lomonosov Moscow State University, Moscow, Russia
- ^{al} Also at Nevis Laboratory, Columbia University, Irvington, NY, USA
- ^{am} Also at Physics Department, Brookhaven National Laboratory, Upton, NY, USA
- ^{an} Also at Moscow Engineering and Physics Institute (MEPhI), Moscow, Russia
- ^{ao} Also at Department of Physics, Oxford University, Oxford, UK
- ^{ap} Also at Institut für Experimentalphysik, Universität Hamburg, Hamburg, Germany
- ^{aq} Also at Department of Physics, The University of Michigan, Ann Arbor, MI, USA
- ^{ar} Also at Discipline of Physics, University of KwaZulu-Natal, Durban, South Africa
- * Deceased